EuCARD-2

Enhanced European Coordination for Accelerator Research & Development

Academic Dissertation

Energy Efficient Beam Transfer Channels for High Energy Particle Accelerators

Gardlowski, Philipp (TUD)

29 January 2016

The EuCARD-2 Enhanced European Coordination for Accelerator Research & Development project is co-funded by the partners and the European Commission under Capacities 7th Framework Programme, Grant Agreement 312453.

This work is part of EuCARD-2 Work Package **3: Energy Efficiency (EnEfficient)**.

The electronic version of this EuCARD-2 Publication is available via the EuCARD-2 web site <http://eucard2.web.cern.ch/> or on the CERN Document Server at the following URL: <http://cds.cern.ch/search?p=CERN-THESIS-2016-044>

Energy Efficient Beam Transfer Channels for High Energy Particle Accelerators

Energieeffiziente Strahlführungssysteme für Hochenergie-Teilchenbeschleuniger

Master-Thesis von Philipp Gardlowski aus Offenbach am Main

29.01.2016

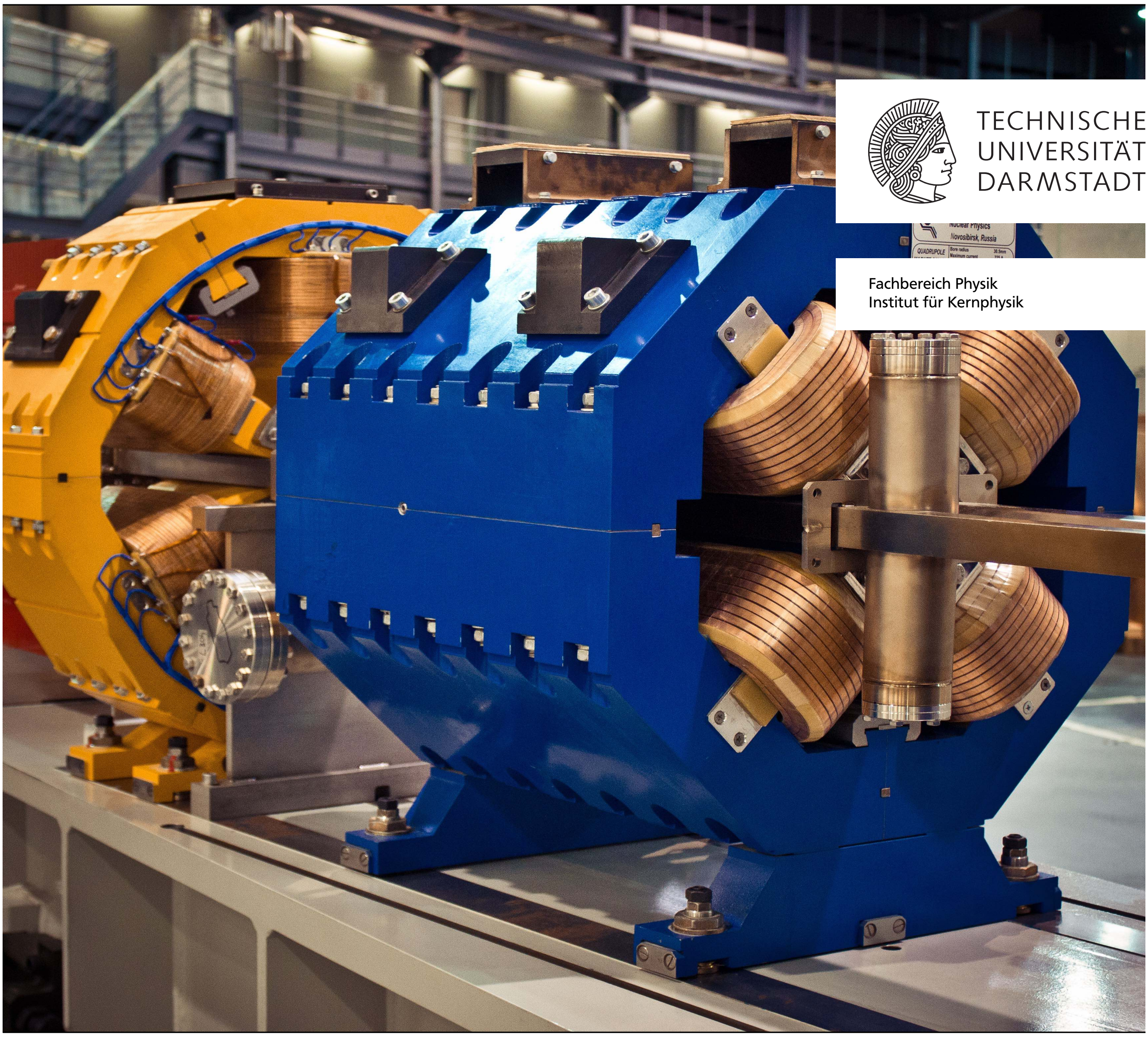

TECHNISCHE UNIVERSITÄT DARMSTADT

Fachbereich Physik
Institut für Kernphysik

Energy Efficient Beam Transfer Channels for High Energy Particle Accelerators
Energieeffiziente Strahlführungssysteme für Hochenergie-Teilchenbeschleuniger

Vorgelegte Master-Thesis von Philipp Gardlowski aus Offenbach am Main

1. Gutachten: Prof. Dr. Dr. h.c./RUS Dieter H. H. Hoffmann
2. Gutachten: Dr. David Ondreka

Tag der Einreichung:

The research leading to these results has received funding from the European Commission under the FP7 Research Infrastructures project EuCARD-2, grant agreement no.312453.

EuCARD-2 is co-funded by the partners and the European Commission under Capacities 7th Framework Programme, Grant Agreement 312453

Erklärung zur Master-Thesis

Hiermit versichere ich, die vorliegende Master-Thesis ohne Hilfe Dritter nur mit den angegebenen Quellen und Hilfsmitteln angefertigt zu haben. Alle Stellen, die aus Quellen entnommen wurden, sind als solche kenntlich gemacht. Diese Arbeit hat in gleicher oder ähnlicher Form noch keiner Prüfungsbehörde vorgelegen.

Darmstadt, den 29. Januar 2016

(Philipp Gardlowski)

Zusammenfassung

Energieeffizienz ist ein zunehmend wichtiger werdendes Kriterium für die Auslegung moderner Teilchenbeschleuniger. Diese Arbeit befasst sich daher mit dem Vergleich unterschiedlicher Magnettechnologien hinsichtlich des Energieverbrauchs und der Gesamtkosten. Da die Anforderungen an Strahlführungen sehr von der jeweiligen Beschleunigeranlage abhängen, sind verallgemeinerte Empfehlungen für die Wahl des Magnettyps nicht möglich. Allerdings gibt es einige Konfigurationen, die für einen bestimmten Bereich der untersuchten Parameter zu signifikant geringeren Gesamtkosten führen können. Für Repetitionsraten unter 0,1 Hz ergibt sich zum Beispiel, dass AC betriebene, konventionelle normalleitende (NC) Magnete oder Hochstrom-gepulste (HCP) Magnete eine ökonomische Lösung bieten. Für Repetitionsraten über 1,0 Hz sind supraleitende Cos(NΘ) (SC) Magnete oder superferrische (SF) Magnete attraktiver; zumindest wenn diese DC betrieben werden und deshalb keine dynamischen Verluste im kryogenen System auftreten. Allerdings gibt es auch Wertebereiche für die Repetitionsrate, in denen keine klare Empfehlung ausgesprochen werden kann. In diesen Fällen ist eine detailliertere Untersuchung für jede individuelle Anlage unumgänglich. Ein ähnliches Verhalten ergibt sich für die magnetische Steifigkeit: Für kleine Werte der magnetischen Steifigkeit ($\leq$10 Tm) sind zum Beispiel NC Magnete aufgrund der geringen benötigten Feldstärken ökonomischer. Je nach Strahlführung sind auch Permanentmagnete (PM) in diesem Bereich eine Alternative. Für große Werte der magnetischen Steifigkeit ($>$100 Tm) werden die benötigten integralen Feldstärken so groß, dass SF oder SC Magnete eine ökonomischere und kompaktere Lösung bieten. Leider gibt es auch hier einen Bereich, in dem sich keine eindeutigen Empfehlungen ergeben.

Um die Modelle einfach aber dennoch anwendbar auf gängige Beamlinedesigns existierender Beschleunigeranlagen zu machen, wird in den Rechnungen in dieser Arbeit eine FODO Transferlinie für alle Beispiele angenommen. Für die Untersuchung der Eignung der verschiedenen Magnettechnologien hinsichtlich der Energieeffizienz wird zunächst die Abhängigkeit des Energiebedarfs von Parametern wie der Strahlgröße beziehungsweise der Aperturgröße, der Repetitionsrate und der kinetischen Energie des Strahls beziehungsweise der magnetischen Steifigkeit ermittelt. Für die Berechnung des Energiebedarfs der verschiedenen Magnete ist der Ausgangspunkt folglich eine Charakterisierung der Transferstrecke hinsichtlich der Hauptparameter. Die Emittanz und die magnetische Steifigkeit beeinflussen die Apertur der Magnete, die sich aus der maximalen Amplitude der Betatronschwingung ergibt. Außerdem definiert die magnetische Steifigkeit die nötigen integralen Feldstärken der Dipole und der Quadrupole. Die Repetitionsrate legt die Zeitstruktur des Transferkanals – und somit auch den Betriebsmodus der beteiligten Geräte – fest. Die Untersuchungen der allgemeinen Eigenschaften von FODO Transferkanälen zeigt, dass das Fokussiersystem einer Beamline vorrangig von der kleinsten magnetischen Steifigkeit abhängt, die von der Transferlinie unterstützt werden soll. Der Transport von Strahlen mit einer größeren magnetischen Steifigkeit ist durch den Effekt der adiabatischen Dämpfung stets gewährleistet. Somit können auch Beamlines mit einem Fokussiersystem fester Stärke für den Transport von Strahlen unterschiedlicher magnetischer Steifigkeit genutzt werden. Basierend auf den Eigenschaften von FODO Transferlinien wird der Energiebedarf verschiedener Magnettechnologien als Funktion der Aperturgröße, der Repetitionsrate und der

magnetischen Steifigkeit bestimmt. Anhand einer exemplarischen Elektronenbeamline, einer exemplarischen Protonenbeamline und einer exemplarischen Schwerionenbeamline wird so die Abhängigkeit des Energiebedarfs von jenen Parametern diskutiert. In einem zweiten Schritt wird die Wirtschaftlichkeit der Magnettypen für verschiedene Anwendungsfelder untersucht, indem die Gesamtkosten des Magnetsystems abgeschätzt werden.

Die Ergebnisse dieser Thesis sind in einer Tabelle zusammengefasst, in der Empfehlungen für die geeigneten Magnettechnologien in Abhängigkeit der magnetischen Steifigkeit des Strahls, der Repetitionsrate der Transferlinie und des Strahlführungstyps gegeben werden. Die untersuchten Strahlführungstypen sind Elektronenstrahlführungen, Protonenstrahlführungen und Schwerionenstrahlführungen. Die Empfehlungen basieren auf den erwarteten Gesamtkosten für einen kontinuierlichen Betrieb über 20 Jahre. Die Gesamtkosten beinhalten die Betriebskosten, die durch den elektrischen Energiebedarf und den Wasserverbrauch bedingt werden, sowie die jeweiligen Investitionskosten der Subsysteme.

Abstract

Energy efficiency becomes an increasingly important aspect in regard to the design of modern particle accelerators. Thus, this thesis examines the comparison of different magnet technologies by means of the energy consumption and the total costs. As the requirements on beamlines highly differ among the different existing accelerator facilities, generalised recommendations on the choice of the magnet type are not possible. However, a few configurations are found, which may deliver significantly lower total costs for specific ranges of the investigated parameters. For low repetition rates below 0.1 Hz, for example, AC operated conventional normal conducting (NC) magnets or high current pulsed (HCP) magnets are an economic solution. For high repetition rates above 1.0 Hz, superconducting Cos(NΘ) (SC) magnets or superferric (SF) magnets are more attractive; at least if they are operated in DC mode and if no dynamic losses occur in the cryogenic system. Unfortunately, a range between these values exist, in which no clear recommendation can be given. Here, a more detailed investigation is necessary for each individual facility. A similar behaviour appears for the magnetic rigidity: For small values of the magnetic rigidity (≤10 Tm), for example, the NC magnets are more economic due to the low necessary field strengths. Depending on the beamline, permanent magnets (PM) can be an alternative, as well. For large values of the magnetic rigidity (>100 Tm), the necessary integrals field strengths become this large that the SF magnets or the SC magnets represent a more economic respectively more compact solution. Unfortunately, a range also exists, in which no clear recommendation can be given.

To keep the models simple but make them still applicable to common beamline designs of existing accelerator facilities, a FODO lattice is assumed for all beamline examples in this thesis' calculations. To investigate the different magnet technologies' suitability by means of energy efficiency, the dependency of the energy consumption from parameters like the beam size respectively the aperture radius, the repetition rate, and the beam's kinetic energy respectively the magnetic rigidity has to be determined first. Thus, the start point of the calculation of the different magnets' energy consumption is the characterisation of the transfer line by means of the major input parameters. The emittance and the magnetic rigidity affect the magnets' aperture resulting from the maximum amplitude of the beta oscillation. The magnetic rigidity further defines the necessary dipoles' and quadrupoles' integral field strengths. The repetition rate accounts for the time structure; and therefore, it accounts for the operation mode. Investigations on the properties of FODO transfer channels show the focussing system of a beamline primarily depends on the minimum value of the beam's magnetic rigidity. For beams with a larger value of the magnetic rigidity, the beam will also be transported due to the effect of adiabatic damping. Thus, fixed-strength beamlines also have the ability to transport beams with varying magnetic rigidity. Based on the found properties of FODO transfer lines, the energy consumption of the different magnet technologies are determined as a function of the aperture size, the repetition rate, and the magnetic rigidity. On the basis of an exemplary electron beamline, an exemplary proton beamline, and an exemplary heavy-ion beamline, the energy consumption's dependency of these parameters are discussed. In a second step, the different magnet types' economic effi-

ciency is examined for different fields of application by making estimates on the total costs of the magnet systems.

The results of this thesis are summarised in a table, which gives recommendations on the applicable magnet technologies depending on the beam's magnetic rigidity, the transfer line's repetition rate, and the type of the beamline (namely electron beamline, proton beamline, or heavy-ion beamline). These recommendations base on the estimated total costs for a continuous operation over 20 years. The total costs include the operation costs due to the electrical energy consumption and the water consumption as well as the particular subsystems' investment costs.

Contents

1 Introduction

Currently, energy efficiency is an important criterion in regard to the design of new, modern industrial facilities. However, in experimental accelerator facilities energy efficiency is often a rather secondary aspect for the machine design. But within the last years, energy efficiency has become increasingly popular for new accelerator facilities as well as for upgrades of existing facilities. Efficiency is often associated with saving operation costs but an energy efficient design can also have further benefits. For example, in accelerator-driven inertial-fusion experiments efficiency is extremely important to realise a break-even for the usage as a power station. Energy efficient medical accelerators lead to a more economic operation; and therefore, result in reduced medical costs due to the reduced operation costs. Large-scale accelerator facilities can have beam-transfer lines with a length of a few km. Here, an energy efficient design is needed to combine the high requirements of the transport system with the given local energy infrastructure. This master thesis will give recommendations on choosing the most energy efficient respectively the most economic magnet system by analysing the fundamental parameters affecting the energy consumption and the total costs. As magnets are both one of the major consumers of electrical energy and one of the major components with high investment costs in any accelerator facility, it is reasonable to optimise this part of the machine with respect to efficiency.

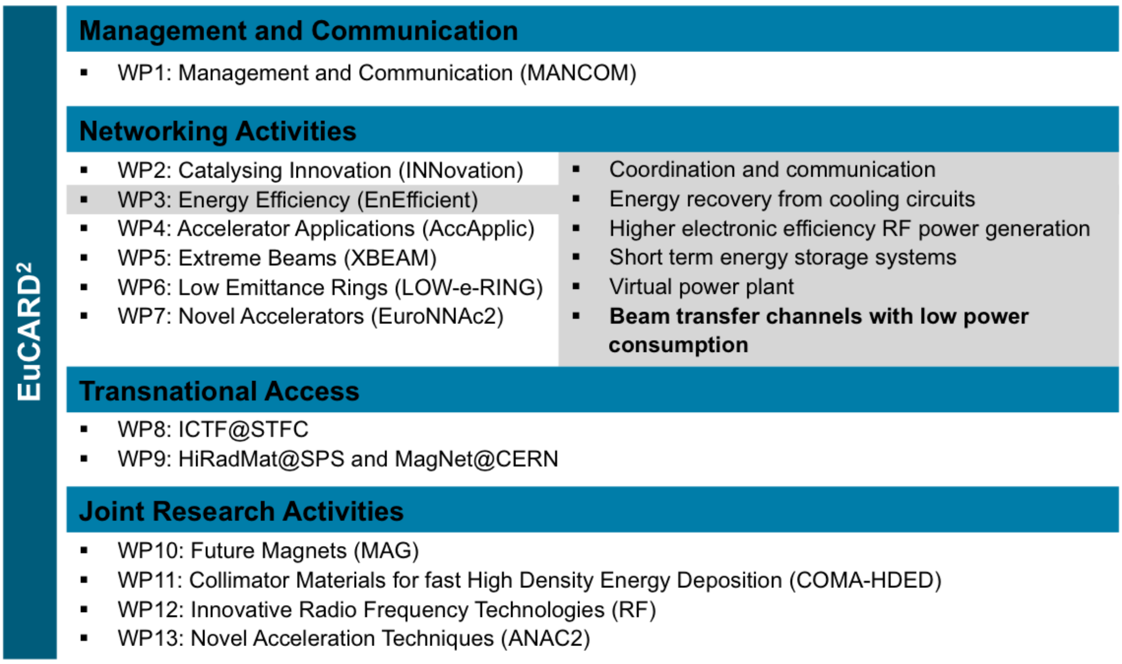

Figure 1.1.: Project structure of EuCARD^2 with special focus on work package WP3: Energy Efficiency (EnEfficient). This master thesis is dedicated to "Beam transfer channels with low power consumption".

To provide new and energy efficient technologies to the European accelerator facilities, the EuCARD^2 (Enhanced European Coordination for Accelerator Research & Development) project was founded. This project merges 40 partners out of 15 European countries. Those participating partners are accelerator facilities as well as universities, research institutes, and industry partners. This master thesis is dedicated to the work package Energy Efficiency (EnEfficient) respectively the task "Beam transfer channels with low power consumption". An executive summary of this thesis was published within the EuCARD^2 project in October 2015 (cf. P. Gardlowski, *Energy Efficiency of Beam Transfer Channels*, EuCARD2 Deliverable D3.3, October 2015 [1]).

2 Physical Basics

2.1 Deflexion of Charged Particles in Electromagnetic Fields

The acceleration and deflexion of charged particles in particle accelerators is caused by electric and magnetic fields. This acceleration is due to the Lorentz force, which is the force acting on a particle with the charge q and the velocity $\vec{v}$ in an electromagnetic field with the electric field strength $\vec{E}$ and the magnetic field strength $\vec{B}$ [2].

$$\vec{F} = q \cdot (\vec{E} + \vec{v} \times \vec{B}) \tag{2.1}$$

The parallel component of the electric field $E_{\parallel}$ yields an acceleration parallel to the direction of travel. The transversal components $E_{\perp}$ and $B_{\perp}$ cause a radial acceleration of the charged particles [2]. The value of the electric field has to be greater than the value of the magnetic field to reach the same effect of the electric and the magnetic field at relativistic velocities [3]; this follows from the relation $\vec{E} = c\vec{B}$. Usually, the necessary electric field strength to deflect charged particles in a particle accelerator is larger than the technically feasible field strengths. For this reason, magnetic fields are used for the deflexion of charged particles, especially at high particle energies. The electric field will be neglected below [3].

Assuming that the particles propagate linearly with the velocity of $\vec{v} = (0, 0, v_s)^T$ and the magnetic field $\vec{B} = (B_x, B_y, 0)^T$ only has transversal components, this yields the Lorentz force [3]:

$$\vec{F} = q \begin{pmatrix} 0 \\ 0 \\ v_s \end{pmatrix} \times \begin{pmatrix} B_x \\ B_y \\ 0 \end{pmatrix} = q \begin{pmatrix} -v_s B_y \\ v_s B_x \\ 0 \end{pmatrix} \tag{2.2}$$

This force causes that the beam will describe a circular path in the horizontal plane, so there is an equilibrium of the Lorentz force and the centrifugal force [3]

$$F = \frac{\gamma m v_s^2}{\rho}. \tag{2.3}$$

Here, $\gamma = 1/\sqrt{1-\beta^2}$ is the relativistic Lorentz factor, $\beta = v/c$ is the relativistic beta factor, and ρ is the bending radius. In consideration of the momentum $p = \gamma m v_s$, the following relation results from the equilibrium of the forces [3]:

$$\frac{1}{\rho(x, y, s)} = \frac{q}{p} B_y(x, y, s) \tag{2.4}$$

Using a multipole expansion of the magnetic field near the ideal trajectory ($x = 0$) shows the individual multipole parts that form the magnetic field [3]:

$$\frac{q}{p}B_y(x) = \frac{q}{p}B_y(0) \quad + \frac{q}{p}\left.\frac{dB_y}{dx}\right|_{x=0} \cdot x \quad + \frac{1}{2!}\frac{q}{p}\left.\frac{d^2B_y}{dx^2}\right|_{x=0} \cdot x^2 \quad + \frac{1}{3!}\frac{q}{p}\left.\frac{d^3B_y}{dx^3}\right|_{x=0} \cdot x^3 \quad + \dots \tag{2.5}$$

$$= \frac{1}{\rho} \quad + kx \quad + \frac{1}{2!}mx^2 \quad + \frac{1}{3!}ox^3 \quad + \dots \tag{2.6}$$

$$Dipole \qquad Quadrupole \qquad Sextupole \qquad Octupole$$

Linear beam optics include the zeroth and first order of this expansion. The dipole part $\frac{1}{\rho} = \frac{q}{p}B_y(0)$ effects a deflexion of the beam. The quadrupole part $k = \frac{q}{p}\frac{dB_y}{dx}$ effects a focussing respectively a defocussing of the beam. Higher multipole parts are either undesired or used to correct field errors [2, 3].

2.2 Magnetic Rigidity

For a constant magnetic field $\vec{B} = (0, B, 0)^T$ and a constant radius $\rho(x, y, s) = \rho =$ constant, rewriting equation 2.4 yields the magnetic rigidity $B\rho$ – a value that is common in accelerator physics. It depends on the momentum $p = mc\beta\gamma$ and the charge q [2]:

$$B\rho = \frac{p}{q} = \frac{mc}{q} \cdot \beta\gamma \tag{2.7}$$

In accelerator physics the momentum is usually given in units per nucleon. The momentum per nucleon as a function of the energy per nucleon results from the relativistic energy-momentum equation [2].

$$E_{total} = E_{kin} + E_0 = \sqrt{p^2c^2 + E_0^2} \quad \Rightarrow \quad p(E_{kin}) = \frac{\sqrt{E_{kin}^2 + 2E_{kin}E_0}}{c} \tag{2.8}$$

Here, E_{total} is the total energy per nucleon, E_{kin} is the kinetic energy per nucleon, E_0 is the rest energy per nucleon, and c ist the speed of light. Hence, the magnetic rigidity as a function of the kinetic energy per nucleon can be written as

$$B\rho = \frac{A}{Qe}\frac{\sqrt{E_{kin}^2 + 2E_{kin}E_0}}{c}. \tag{2.9}$$

In this equation, e is the elementary electrical charge and A is the effective mass number following from the mass number A_0 of the neutral atom, the charge number Q, and the mass number A_e of an electron.

$$A = A_0 - Q \cdot A_e \tag{2.10}$$

2.3 Effective Magnet Length and Integral Field Strength

As the magnetic field lines exceed the magnet's geometric length, which is in general the length of the iron yoke, the effective length of a magnet including these edge fields is defined as the integral of the field strength $B(s)$ along the beam axis, which is normalised to the value of the magnetic field strength B in the center of the magnet [2]:

$$L = \frac{1}{B}\int_{-\infty}^{+\infty} B(s)ds = \alpha\rho \tag{2.11}$$

Multiplying equation 2.11 with the magnetic field strength B yields the integral magnetic dipole field strength, which is a function of the deflexion angle α and the magnetic rigidity $B\rho$:

$$BL = \alpha \cdot B\rho \tag{2.12}$$

Analogously, the integral gradient $B'L$ of a quadrupole magnet is a function of the focussing strength kL and the magnetic rigidity $B\rho$:

$$B'L = kL \cdot B\rho \tag{2.13}$$

The following equations are used as an approximation of the effective magnet length. These can be found in literature [2]:

$$L_{\text{eff,dip}} \approx L_{\text{yoke}} + 1.3g \tag{2.14}$$

$$L_{\text{eff,quad}} \approx L_{\text{yoke}} + a \tag{2.15}$$

Here, L_{yoke} is the length of the iron yoke, g is the dipole's gap, and a is the quadrupole's pole-tip radius. These equations are for iron dominated magnets. Further edge fields, e.g., caused by the coil ends of the superconducting cos(NΘ) magnets' saddle coils are not investigated here.

2.4 Beta Function

The motion of a beam of charged particles in a machine without dipoles ($1/\rho = 0$) and with a fixed single energy ($\Delta p/p = 0$) can be expressed by Hill's differential equation [3]:

$$x''(s) - k(s)x(s) = 0 \tag{2.16}$$

Here, the beam size $x(s)$ and the quadrupole strength $k(s)$ are both a function of the position s, which result in a transversal betatron oscillation. Hence, the mathematical approach [3]

$$x(s) = Au(s)\cos(\Psi(s) + \phi) \tag{2.17}$$

is used to describe this oscillation. The factor A and the phase ϕ are constant. Considering the definition of the beta function $\beta(s) := u^2(s)$, the solution is [3]

$$x(s) = \sqrt{\epsilon}\sqrt{\beta(s)}\cos(\Psi(s) + \phi) \tag{2.18}$$

with $\Psi(s) = \int_0^s \frac{d\sigma}{\beta(\sigma)}$ and the emittance ϵ. Analogously, the motion in the perpendicular transverse plane y can be described. Thus, the beam size at a position s is [3]

$$x(s) = \sqrt{\epsilon_x\beta_x(s)} \tag{2.19}$$

respectively

$$y(s) = \sqrt{\epsilon_y\beta_y(s)}. \tag{2.20}$$

2.5 Emittance and Acceptance

The emittance ϵ – except for a factor π – is the area of the transversal phase space ellipse in the $x - x'$ plane [3]. Hence, the real area of the transversal phase space ellipse is $\pi\epsilon$. According to Liouville's theorem, this area – and therefore the emittance – is a conserved quantity. To compare the emittance of different machines, the so called normalised emittance ϵ_n is often used, which is defined as [2]

$$\epsilon_n = \epsilon\beta\gamma. \tag{2.21}$$

As mentioned before, $\beta = v/c$ is the relativistic beta factor and $\gamma = 1/\sqrt{1-\beta^2}$ is the relativistic gamma factor.

The acceptance of a machine is given by the radius of the vacuum chamber d and the maximum value of the beta function $\beta_{\max}$ [3]:

$$A = \frac{d^2}{\beta_{\max}} \tag{2.22}$$

To minimise beam losses, the ratio A/ϵ is about 2-10 for proton and heavy-ion machines, whereas it can be larger for electron machines. For example, the SLS at PSI has a horizontal emittance of $5\,\mu$m mrad and a horizontal acceptance of 80 mm mrad [4], which yield A/ϵ=16000.

2.6 Adiabatic Damping

When the particle beam is accelerated in longitudinal direction, the longitudinal momentum will change, whereas the momentum in transversal direction will remain constant [2]. Therefore, the angle x' and thus the transversal emittance will decrease with increasing momentum in longitudinal direction, if the energy loss due to synchrotron radiation is sufficiently small. The normalised emittance is conserved when the momentum is changed. This effect of decreasing the emittance due to the longitudinal acceleration of the beam is called adiabatic damping.

As the normalised emittance is conserved, it can be written as:

$$\epsilon_n = \epsilon_0\beta_0\gamma_0 = \epsilon\beta\gamma \tag{2.23}$$

Here, ϵ_0 is the transversal emittance of the beam before the acceleration and ϵ is the transversal emittance of the accelerated beam. β_0 and γ_0 are the relativistic beta factor and gamma factor before the acceleration and β and γ are the ones after the acceleration. Solving equation 2.23 for ϵ yields

$$\epsilon = \epsilon_0 \frac{\beta_0\gamma_0}{\beta\gamma}. \tag{2.24}$$

As $\beta\gamma$ is proportional to the magnetic rigidity $B\rho$ (cf. equation 2.7), the emittance change of the particle beam with an emittance ϵ_0 and a magnetic rigidity $(B\rho)_0$ is inversely proportional to the magnetic rigidity $B\rho$:

$$\epsilon = \epsilon_0 \frac{(B\rho)_0}{B\rho}. \tag{2.25}$$

2.7 Beam Size

The beam size contains a part, which results from the transversal betatron oscillation (cf. equation 2.19), and a part, which results from dispersion respectively the beam's momentum spread [3, 5]:

$$x_{\text{beam}}(s) = x_\beta(s) + x_D(s) = \sqrt{\epsilon\beta(s) + \left(D(s)\frac{\Delta p}{p}\right)^2} \tag{2.26}$$

Here, $x_{\text{beam}}(s)$ is the RMS beam size, ϵ is the RMS emittance, $D(s)$ is the dispersion function, and $\Delta p/p$ is the beam's momentum spread. For large values of the emittance and small values of the momentum spread, which often occur in hadron accelerators, the first term dominates over the dispersive term. Typically for electron accelerators, the emittance is quite small and the dispersion term is nit negligible. However, in the following calculations the beam size is assumed to be only a function of the emittance. The neglected dispersion term is compensated by an accordingly higher emittance in the calculation of the necessary aperture sizes.

2.8 Power Loss and Energy Consumption

The active power P can be calculated from the voltage U and the current I [6]:

$$P = U \cdot I \tag{2.27}$$

With Ohm's law $U = R \cdot I$ [6], the power loss P_{loss} can be determined as:

$$P_{\text{loss}} = R \cdot I^2 \tag{2.28}$$

The average power loss is the integral of the actual power loss over time normalised by the cycle time T:

$$P_{\text{avg}} = \frac{1}{T}\int_0^T P_{\text{loss}}(t)dt = \frac{1}{T}\int_0^T RI^2(t)dt \tag{2.29}$$

Assuming a linear rise and fall of the current within the duration of ramping T_{ramp} as well as a constant flattop current I within the duration of the flattop T_{flat}, the average power loss is

$$P_{\text{avg}} = \frac{1}{T}RI^2\left(\frac{2}{3}T_{\text{ramp}} + T_{\text{flat}}\right). \tag{2.30}$$

The energy consumption is the product of the average power loss P_{avg} and the assumed time interval t [6]

$$E = P_{\text{avg}} \cdot t. \tag{2.31}$$

The energy consumption per year consists of the energy consumption during the operation as well as the energy consumption during shutdown. During operation, a continuous operation of the facility with a constant average power loss is assumed. During shutdown, only the average power loss of the cooling system, which is running the entire year in the following model, is assumed. Hence, the energy consumption per year is

$$E = E_{\text{operation}} + E_{\text{shutdown}}. \tag{2.32}$$

3 Properties of FODO Beam-Transport Lines

The beam transport between two accelerators, for example, a booster synchrotron and a main synchrotron or a storage ring, or the beam transport from an accelerator to a target, is often realised as a FODO structure. This structure combines a strong focussing and gradients, which are lower than in other focussing systems. Hence, this focussing system is inherently energy efficient. This FODO structure is a periodic structure consisting of alternating focussing (F) and defocussing (D) quadrupole magnets, and a drift space (O) between them (see figure 3.1). The drift space between the focussing and defocussing quadrupole is the same one as between the defocussing and focussing ones. The technical designs of the quadrupoles are identical, as well. For bending the beam, dipole magnets are inserted in the drift spaces. In the following calculations, it is assumed that the weak focussing as well as the edge focussing of the dipole magnets are negligible small compared to the effect of the gradient of the quadrupole magnets. Also, a straight beam-transfer line without any dipoles is possible. Furthermore, a transfer line, which is long enough to comply with the periodic boundary conditions of the beam parameters, is assumed. The matching sections at the start and the end of the beamline are neglected. In the following calculations the start point and end point of each FODO cell is in the center of

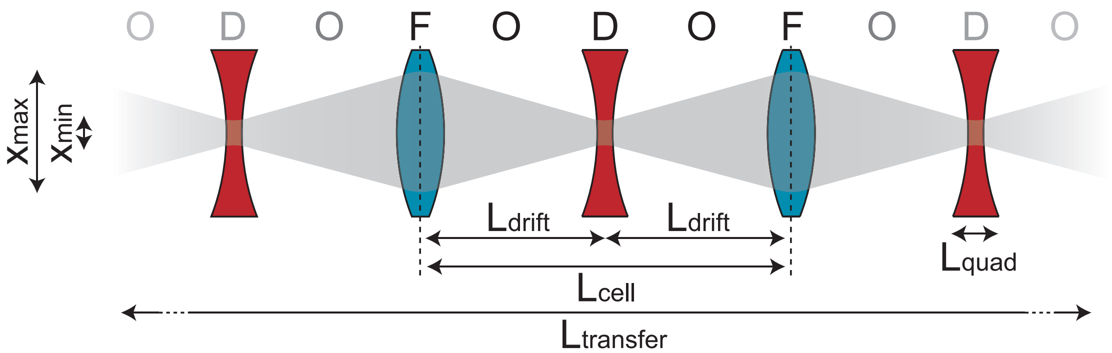

Figure 3.1.: Schematic structure of a FODO beam-transport line consisting of a periodic sequence of focussing quadrupoles (F, blue) and defocussing quadrupoles (D, red) and drift spaces (O) between them. The horizontal plane is shown. In the vertical plane focussing and defocussing quadrupoles are inverted. All quadrupoles have an equal length of L_{quad} and an equal integral focussing strength but with alternating sign. The drift spaces have a length of L_{drift}. The thin-lens approximation yields a cell length of $L_{\text{cell}} = 2L_{\text{drift}}$. The total length of the transfer line L_{transfer} is an integer multiple of L_{cell}. The maximum of the beam envelope $x_{\max}$ is in the center of the focussing quadrupoles, the minimum of the beam envelope $x_{\min}$ is in the center of the defocussing quadrupoles.

the focussing quadrupoles. The properties of such a FODO transfer line can be derived from literature [2, 3, 7].

In the thin-lens approximation, the transport matrix of a FODO cell consisting of quadrupoles with focal lengths f_1 and $-f_2$ and drift spaces of the length d is determined by multiplication of the transport matrices of all elements in the cell [7]:

$$M = M_{\frac{1}{2}\mathrm{QF}} M_{\mathrm{D}} M_{\mathrm{QD}} M_{\mathrm{D}} M_{\frac{1}{2}\mathrm{QF}} \tag{3.1}$$

$$= \begin{pmatrix} 1 & 0 \\ -\frac{1}{2f_1} & 1 \end{pmatrix} \begin{pmatrix} 1 & d \\ 0 & 1 \end{pmatrix} \begin{pmatrix} 1 & 0 \\ \frac{1}{f_2} & 1 \end{pmatrix} \begin{pmatrix} 1 & d \\ 0 & 1 \end{pmatrix} \begin{pmatrix} 1 & 0 \\ -\frac{1}{2f_1} & 1 \end{pmatrix} \tag{3.2}$$

$$= \begin{pmatrix} 1 + \frac{d}{f_2} - \frac{d}{f_1} - \frac{d^2}{2f_1 f_2} & 2d\left(1 + \frac{d}{2f_2}\right) \\ \frac{1}{f_2} - \frac{1}{f_1} - \frac{d}{f_1 f_2} + \frac{d}{2{f_1}^2} + \frac{d^2}{4{f_1}^2 f_2} & 1 + \frac{d}{f_2} - \frac{d}{f_1} - \frac{d^2}{2f_1 f_2} \end{pmatrix} \tag{3.3}$$

In the case of identical quadrupoles with an alternating gradient, equation 3.3 can be simplified to [7]

$$M = \begin{pmatrix} 1 - \frac{d^2}{2f^2} & 2d\left(1 + \frac{d}{2f}\right) \\ -\frac{d}{2f^2}\left(1 - \frac{d}{2f}\right) & 1 - \frac{d^2}{2f^2} \end{pmatrix}. \tag{3.4}$$

with the focal length f for both focussing and defocussing quadrupoles. The phase advance per cell as well as the maximum of the beta function follow from the standard form of the Twiss matrix [7]

$$M_{\mathrm{Twiss}} = \begin{pmatrix} \cos\Phi + \alpha \sin\Phi & \beta \sin\Phi \\ -\gamma \sin\Phi & \cos\Phi - \alpha \sin\Phi \end{pmatrix}. \tag{3.5}$$

The phase advance is given by [7]:

$$\cos\Phi = \frac{1}{2}\operatorname{Tr} M = 1 - \frac{d^2}{2f^2} \tag{3.6}$$

$$\sin\frac{\Phi}{2} = \frac{d}{2f} \tag{3.7}$$

The condition $|\cos\Phi| \leq 1$ causes an upper limit of the drift spaces between the quadrupoles respectively a lower limit of the focal length [2]:

$$d_{\mathrm{max}} = 2f \tag{3.8}$$

$$f_{\mathrm{min}} = \frac{d}{2} \tag{3.9}$$

Comparing the transport matrix of the cell in equation 3.4 with the standard form of the Twiss matrix in equation 3.5 and substitution into equation 3.6 yield the maximum value of the beta function in the center of the focussing quadrupoles [7]:

$$\beta_{\max} = \frac{2d\left(1+\frac{d}{2f}\right)}{\sin\Phi} \tag{3.10}$$

$$= \frac{2d\left(1+\frac{d}{2f}\right)}{\sqrt{1-\cos^2\Phi}} \tag{3.11}$$

$$= \frac{2d\left(1+\frac{d}{2f}\right)}{\sqrt{\frac{d^2}{f^2}-\frac{d^4}{4f^4}}} \tag{3.12}$$

$$= \frac{2f\left(1+\frac{d}{2f}\right)}{\sqrt{1-\frac{d^2}{4f^2}}} \tag{3.13}$$

Due to equation 3.13, the maximum value of the beta function is proportional to the focal length f for sufficiently large values of the focal length. Furthermore, the focal length is a function of the magnetic rigidity $B\rho$ and the integral gradient $B'L$ [2]:

$$f = \frac{1}{kL} = \frac{B\rho}{B'L} \tag{3.14}$$

Hence, the maximum value of the beta function is proportional to the magnetic rigidity for sufficiently large values of the magnetic rigidity.

From equation 3.13 follows that the maximum value of the beta function is a function of the drift length d and the focal length f. The behaviour of the maximum value of the beta function depending on these two parameters is illustrated in figure 3.2. For a given maximum value of the beta function, a family of possible combinations of d and f exist. For an exemplary value of the beta function of 50 m, these combinations are indicated as a thick line in figure 3.2. To optimise the parameters d and f, the following algorithm is used: The maximum value of the beta function $\beta_{\max}$ has a minimum for a fixed value of the drift length d. The corresponding focal length $f_0(d)$ for this minimum can be calculated from the beta function's derivative $d\beta_{\max}(d,f)/df = 0$. Starting from a minimum drift length d_0 and iteratively increasing it, the beta function's maximum value is calculated for every combination of d and $f_0(d)$. For each combination, the value of $\beta_{\max}(d_0, f_0(d_0))$ is calculated. The algorithm stops if the resulting value of the beta function is larger than the limit, which is defined by the acceptance respectively the beam's emittance as well as the aperture (cf. equation 2.22). The corresponding values of the beta function's maximum values following from the algorithm are indicated as red points in figure 3.2. The algorithm's return value is the combination of d and f, which is the closest point to the line representing the family of solutions. Moreover, the found combination of d and f is the solution with the larges possible drift length. This yields the smallest number of magnets required for the beamline. The integral gradient used for the beamline design is

$$B'L_{\text{opt}} = \frac{B\rho}{f_{\text{opt}}}. \tag{3.15}$$

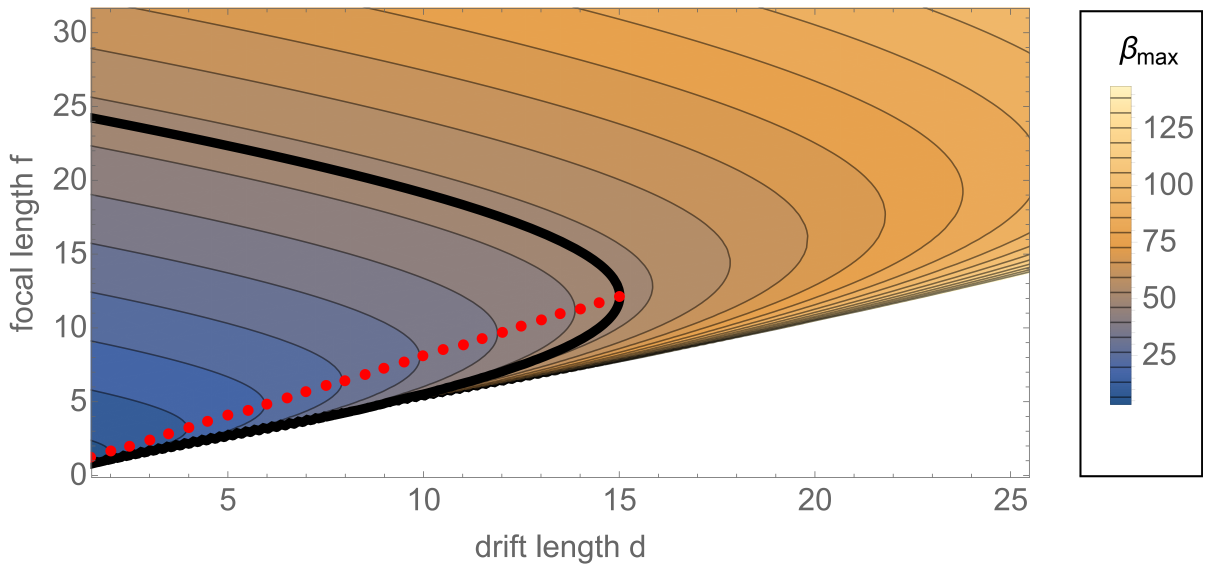

Figure 3.2.: Maximum value of the beta function as a function of the drift length d and the focal length f. The red points indicate the approximation algorithm for finding an optimised solution for an exemplary value of the maximum beta function of 50 m, which is represented by the thick line.

In this equation, $B\rho$ is the magnetic rigidity and f_{opt} is the focal length following from the optimisation algorithm.

Assuming now an emittance change according to adiabatic damping (which is inversely proportional to the magnetic rigidity, see equation 2.25) and the behaviour of the maximum value of the beta function following from equation 3.13 and equation 3.14, the beam envelope x_{max} converges to a constant value for sufficiently large values of the magnetic rigidity:

$$x_{\text{max}} = \sqrt{\epsilon \beta_{\text{max}}} \xrightarrow{\text{large B}\rho} \text{constant} \tag{3.16}$$

As a variation in the focal length due to different magnetic rigidities also results in a change in the phase advance, matching sections are necessary. But as mentioned before, these matching sections are neglected in the following calculations and only the beamline's FODO part is investigated. The beam envelope x_{max} as a function of the magnetic rigidity considering adiabatic damping is shown in figure 3.3 to illustrate the properties of an exemplary beamline. The shown behaviour is important for the design process because of a minimum magnetic rigidity, for which the beam envelope fits into the magnet aperture. If the beam is accelerated further, the beam envelope decreases and the beam always fits into the magnet aperture for magnetic rigidities larger than the minimum necessary magnetic rigidity although the gradient is fixed. This behaviour can be used to realise transfer lines, which contain magnets with a fixed gradient, for example, permanent magnetic quadrupoles, even for applications with varying magnetic rigidities. Thus, for the design of a straight beamline one only has to determine the smallest magnetic rigidity, and the beam envelope will fit into the aperture of the quadrupole magnets for larger magnetic rigidities, as well. This behaviour is, of course, applicable only for straight beamlines without dipole magnets. Using permanent magnetic dipoles with fixed dipole fields, beams with different magnetic rigidities will lead to different deflexion angles. Hence, hybrid

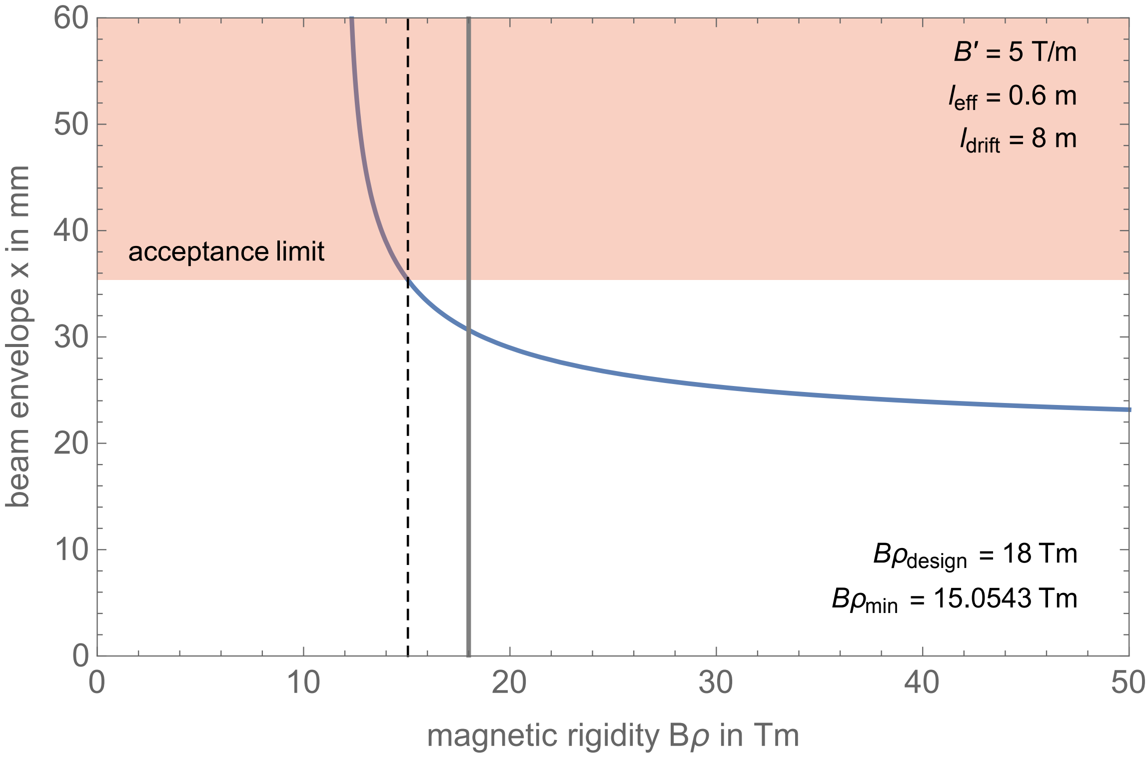

Figure 3.3.: Beam envelope $x_{\max}$ as a function of the magnetic rigidity considering adiabatic damping for an ion beam with a design emittance of 35 mm mrad at a design magnetic rigidity of 18 Tm (continuous line). The gradient B', the effective magnet length l_{eff}, and the drift length l_{drift} are fixed. The red area marks the prohibited aperture range resulting from the acceptance limit. The dashed line symbolises the minimum magnetic rigidity so that the beam envelope is still in the permitted aperture range. The beam envelope decreases with increasing magnetic rigidity and converges to a constant value for large values of the magnetic rigidity.

beamlines consisting of PM quadrupoles and NC dipoles will also be considered in the following calculations.

In the following calculations, the beams' range of magnetic rigidity, which shall be transported by the beamline, is used to design the transport system: The lowest value of the magnetic rigidity defines the necessary parameters of the focussing system and the largest value of the magnetic rigidity defines the necessary parameters of the dipole magnets to ensure the successful transport in bended transport lines.

4 Modelling of Different Magnet Types

4.1 Properties of Different Magnet Types and Magnet Models

In this section, the modelled magnet types' essential properties are summarised. Generally, all losses are considered, which are caused by magnets, power converters, and supply cables as well as cooling (water cooling or liquid helium (LHe) cooling) of these components. Furthermore, a standard design is chosen for the magnets to cover a wide field of application. However, not all aspects can be modelled in detail (e.g., special requirements on radiation hardness, special designs for more compact magnets, or other reasons, why one cannot use the standard magnets described in this chapter). The magnet cross-sections shown in this section illustrate the rough designs of the magnets used in the following calculations but the dimensions of the magnets (horizontal/vertical aperture, magnet length etc.) can be scaled to fit the magnet properties to the necessary values for each individual beamline.

4.1.1 Normal Conducting Magnets (NC)

Normal conducting (NC) magnets are one of the most common magnets in particle accelerators. Due to the long history of these electromagnets, the engineering design is well-known. Hence, no expensive R&D is necessary for this magnet type.

Engineering Design and Physical Range of Operation

There is a variety of different magnet designs for NC magnets. In this thesis, a H-magnet geometry is chosen for the NC dipoles. The rough design of this magnet type is shown in figure 4.1(a). The magnetic field is excited by rectangular race-track coils. The necessary current I and the winding number n can be determined by using the following equation [2]:

$$B \approx \mu_0 \frac{nI}{g} \quad \Rightarrow \quad nI \approx \frac{Bg}{\mu_0} \tag{4.1}$$

The dipole field is formed by the geometry of the iron yoke, which is made of lamellas stamped out of electrical steel. To improve the field quality, a Rogowski profile can be used for the edges of the pole shoes.

For the NC quadrupoles, a classical design was chosen, which is shown in figure 4.1(b). The quadrupole field is formed by the hyperbolic pole profile. The necessary current I and the winding number n can be determined by using [2]:

$$B' \approx 2\mu_0 \frac{nI}{a^2} \quad \Rightarrow \quad nI \approx \frac{B'a^2}{2\mu_0} \tag{4.2}$$

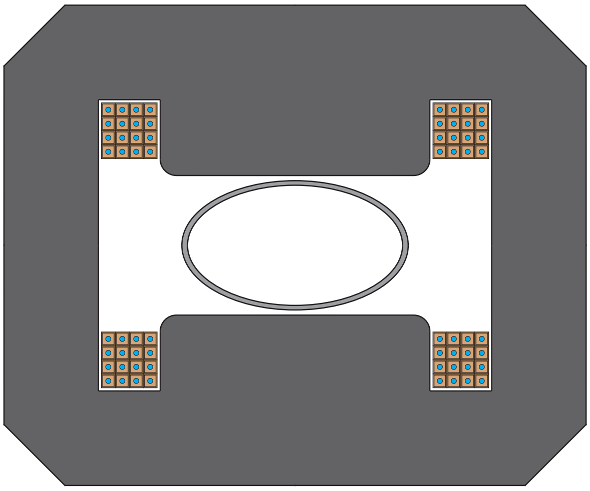

(a) Cross-section of a NC dipole.

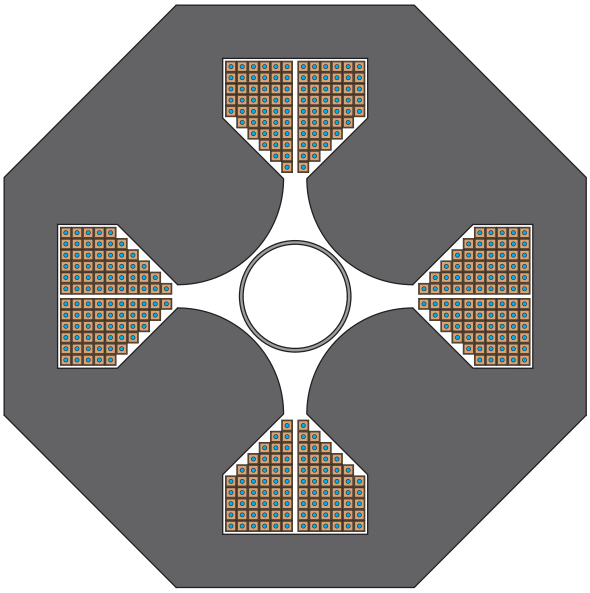

(b) Cross-section of a NC quadrupole.

Figure 4.1.: Cross-sections of the modelled NC magnets . The coil is made of copper cables with a cooling channel. The iron yoke forms the magnetic dipole field.

The coil of the quadrupole has a trapezoidal cross-section to minimise saturation effects in the iron yoke. Like the dipole yokes, the yokes of the modelled quadrupole magnets are made of laminated electrical steel.

In the following calculations, a field quality of both the dipoles and quadrupoles of $\Delta B/B = 0.005$ is assumed. Therefore, the magnet's pole widths are optimised to ensure this value of the field quality within the good-field region $r_{\text{good-field}}$ (usable aperture). The necessary dipole's pole width w can be taken from literature [8]:

$$w = 2 \cdot \left(r_{\text{good-field}} + \frac{g}{2} \cdot x \right) \tag{4.3}$$

For the quadrupole's horizontal and vertical cut-off position x_c of the hyperbolic pole shoes, the following equation is used [8]:

$$x_c = r \cdot \sqrt{\frac{1}{2} \left(\sqrt{\left(\left(\frac{r_{\text{good-field}}}{r} \right)^2 + x \right)^2 + 1} + \left(\frac{r_{\text{good-field}}}{r} \right)^2 + x \right)} \tag{4.4}$$

In these equations, g is the dipole's gap and r is the quadrupole's pole-tip radius. Furthermore, x is defined as $x = -0.14 \cdot \log \frac{\Delta B}{B} - 0.25$.

Due to saturation effects in the iron yoke, the magnetic field strength of NC magnets is limited to a value of $B \leq 2$ T [3]. In practise, lower field strengths are used. Hence, the dipole field is limited to 1.6 T [9] in the following calculations. The pole-tip fields of the quadrupoles are limited to 0.8 T [9]. Furthermore, the yoke width is scaled to limit the magnetic flux in the yoke to $B_{\text{iron}} \leq 1.5$ T [9].

Usually, the coil cable is made out of copper due to the good properties of copper with respect to electrical and thermal conductivity. The cable has a quadratic cross-section, an insulation layer, and a cooling channel for water cooling in the center of the cable. The arising coil is then insulated with a further insulation layer. The maximum current density in the coil cable is set to $5\,A/mm^2$ to reduce resistive losses in the coil [9]. The cable cross-section is scaled to keep the pressure drop of the cooling water in the cable below 10 bar [10]. The coil's resistance follows from the length of the conductor, which depends on the number of windings and the geometry of the magnet. The power loss of the NC magnets can be determined by using equation 2.28 with the resulting resistance and the current following from equation 4.1 respectively 4.2.

Since the ampere turns nI are proportional to the gap g respectively to the square of the pole-tip radius a, the power loss (see equation 2.27) of dipoles is proportional to g^2 and the power loss of quadrupole magnets is proportional to a^4 if the number of turns is kept constant. Hence, the aperture of this magnet type should be kept as small as possible for each individual application to allow magnet designs with low energy consumption.

Operation Mode

NC magnets can be used for DC operation and AC operation (ramped operation or pulsed operation). On the one hand, AC operation has the advantage of a lower mean power loss compared to DC operation. On the other hand, AC operation is also resulting in additional active power peaks, which requires more complex power converters.

The NC magnets modelled in this thesis are operated in AC mode if possible. This means that the magnets are operated at their nominal field for the duration of the beam transfer (for fast-extraction transfers only a few μs). These magnets are operated in DC mode, if it is not possible to ramp down the magnet between two successive transfers. The ramp time – which is the time duration from zero to the nominal value of the magnetic field – is limited due to the magnets' inductance. The inductance depends on the pole geometry, the magnet length, the aperture, and the number of windings [11]. As the ramp time is proportional to the inductance for a fixed ramping voltage, magnets with a higher inductance have higher ramp times. Since the ramp time limits the range of repetition rates, in which an AC operation is possible, this has an effect on the field of application. Common values of the ramp time resulting from the inductance and resistance of existing magnets are in the range of 0.1-1.0 s [9]. In the following calculations, a ramp time of 0.5 s is assumed for the NC magnets.

Cooling

In general, the coils of NC magnets are water-cooled. The necessary diameter of the cooling channel in the coil cable can be determined with the following equation, which can be found in the literature [10]:

$$d = 5,59 \cdot 10^{-3} \left(\frac{P}{\Delta T K_W} \right)^{0,368} \left(\frac{l}{\Delta p} \right)^{0,21} \tag{4.5}$$

In this equation, P is the power loss of the coil, l is the effective length of the coil cable, ΔT is the temperature rise of the cooling water, K_W is the number of cooling circuits, and Δp is the pressure drop in the coil. The maximum permitted pressure drop is set to 10 bar and the maximum permitted temperature rise ΔT is set to 20 °C. For the standard magnets modelled in this thesis, the number of cooling circuits K_W is limited to 4 circuits. Hence, the necessary diameter of the cooling channel depends only on the effective length of the coil cable and the power loss.

To choose the coil cable, a set of cables with common dimensions is taken [12]. From this set of possible cables, for every cable the effective length, the winding number as well as the resulting power loss are determined. Then, only the cables with a cooling-channel diameter larger than the necessary diameter are selected. From these candidates, the one with the lowest power loss will be chosen to minimise the energy consumption of the magnet. This might lead to a coil design that is not the most compact design. Thus, this type of magnet will cost more than a magnet with a more compact coil. For long-term operation, the savings in operation costs will prevail over the investment costs in most cases.

4.1.2 Superferric Magnets (SF)

Superferric (SF) magnets are iron dominated magnets using a yoke design similar to the one of NC magnets but using a superconducting coil instead of a normal conducting coil. This magnet type is also limited due to saturation effects in the yoke. As this magnet type uses superconducting coils producing no resistive losses within the magnet, the economically achievable field strengths are higher than for the NC magnets. A further benefit of cold magnets is the effect of cryo pumping. Hence, a high vacuum quality is possible with this magnet type. The SF magnets discussed in this section base on the design of the SIS100 magnets for FAIR [13, TDR from 2008]. As SF magnets require a complex engineering design (including a cryostat and a cryogenic infrastructure) and as they are rare in the existing accelerator facilities compared to NC magnets, R&D and prototyping are necessary. These points are not included in the following calculations.

Engineering Design and Physical Range of Operation

SF magnets use a yoke design, which is in general similar to NC magnets. Nevertheless, these magnets have a coil made of superconducting cables instead of copper cables. The used superconductor is NbTi. The modelled dipole is a window-frame magnet, whose cross-section is illustrated in figure 4.2(a). It consists of an iron yoke, which is forming the dipole field, and a superconducting coil. The coil design depends on the desired operation; for AC operation a single layer or double layer coil is used in the model to minimise the inductance (high current, low number of windings), for DC operation it is possible to use a lower current but with more layers (low current, high number of windings) to minimise the power loss of the normal conducting parts of the magnet system like supply cables and power converters. The coil cables' cross-sections are identical to the SIS100 dipole cable [13] respectively to the SIS100 quadrupole cable [13] but the cross-sectional area can be scaled to fit the cable also to smaller magnets. In the center of the coil cable is a cooling channel for liquid helium (LHe), which is used for a direct cooling of the coil cable. The LHe-return lines are used to cool the iron yoke.

The dipole's magnetic field strength respectively the ampere turns can be calculated by using the same equations like for the NC magnets (cf. equation 4.1). For the quadrupole's gradient respectively the ampere turns, the same equations like for the NC magnets (cf. equation 4.2) can be applied, as well.

As the superconducting cable of the SF magnets allows currents up to several kA, significantly less windings are necessary compared to the NC magnets for the same magnetic field strength. Hence, the coils and also the yokes are smaller compared to the NC magnets. This is a benefit; especially for large apertures, for which the coils of NC magnets become much larger than coils of SF magnets. On the other hand, magnets with lower currents but a higher number of windings can be used to create energy efficient magnets for DC operation. In this model, a maximum current for DC operation of 3.5 kA and a maximum current for AC operation of 12.7 kA are assumed [13].

The SF quadrupole design is similar to the NC quadrupole design but with coils made of the SIS100 quadrupole cable. The magnet cross-section is illustrated in figure 4.2(b). The cable's cross-sectional area can also be scaled and – like for the SF dipole – the number of windings can be fitted to the desired operation (low current and high number of windings for DC operation or high current and low number of windings for AC operation). The assumed maximum current

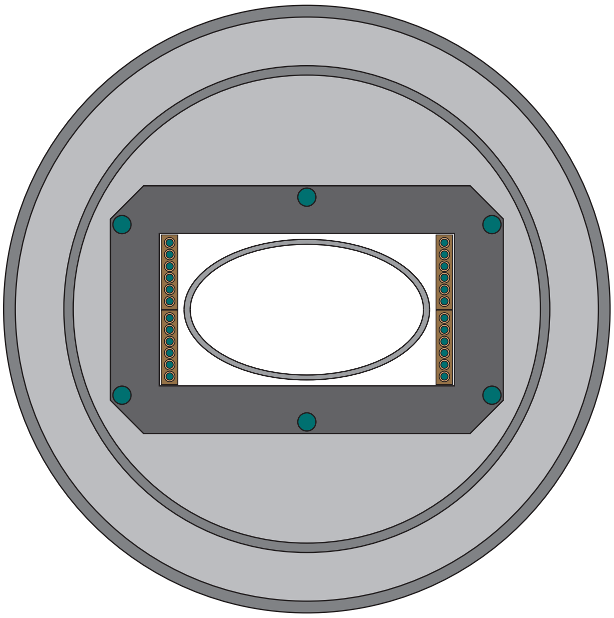

(a) Cross-section of a SF dipole.

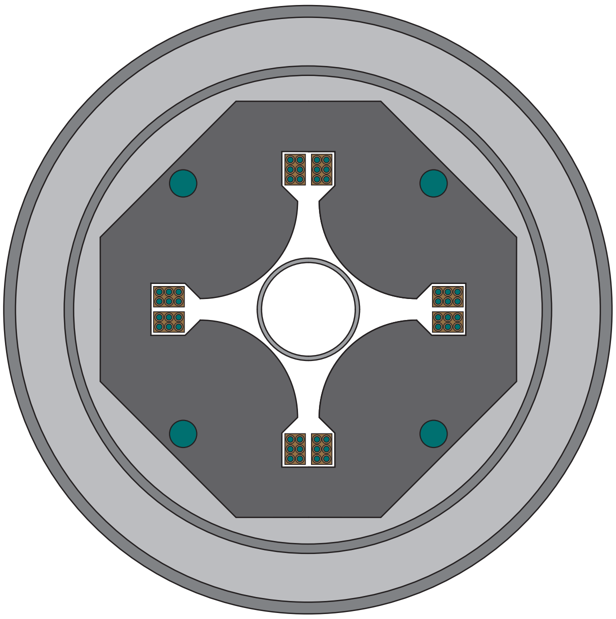

(b) Cross-section of a SF quadrupole.

Figure 4.2.: Cross-sections of the modelled SF magnets. The coils are made out of a superconducting cable with a cooling channel for liquid helium. The iron yoke forms the magnetic dipole field respectively the magnetic quadrupole field. The helium-return line is used to cool the iron yoke. An inner 4 K part and an outer 80 K part exist.

for DC operation is 2.5 kA and the maximum current for AC operation is 4.5 kA [13]. According to the number of windings, the coil cross-section is rectangular for up to 12 windings and trapezoidal for more windings.

The quadrupole field is formed by the hyperbolic pole shoes. The quadrupole's pole width is optimised to ensure a field quality of $\Delta B/B = 0.005$ within the good-field region (cf. section 4.1.1, NC magnets) by using the field quality as a function of the yoke geometry, which can be taken from literature [8].

As the coil's resistance is zero, the magnet itself produces no resistive losses. The only resistive losses assumed for this magnet type come from the resistive supply cables and the power converters. Due to the absence of resistive losses in the magnet, higher currents can be used to generate the magnetic field. Therefore, slightly higher field strengths are achievable compared to the NC magnets. Nevertheless, the field strength is limited due to saturation effects in the yoke. The SIS100 dipole magnets have a nominal field strength of 1.9 T, the SIS100 quadrupole magnets have a nominal pole-tip field of 1.35 T [13]. These values are also used for the modelled magnets in this thesis.

All magnets are placed in a continuous cryostat to avoid cold-warm transitions. The magnets' cryostat has an inner 4 K part and an outer 80 K part, which both are insulated by superinsulation [14]. The cold iron yoke is fixed in the cryostat by a suspension system. As the cross-sectional area of the suspension is proportional to the cold mass, the thermal current and thus also the static losses are proportional to the cold mass [14].

A further necessary feature of SF magnets is a system for quench detection and protection. Otherwise, significant damages can result when the magnet is quenching. The operation and investment costs of such a system are not included in the model.

Depending on the design of the SF magnet, it is possible to manufacture magnets with a cold yoke or a warm yoke. This has an effect on the energy consumption of the cooling system. The modelled magnets use cold yokes similar to the SIS100 magnets. The SF magnet designs with a warm iron yoke are not considered here.

Operation Mode

The duration for ramping the magnets from zero to the nominal value is assumed to be 1 s for AC operation. For DC operation, the duration for initial ramping or for changing to another level is set to 60 s to decrease the power converters' ramping voltage. Thus, only for repetition rates below 0.5 Hz an AC operation is possible. For repetition rates above 0.5 Hz a DC operation is assumed. An AC operation yields eddy currents in the yoke, which cause additional heat loads in the magnets' inner 4 K parts. Hence, a fast AC operation (high repetition rate up to 0.5 Hz) of a transfer channel should be avoided if possible and should be replaced by DC operation. However, slow AC operation (repetition rate $\ll$ 0.5 Hz) can be more efficient since the average power converter losses are larger in DC operation.

Cooling

Based on the SIS100 magnets' calculated heat loads, the cooling losses of the SF magnets are calculated by scaling the static losses with the magnets' cold mass. The dynamic losses are calculated by scaling the SIS100 magnets' dynamic losses linearly with the cold mass but also linearly with the repetition rate [13, 14]. These losses base on a reference repetition rate of 0.5 Hz [13, 14]. In addition, the main components of the cryogenic infrastructure are assumed in the cooling model, which will be discussed in section 4.4.2. This cryogenic infrastructure is assumed to be identical to the one for the SC magnets. Table 4.1 gives an overview on the static and dynamic losses of the SF dipole and quadrupole magnets, which are assumed in this model.

Dipole	**Losses 4 K**	**Losses 50-80 K**
Static losses	0.7 W_{4K}/m	2.6 W_{80K}/m
Dynamic losses (repetition rate 0.5 Hz)	4.1 W_{4K}/m	
Quadrupole	**Losses 4 K**	**Losses 50-80 K**
Static losses	1.2 W_{4K}/m	4.6 W_{80K}/m
Dynamic losses (repetition rate 0.5 Hz)	4.9 W_{4K}/m	
Connection Cryostat	**Losses 4 K**	**Losses 50-80 K**
Static losses	1.0 W_{4K}/m	5.0 W_{80K}/m

Table 4.1.: Overview on the static and dynamic losses of the modelled SF dipole magnets and quadrupole magnets.

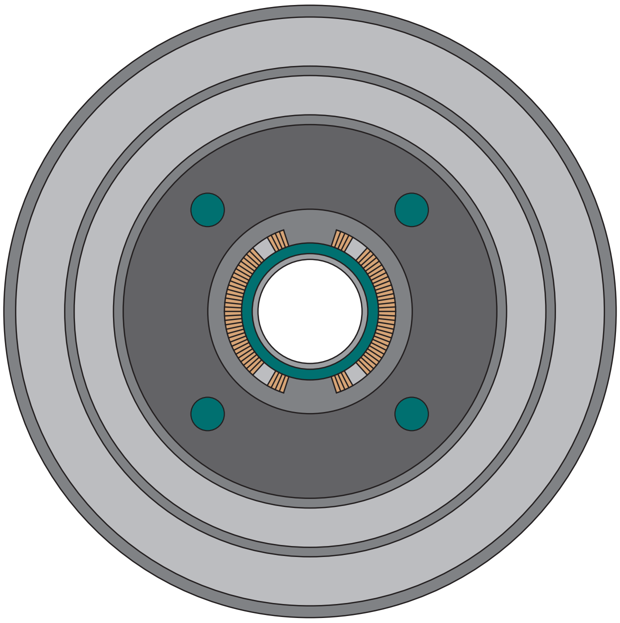

(a) Cross-section of a SC cos(Θ) dipole.

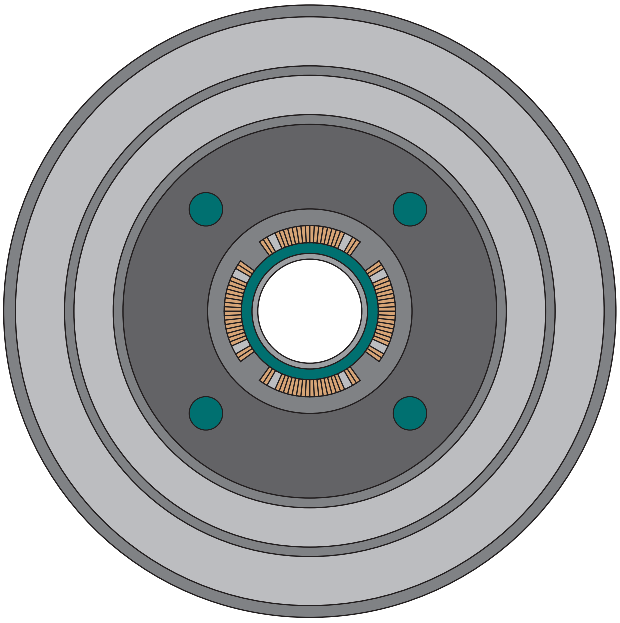

(b) Cross-section of a SC cos(2Θ) quadrupole.

Figure 4.3.: Cross-sections of the modelled SC magnets. The geometry of the conductor blocks approximates the cos(NΘ)-distributed current. The current distribution forms the magnetic dipole field respectively the magnetic quadrupole field. The coil is made out of superconducting Rutherford cable. An inner 4 K part and an outer 80 K part exist. The helium-return line is used to cool the cold mass.

4.1.3 Superconducting Cos(NΘ) Magnets (SC)

Superconducting (SC) cos(NΘ) magnets are not iron dominated like the NC or the SF magnets but they are current dominated. As no resistive losses occur in the magnet, high field strengths can be achieved. The designs of the modelled magnets in this section base on the magnet designs of the SIS300 magnets for FAIR and the RHIC magnets at BNL. Similar to the SF magnets, the engineering design is complex and R&D is generally necessary. This is not included in the model.

Engineering Design and Physical Range of Operation

The magnet cross-sections of the modelled SC dipoles and quadrupoles are shown in figures 4.3(a) and 4.3(b). These magnets have single-layer saddle coils consisting of Rutherford cables [15] out of NbTi. With this superconductor, magnetic field strengths up to 8 T are possible, for example, in the LHC at CERN. With superconductors like Nb_3Sn even higher fields are possible. The chosen geometry of the conductor blocks approximates the cos(NΘ)-distributed current ($I = I_0 \cos(N\Theta)$), which generates the dipole ($N = 1$) respectively the quadrupole field ($N = 2$). The total angular width of the dipole's coil sectors is 60° and the total angular width of the quadrupole's coil sectors is 30° [16]. To eliminate the first two higher harmonics of the magnetic field an optimised geometry of the conductor blocks, which uses wedges between the conductor blocks, is chosen [16]. In the following calculations, one-wedge coils are assumed.

They are also illustrated in figures 4.3(a) and 4.3(b). The coils are fixed by collars surrounded by a magnetic shielding.

The number of turns n is a function of the pole-tip radius in this model. To determine the number of turns, the total angular width is filled with Rutherford cables [15]. Hence, the number of turns can be approximated by the following equation:

$$n \approx 2 \cdot \frac{r\alpha}{w} \frac{2\pi}{360} \tag{4.6}$$

In this equation, r is the inner radius of the conductor shell (pole-tip radius), α is the total angular width in degree (i.e., 60° for dipole magnets and 30° for quadrupole magnets), and w is the width of the Rutherford cable's inner edge. The factor 2 follows from coil design that consists of two half shells. The necessary current I_0 needed to generate the magnetic field strength B is a function of the magnetic field strength B and the inner radius of the conductor shell r [17]:

$$B = \frac{\mu_0 I_0}{2r} \quad \Rightarrow \quad I_0 = \frac{2Br}{\mu_0} \tag{4.7}$$

For the quadrupole gradient it follows [17]:

$$B' = \frac{\mu_0 I_0}{2r^2} \quad \Rightarrow \quad I_0 = \frac{2Br^2}{\mu_0} \tag{4.8}$$

Hence, the necessary current is $I = I_0/n$. Typically, currents of a few kA are common. As the coil is superconducting, no resistive losses exist in the magnet itself but resistive losses exist in the normal conducting supply cables and the power converters.

The whole magnet is placed in a cryostat consisting of an inner 4 K part and an outer 80 K part. They are both insulated by superinsulation [14]. The coils are cooled with LHe. The LHe-return line is used for cooling of the magnetic shielding. Like the SF magnets, all SC magnets are placed in a continuous cryostat to avoid cold-warm transitions. Also, the magnet is fixed in the cryostat by a suspension system. It's cross-sectional area is proportional to the cold mass and therefore the static losses are also proportional to the cold mass [14].

In the following calculations, the maximum dipole field is set to 4.5 T [18] and the maximum equivalent pole-tip field of the quadrupoles is set to 2.7 T [18]. These are common values of existing facilities using this technology. Since the coil ends of the saddle coil reserve additional space, it is common to manufacture magnets being at least 1 m long. Hence, this value was chosen as the minimum magnet length of the SC magnets in the model.

Operation Mode

The duration for ramping the magnets from zero to the nominal value is assumed to be 5 s for AC operation (similar to the SIS300 magnets [18]). For DC operation, the duration for initial ramping or for changing to another level is set to 60 s to decrease the power converters' ramping voltage. Hence, only for repetition rates below 0.1 Hz an AC operation is possible; above this value DC operation is assumed. As additional dynamic losses occur in AC operation, DC operation can be more efficient than AC operation. However, DC operation can result in higher power converter losses compared to AC operation for low repetition rates ($\ll 0.1$ Hz).

Dipole	**Losses 4 K**	**Losses 50-80 K**
Static losses	0.9 W_{4K}/m	4.9 W_{80K}/m
Dynamic losses (repetition rate 0.1 Hz)	6.2 W_{4K}/m	
Quadrupole	**Losses 4 K**	**Losses 50-80 K**
Static losses	1.5 W_{4K}/m	9.8 W_{80K}/m
Dynamic losses (repetition rate 0.1 Hz)	6.3 W_{4K}/m	
Connection Cryostat	**Losses 4 K**	**Losses 50-80 K**
Static losses	0.6 W_{4K}/m	2.8 W_{80K}/m

Table 4.2.: Overview on the static and dynamic losses of the modelled SC dipole magnets and quadrupole magnets.

Cooling

Based on the SIS300 magnets' calculated heat loads [14], the cooling losses of the SC magnets are calculated by scaling the static losses with the magnets' cold mass. The values of the static losses base on the SIS300 magnets' cold mass. The dynamic losses scale linearly with the cold mass and also scale linearly with the repetition rate [14]. The reference value for the dynamic losses base on the dynamic losses of the SIS300 magnets at a repetition rate of 0.1 Hz. In addition, the main components of the cryogenic infrastructure are assumed in the cooling model. These are introduced in section 4.4.2. The cryogenic infrastructure is assumed to be identical to the one for the SF magnets. The assumed static losses and dynamic losses of the SC dipole and quadrupole magnets are summarised in table 4.2.

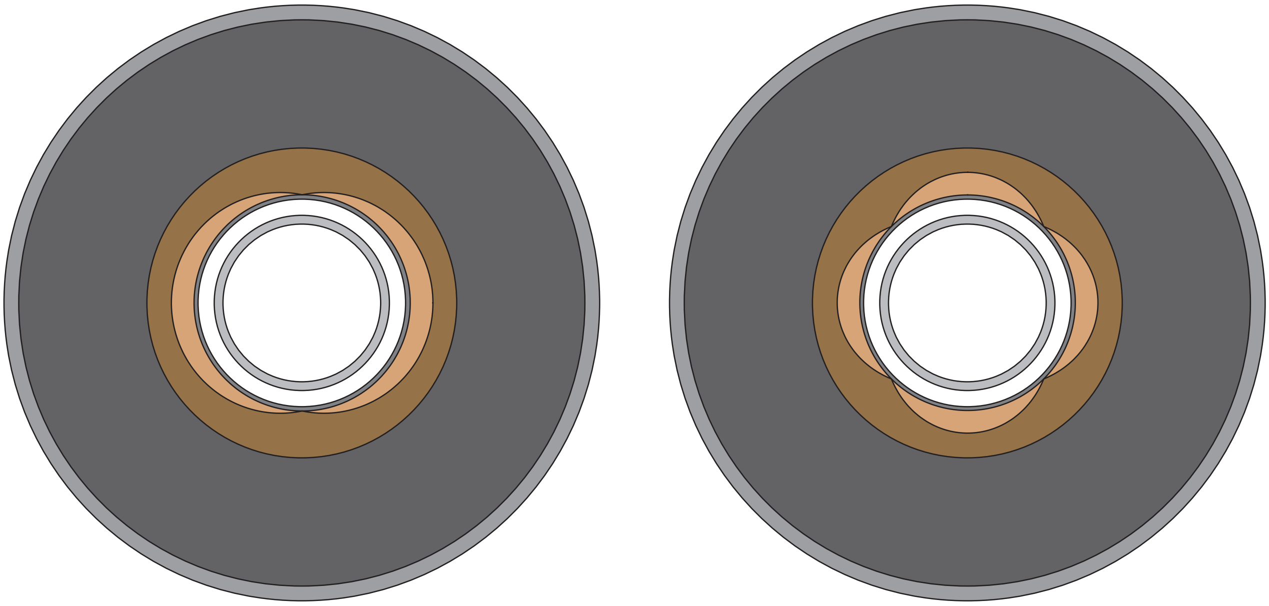

(a) Cross-section of a HCP dipole. (b) Cross-section of a HCP quadrupole.

Figure 4.4.: Cross-sections of the modelled HCP magnets. The current distribution of the cos(NΘ)-shaped array of copper strands forms the magnetic dipole field (N = 1) respectively the magnetic quadrupole field (N = 2). The coil has one winding and is fixed by PEEK collars, which are surrounded by a magnetic shielding.

4.1.4 High Current Pulsed Magnets (HCP)

GSI has built a prototype of an high current pulsed (HCP) quadrupole magnet [19]. This magnet type is a cos(NΘ) magnet (N = 1 for a dipole, N = 2 for a quadrupole), which uses a cos(NΘ)-shaped array of twisted copper wires instead of approximative conductor shells like the SC magnets do. As the magnet at GSI is a prototype, further R&D is necessary before this magnet type can be used in real transfer channels. There is no concept for the HCP dipole magnet yet. However, the general engineering design of the quadrupole prototype can be adopted for the dipole magnet.

Engineering Design and Physical Range of Operation

The geometry of the modelled magnets is similar to the one of the prototype at GSI. The magnet cross-sections are shown in figures 4.4(a) and 4.4(b). Those magnets' coils have one winding and the conductor is a cos(NΘ)-shaped array of twisted copper wires. In total, the coil consists of around 600 strands, which have a diameter of 0,355 mm. To reduce the skin effect and to generate a homogeneous current distribution over the full conductor cross-section, all strands are isolated and are operated in parallel. The copper wires are fixed in epoxy resin. The resulting coil is then fixed in a PEEK collar surrounded by a magnetic shielding of silicon iron. The collars and brackets have to withstand forces up to 200 kN.

To create the high-current pulse, the prototype's capacitor bank of 450 μF is charged to several kV by an external power supply. Then it is discharged through the coil and a damping resistor.

For the switch, a pseudospark switch is used. The necessary current I_0 needed to generate the magnetic field strength B is a function of the magnetic field strength B and the inner radius of the conductor r. The equations are identical to the ones of the SC magnets (cf. equation 4.7 for dipoles and equation 4.8 for quadrupoles).

The prototype uses a critically damped oscillating circuit, whose current pulse has a design duration of a few μs. The duration of the flattop within which the current fluctuates by less than the desired accuracy (in the model an accuracy of 0.1% is assumed) can be influenced by modifying the resistance of the damping resistor. The inductance of the dipole respectively the quadrupole coil can be determined by approximations, which can be found in literature [20].

As the energy, which is stored in the capacitor, is $E = \frac{1}{2}CU^2$ [6], the energy consumption per pulse can be determined as

$$E = \frac{1}{2}(1-\eta)CU^2. \tag{4.9}$$

Here, η is the efficiency of the oscillating circuit, C is the capacitance of the capacitor bank, and U is the voltage. For the prototype at GSI, a critically damped oscillating circuit is used, which yield $\eta = 0$. With an energy-recovery circuit, which technically can be realised in general, it is possible to recover up to 80% of the energy per pulse ($\eta = 0.8$). This is assumed in the following calculations [21].

As the prototype's design value of the equivalent pole-tip field is 4.5 T, this value is applied to the maximum values of the equivalent pole-tip field respectively the dipole field of the modelled magnets. The prototype's aperture radius of 40 mm respectively the equivalent pole-tip radius of 56 mm yield a maximum gradient of 80 T/m [19]. The field quality of the quadrupole prototype has not been completely measured yet and a dipole version of it does not exist. Nevertheless, the expected field quality should be in the range of SC cos(NΘ) magnets.

Operation Mode

Due to high currents up to 400 kA [19] and the absence of an active cooling of the coil, this magnet type has to be operated in pulsed mode. Otherwise, the thermal stress of the copper wires would result in a destruction of the coil. Hence, a DC operation is not possible with the design of the prototype. As the duration of the flattop is only a few μs, this magnet type is not compatible with machines using slow extraction. The maximum repetition rate depends on the thermal stress in continuous operation and the power converters' duration for recharging the capacitor for the next transfer. As the lifetime of the switch is limited to about 100 million cycles (depending on the switch type), this magnet type has limited suitability; especially for high repetition rates due to the necessary replacement of these components [21]. R&D would be useful to increase the lifetime at high repetition rates.

Cooling

The prototype's engineering design does not contain an active cooling [19]. Hence, repetition rates up to about 0.5 Hz result in an operation temperature of up to 55°C (ambient temperature of 25°C and temperature difference of up to 30 K) [21]. Repetition rates up to about 1.5 Hz are applicable if an increased operation temperature of about 80°C (temperature difference of up to 55 K) is possible [21]. For higher repetition rates, an active cooling is necessary. However, the HCP magnets are modelled as magnets without any cooling. The air cooling (convection cooling) of the power converters, which charge the capacitors, is also not included.

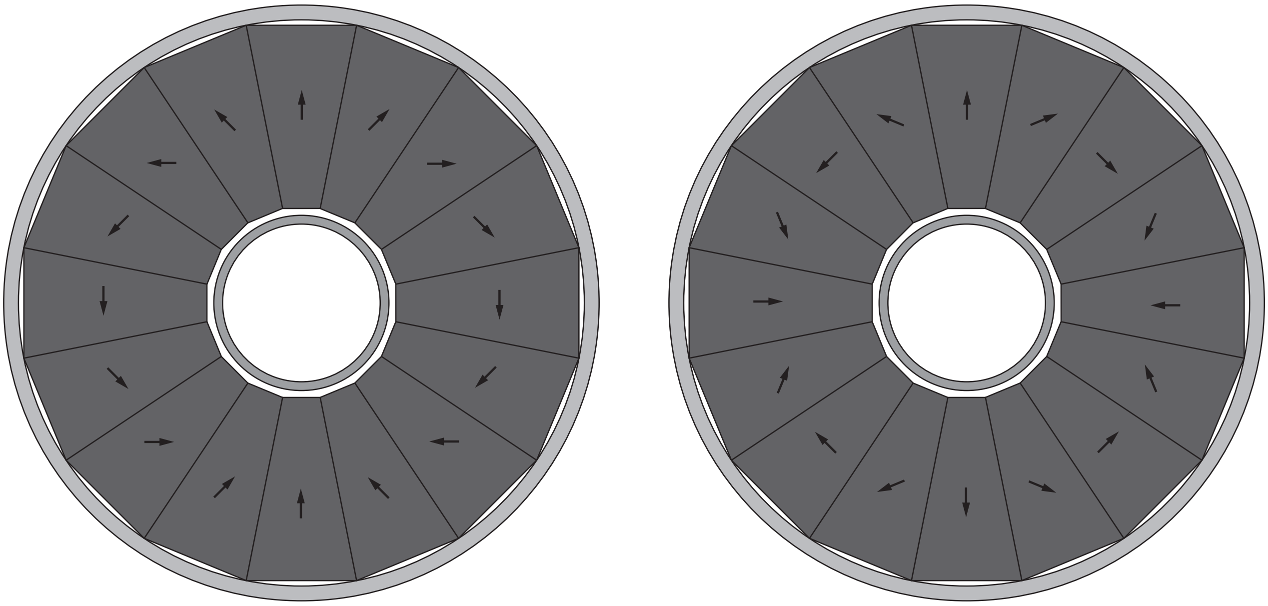

(a) Cross-section of a PM dipole. (b) Cross-section of a PM quadrupole.

Figure 4.5.: Cross-sections of the modelled PM magnets, which are Halbach arrays consisting of 16 Sm_2Co_{17} wedges. The direction of the magnetisation changes from one to the next by an angle of $\pi/8$ for the dipole and by an angle of $\pi/4$ for the quadrupole. The collar, which is made of non-magnetic material like aluminium, has to withstand large forces.

4.1.5 Permanent Magnets (PM)

As a last magnet type, permanent magnets (PM) will be introduced. These magnets' engineering designs differ a lot among the different fields of application. Here, only the Halbach array is discussed because this design is well-known and is not too complex. There are hybrid magnets, which consist of permanent magnetic material and electric coils, on the market as well. These magnets have the benefit of a tunable field strength. However, the modelled magnets in this thesis are limited to pure PM magnets without electrical coils.

Engineering Design and Physical Range of Operation

Depending on the field of application, a few permanent magnetic materials are possible to build accelerator magnets. The common materials each have both advantages and disadvantages. For example, $Nd_2Fe_{14}B$ and Sm_2Co_{17} have comparable remanence fields of 1.2 T respectively 1.1 T [22]. However, $Nd_2Fe_{14}B$ is less radiation hard compared to Sm_2Co_{17} but handling of this material is better due to the brittle consistence of Sm_2Co_{17} [22, 23]. In the model, Sm_2Co_{17} is used as PM material.

The PM magnets' cross-sections are shown in figure 4.5(a) and 4.5(b). These magnets consist of 16 wedges of PM material, which are arranged in a Halbach array [24]. This means that the magnetisation direction of the wedges changes from one to the next by an angle of $\pi/8$ for dipoles respectively $\pi/4$ for quadrupoles. This magnet design results in fixed-strength dipole and quadrupole magnets. The collar around the Halbach array holds the wedges together and has to withstand the repulsive forces. The collars are manufactured from non-magnetic material such as aluminium.

To calculate the dipole field strength respectively the pole-tip field, the equations in literature [22] and [24] can be used. The field strength depends on the inner radius r_1 and the outer radius r_2 of the PM wedges as well as on the number of wedges m and the remanence field strength B_r. The resulting dipole field strength is [24]

$$B_{\text{dipole}} = B_r \ln\left(\frac{r_2}{r_1}\right) \cos(\pi/m) \sin(\pi/m) \frac{m}{\pi}. \tag{4.10}$$

For the quadrupoles' pole-tip field it follows [24]

$$B_{\text{pole-tip}} = 2B_r \left(1 - \frac{r_1}{r_2}\right) \cos^2(\pi/m) \sin(2\pi/m) \frac{m}{2\pi}. \tag{4.11}$$

Depending on the amount of PM material, which follows from the magnet's geometry (inner radius r_1, outer radius r_2, number of wedges m), and the type of PM material, field strengths of up to 1.5-1.8 T are practicable for common aperture sizes. The field quality depends also on the magnet's geometry and gets better the more segments are used. With increasing magnet size, manufacturing issues can occur due to the high forces and the materials' brittle consistence. For the modelled magnets using Sm_2Co_{17}, a range of the field strength of about 1.2-1.6 T is assumed. The amount of the PM material increases with the aperture to keep the field strength constant. Hence, this magnet design is applicable especially for small apertures common, for example, in electron machines like synchrotron light sources.

As neither electrical components nor power converters are required for this magnet type, an active cooling does not exist in general, too. This magnet system does not require a control system for the magnets itself if these are fixed-strength magnets. However, to ensure the transport of a beam, whose magnetic rigidity deviates from the design value, the use of steerers is obligatory due to the absence of any tunability of the magnets. As mentioned before, this disadvantage could be compensated by hybrid magnets with a PM part for the nominal level and steering coils for deviations [25] but with a completely different magnet design than the PM magnets assumed in this thesis. Another option is the mechanical movement of the PM material, which also requires a special magnet design [26].

A further disadvantage is the process of demagnetisation due to radiation. Depending on the used PM material and the accelerated particles respectively the produced secondary particles, this effect can become an issue if the magnets are located in high radiation environments, e.g., near targets or collimators. The effect of demagnetisation can also be an issue in electron machines not only due to the electron beam itself but also due to synchrotron radiation. Hence, additional operation costs resulting from a remagnetisation of the PM material can occur. As the environments differ from beamline to beamline, these costs are not considered in the model.

Operation Mode

The magnetic field of the PM magnets is – except for demagnetisation effects – constant over time. Hence, this magnet type is applicable for the full spectrum of repetition rates as well as for fast beam transfers (a few μs) and slow beam transfers (several s or continuous beam).

4.2 FODO Lattice

The FODO lattice assumed for the beam-transport lines and described in chapter 3 consists of a periodical sequence of quadrupole magnets and dipole magnets. The drift space between the quadrupoles' centers is constant. In the modelled FODO structure, the dipole magnets are places in the center of each drift space. A disadvantage resulting from this assumption is the fact that especially for long transfer lines with a small total deflexion angle a lot of dipoles are used but with very low field strengths. This can be interesting for PM magnets but for the other magnet types this would be less practical. In practice, one would prefer less magnets with a higher field per magnet to reduce the system's investment costs.

To compare the dimensions of the different magnet types in the FODO lattice, figure 4.6 illustrates a scheme of exemplary FODO structures according to the different magnet types. All FODO cells have equal integral gradients and equal integral dipole field strengths. Due to the different pole-tip fields, the magnet lengths vary to keep the integral gradient respectively the integral dipole field constant. The minimum magnet lengths of the dipole and quadrupole magnets as well as the maximum field strengths of each magnet type are summarized in table 4.3. Furthermore, the free drift spaces between the magnets, which can be used, e.g., for beam diagnostics etc., vary among the different magnet lengths of the magnet types, as well. The additional space required for the cryostats of the SC magnets and the SF magnets is also indicated in figure 4.6 for these magnet types.

The integral dipole field respectively the integral gradient are calculated using the algorithm introduced in chapter 3. Then, the effective magnet length can be determined for each magnet type by using

$$L_{\mathrm{eff,dip}} = \frac{BL}{B_0} \tag{4.12}$$

respectively

$$L_{\mathrm{eff,quad}} = \frac{B'L}{B_0/a} \tag{4.13}$$

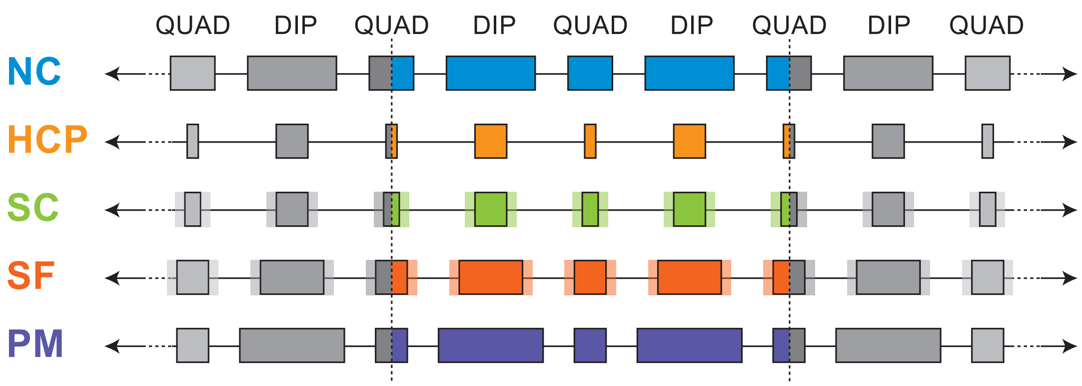

Figure 4.6.: Scheme of the FODO lattices according to the different magnet types. The magnet lengths vary due to the different pole-tip fields. The cryostats of the SC magnets and the SF magnets are indicated as transparent parts. The drift length between the quadrupoles' centers is equal for all magnet models.

	NC	SF	SC	HCP	PM
Minimum dipole length	0.3 m	0.5 m	1.0 m	0.5 m	0.3 m
Minimum quadrupole length	0.3 m	0.5 m	1.0 m	0.5 m	0.3 m
Maximum dipole field	1.60 T	1.90 T	4.50 T	4.50 T	1.22-1.52 T
Maximum quadrupole pole-tip field	0.80 T	1.35 T	2.70 T	4.50 T	1.40-1.56 T

Table 4.3.: Assumptions on the minimum magnet lengths and maximum field strengths for the different magnet types. The maximum field strengths of the PM magnets vary due to the dependency of the field strength on the aperture size and the used amount of permanent magnetic material.

and substituting B_0 with the specific value of the maximum dipole field respectively the maximum quadrupole pole-tip field given in table 4.3. The real magnet lengths can be determined by using equations 2.14 and 2.15. For the FODO lattice, the effective magnet length, which follows from the edge fields caused by the yoke geometry (aperture size), is used. Edge fields caused by the coil ends – especially the coil ends of the SC magnets' saddle coils – are not assumed in the model. If the necessary magnet length is smaller than the minimum magnet length given in table 4.3, e.g., due to very low field strengths, the minimum magnet length is used and the dipole field respectively the gradient are reduced to match with the requirements of the FODO lattice. Otherwise, i.e. if the necessary magnet length is larger than the minimum magnet length, the maximum value of the dipole field strength respectively the gradient are used and the magnet length is scaled to match with the necessary parameters of the FODO lattice.

When the magnetic rigidity increases, the integral gradients and integral dipole fields will also increase. This dependency is implemented in the model as the gradient respectively the dipole field are increased until a limit is reached. If the desired value for the integral field strength is higher than the magnets' integral field strength, which result from the magnet type's maximum field and the minimum magnet length given in table 4.3, the magnet length will be increased to increase the integral gradient or integral dipole field further. This method was chosen to keep the magnets as compact as possible to minimise the investment costs.

4.3 Power Converters

4.3.1 Power Converters for NC, SC, and SF Magnets

Two different power converter types are used within the model for the NC, SC, and SF magnets. They cover two different fields of applications. For currents up to 2 kA and voltages up to 600 V, switch mode (SM) power converters are used in the model. For higher nominal values for the current respectively the voltage, silicon controlled rectifier (SCR) power converters will be chosen. The algorithm for calculating these power converters' power losses depending on the required flattop current is provided by the power converters department at GSI [27]. To determine the power loss of the power converters, first the ramping voltage, which is the voltage applied while ramping the magnets, is calculated. This results from the magnet system's total inductance L, the total resistance R, and the desired value of the rise time t_{ramp} of the current from zero to the flattop value I_{flattop} [6]:

$$I(t) = \frac{U_{\text{ramp}}}{R}\left(1 - e^{-\frac{R}{L}\cdot t}\right) \quad \Rightarrow \quad U_{\text{ramp}} = \frac{I_{\text{flattop}} \cdot R}{1 - e^{-\frac{R}{L}\cdot t_{\text{ramp}}}} \tag{4.14}$$

In the following calculations, the NC magnets' rise time is set to 0.5 s, the SF magnets' rise time is set to 1.0 s, and the SC magnets' rise time is set to 5.0 s. The flattop voltage is calculated from the flattop current I_{flattop} and the system's total resistance R [6]

$$U_{\text{flattop}} = I_{\text{flattop}} \cdot R. \tag{4.15}$$

Considering the ramping voltage, the flattop voltage, and the flattop current, the total power loss of the power converters' essential components, such as the ripple filter choke, the rectifier, the transformer, and further internal losses, can be calculated with the algorithm.

Moreover, the SM power converters can store the energy from the ramp-down process in capacitors to reuse it for the next ramping. For storing this energy in the capacitor, an efficiency of 95% is assumed [28]. It has to be considered, that both the SM and the SCR power converters have water-cooled parts resulting in additional power losses. Without reference to the magnet type, a distance of 100 m from the power converter to the magnet (for NC magnets) respectively the current feedbox (for SC and SF magnets) is assumed [28]. The cross-sectional area of the resulting supply cables scales with the current. Depending on the current, these supply cables can also be water-cooled. To achieve high currents, the cables can be parallel-connected.

As SC and SF magnets have no resistance in the coil and in the links between the individual magnets, the supply cables from the power converter to the current feedbox are the only parts, which causes resistive losses. Therefore, for the SC respectively the SF magnets only one power converter for the dipole magnets and another one for the quadrupole magnets is used in the model. The generally high currents common for those magnet technologies lead to the choice of SCR power converters in the most cases of the following calculations. It is possible to use more power converters, if the inductance of the whole transfer line is too large to realise ramps within the desired time duration. In the case of the NC magnets, significant resistive losses occur not only in the supply cables but also in the magnets itself and the links between them. Hence, it is not recommendable to use one power converter for all magnets of a magnet family. Moreover, it is also not recommendable to use one power converter for each magnet due to the increased investment costs and the resistive losses from the additional power converters and supply cables. Therefore, a compromise between the number of magnets, which are connected in series to one common power converter, and the number of power converters is needed. When the number of magnets per power converter and consequently the connected total resistance increases, the necessary voltage, which is needed to ramp the magnets within the desired time, also increases. Thus, in the model it is checked if the resulting apparent power has a value below 2 MVA in the following calculations.

4.3.2 Power Converters for HCP Magnets

The HCP magnets' power converters are high voltage capacitor charging power supplies. The power supplies provided by industry partners [29] deliver a power of up to several 10 kW, which match with the requirements of the HCP magnets. For example, the prototype at GSI uses a capacitor bank of 450 μF and a voltage of up to 23 kV resulting in a energy of up to about 119 kJ, which is stored in the capacitor bank [19]. Assuming a repetition rate of 1 Hz and an energy recovery circuit with an efficiency of 80%, a power converter with a nominal power of about 24 kW is necessary for continuous operation. The efficiency of those power supplies is specified as about 90% [29]. Hence, the power loss of the HCP magnets' power converters is $P_{\text{pc, HCP}} = 0.1 \cdot P_{\text{loss}}$, where P_{loss} is the power loss of the magnet. In the model, it is assumed that each HCP magnet has its own power converter.

4.4 Cooling

In the model of the magnets' energy consumption only water cooling and liquid helium (LHe) cooling are assumed. The necessary cooling power of air cooling in the tunnel differs strongly among the different accelerator types and the number of additional devices, such as beam diagnostics. Furthermore, in the end the air cooling itself bases on some sort of water cooling. Hence, air cooling is neglected in the model, and it is assumed that all losses are dissipated to the water cooling or LHe cooling.

4.4.1 Water cooling

The electrical power of the pumps can be calculated by the following equation [30]:

$$P_{\text{pump}} = \frac{P_{\text{loss}} \cdot \Delta p}{\Delta T \cdot 4200\ \text{J/kgK} \cdot 998.2\ \text{kg/m}^3} \cdot \eta \tag{4.16}$$

Here, P_{loss} is the power loss of the magnets respectively the power converters. The average temperature difference ΔT of the cooling water is assumed to be 10 K. The pressure drop Δp of the magnets' water cooling is assumed to be 10 bar. For the power converters' water cooling, a value of 5 bar is assumed. The overall efficiency η of the pumps is assumed to be 80%. The total power P_{water} of the water cooling results from a factor of 0.25 W/W_{loss} [14], the power loss P_{loss} of the cooled devices (magnets respectively power converters), and the corresponding power loss P_{pump} of the pumps:

$$P_{\text{water}} = 0.25 \cdot P_{\text{loss}} + P_{\text{pump}} \tag{4.17}$$

Cryogenic Infrastructure	Losses 4 K	Losses 50-80 K
Connections	0.25 W_{4K}/connection	1.5 W_{80K}/connection
Vacuum barrier (1 piece per 130 m)	2.0 W_{4K}/piece	4.0 W_{80K}/piece
Connection box (1 piece per 130 m)	4.0 W_{4K}/piece	10.0 W_{80K}/piece
LHe feedbox (1 per beamline)	20.0 W_{4K}/box	85.0 W_{80K}/box
LHe endbox (1 per beamline)	10.0 W_{4K}/box	50.0 W_{80K}/box
Current feedbox (1 per beamline)	5.0 W_{4K}/box	20.0 W_{80K}/box
Current leads (1 pair per magnet familiy)	10.0 W_{4K}/pair	63.0 W_{80K}/pair

Table 4.4.: Overview on the static losses of the modelled SC and SF magnets' cryogenic infrastructure based on the SIS100 and SIS300 heat loads [14].

The pumps of the water cooling also run during shutdown to avoid dirt in the cooling channels. Hence, a non-zero energy consumption occurs when the magnets are switched off, as well.

The water cooling system is no closed system. Thus, the water consumption due to vaporisation has to be also taken into account within the calculation of the estimated operation costs. The amount of additional water in m^3/h for an average temperature of 25°C approximately is [31]:

$$\dot{V}_{\text{water}} \approx \frac{4}{3} \frac{P_{\text{loss}}}{r_{100} - c_{\text{p,vapour}} \Delta T} \cdot 3.6 = \frac{4}{3} \frac{P_{\text{loss}}}{2260\ \text{kJ/kg} - 1.87\ \text{kJ/kgK} \cdot 75\ \text{K}} \cdot 3.6 \quad (4.18)$$

Here, P_{loss} is the total power loss of the beamline's magnets and power converters. A multiplication of this equation and the time of operation per year yields the water consumption per year.

4.4.2 Liquid-Helium Cooling

The heat losses of the SF magnets and the SC magnets were discussed in section 4.1.2 and in section 4.1.3. To get the power loss of the cryogenic cooling system, these values have to be multiplied with a coefficient of performance, which includes the power loss of the helium refrigeration (250 W/W_{4K} respectively 15 W/W_{80K}) as well as the power loss P_{water} of recooling the water of the cryogenic cooling system's water-cooled components. Hence, the power loss of the cryogenic cooling system is [14]:

$$P_{\text{LHe}} = \left(250 + P_{\text{water}}(250)\right)\ \text{W/W}_{4\text{K}} \cdot P_{\text{loss, 4K}} + \left(15 + P_{\text{water}}(15)\right)\ \text{W/W}_{80\text{K}} \cdot P_{\text{loss, 80K}} \quad (4.19)$$

In addition to the losses of the magnets themselves, further losses of the cryogenic cooling system resulting from the cryogenic infrastructure are generated. These losses are summarised in table 4.4. During shutdown, all magnets are switched off. However, the complete cryogenic cooling of the SF and SC magnets as well as the cryogenic infrastructure run also during shutdown to minimise the duration of cooling down the magnets to operation temperature after the shutdown. Hence, the DC losses are assumed for the entire year. AC losses are additionally assumed within the time of operation, if an AC operation is possible.

5 Modelling of Energy Consumption, Operation Costs, and Investment Costs

In this section, a description of the calculation algorithm of the energy consumption, operation costs, and investment costs is given. Therefore, the input parameters are introduced, as they are necessary to calculate the energy consumption for a FODO beam-transfer line. Considering the current energy price and the current water price including a rough approximation for the future prices, the operation costs can be calculated. The investment costs result from the chosen beamline parameters and include the magnets as well as the power converters and the cooling systems. Furthermore, a rough overview on the model's uncertainties is given.

5.1 Energy Consumption and Operation Costs

The calculation algorithm for the estimated energy consumption of the FODO beam-transfer lines is implemented in *Mathematica*. A rough overview on this algorithm is illustrated in figure 5.1. Based on the properties discussed in chapter 3 and the magnet models introduced in chapter 4, the energy consumption is determined as following: The beam parameters (horizontal and vertical emittance, magnetic rigidity) as well as the desired horizontal and vertical

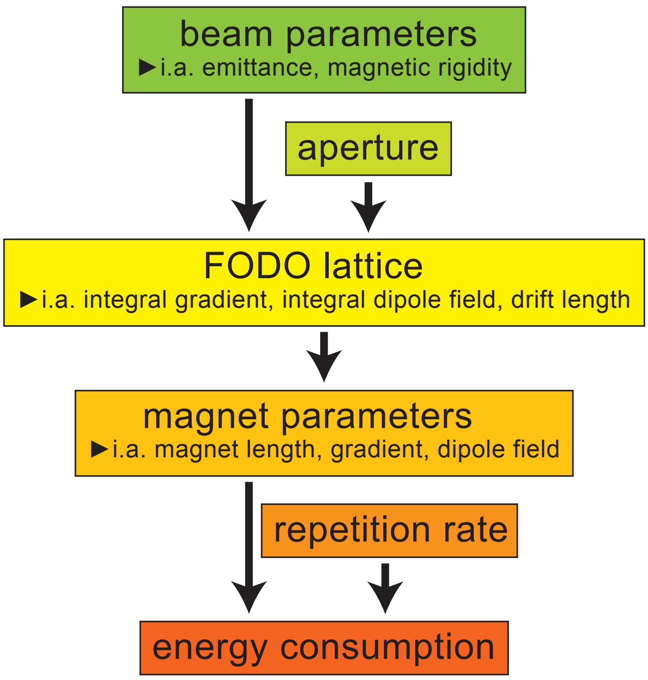

Figure 5.1.: Flowchart of the calculation algorithm for the estimated energy consumption.

aperture are the input parameters. These parameters are used to determine the FODO lattice. This FODO lattice consists of the integral gradient, the integral dipole field, and the drift length. The magnet parameters, which are the pole-tip radius, gap, good-field region and magnet lengths, follow from the limits on the magnetic field strength (cf. section 4.2) and the design of the different magnet types. As the magnets' geometric parameters as well as the optics parameters are known, the magnets' energy consumption can be calculated for each magnet type at a given repetition rate. The transfer channel is made of an integer number of FODO cells. Hence, the resulting total energy consumption per FODO cell yields the total energy consumption of the transfer channel. The power converters' energy consumption follows from the magnets' inductance and resistance as well as the repetition rate and the desired duration for ramping. The energy consumption of the water cooling system depends on the magnets' power loss and the power converters' power loss. For the LHe cooling, the cooling systems energy consumption depends on the magnets' heat loads in the cryogenic system. In the following calculations, only the energy consumption of the magnets, the power converters, and the cooling system are considered. Further devices such as steerers, multipole correctors, and beam diagnostics are not included in the model. The operation costs resulting from electric energy consumption are determined by multiplication of the energy consumption per year and the energy price of 0.12 EUR/kWh [32]. This price is assumed to increase by 0.007±0.002 EUR/kWh per year. For operation, 6000 hours of continuous operation are assumed. The rest of the year is assumed to be a continuous shutdown. The water cooling is assumed to run the whole year to avoid debris in the magnets' cooling channels. The LHe cooling runs the whole year to minimise the effort for cooling the magnets down after a shutdown. Furthermore, it is assumed that the beamline is operated at its maximum magnetic rigidity for the whole operation period; even when it is a beamline, which is designed for a variable range of the magnetic rigidity.

Besides the operation costs due to electric energy, further operation costs are considered, for example, due to water consumption. The water price per m^3 is assumed as 2.79 EUR [33], which is an extrapolated value for 2015 and which is assumed to increase by 2±1% per year. This value also includes water conditioning. The liquid-helium cooling is assumed to be a closed system. Hence, no helium wastage is expected. Thus, helium consumption is neglected in the model.

As the effort of replacing broken components highly differs among magnet types, breakdowns are not considered in the model of operation costs. For example, maintenance work at a superconducting beamline is generally more sophisticated due to the cryogenic infrastructure compared to normal conducting systems. Furthermore, the time duration for maintenance is longer for superconducting machines because the components have to be heated up before maintenance and then cooled down before the next operation. Therefore, a continuous operation without any failures is used in the model to simplify the assumptions on the operation. As an exception, maintenance costs are included for the switches of the HCP magnets, as these can cause large additional costs especially for high repetition rates.

5.2 Uncertainties due to the Model's Fluctuations

For the following investigations, the estimated energy consumption is represented by a discrete function of the aperture size, the repetition rate, or the magnetic rigidity. Figure 5.2 gives an example for the obtained discrete data points. In this example, for each aperture size the energy consumption is calculated separately. Depending on the magnet type, the energy consumption

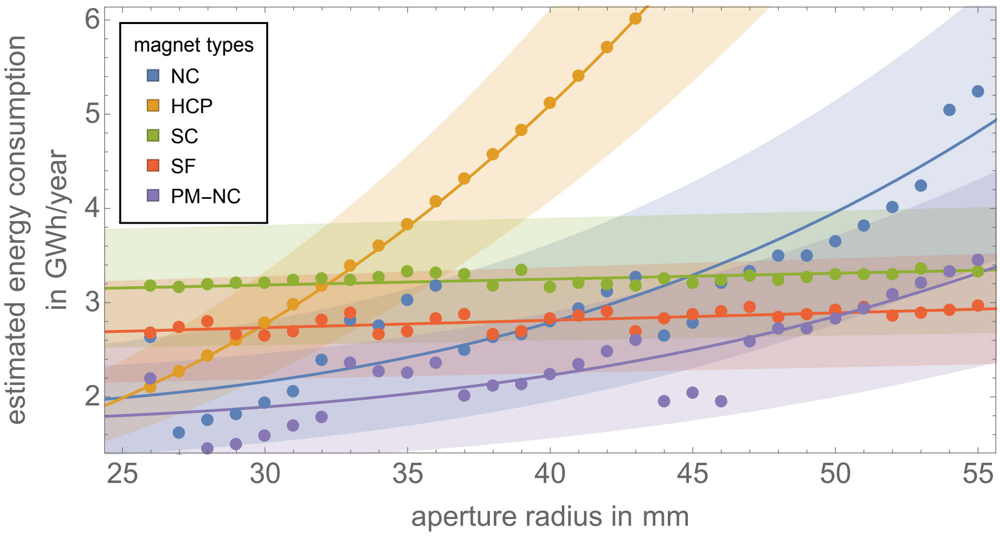

Figure 5.2.: Exemplary data set of the energy consumption as a function of the aperture radius. The original data from the model are illustrated as points. To each data set a trendline is fitted. The corresponding bands indicate the uncertainties due to the model's fluctuations. These fluctuations are approximately 20% on average.

can fluctuate significantly even for small variations of the aperture size. The reasons of these fluctuations are different for each magnet type. However, they can be explained by fluctuations in the magnets', the power converters' and the cooling systems' parameters. For example, as the pole-tip field varies for different aperture sizes respectively different magnetic rigidities, the necessary number of windings in the coil may jump from N windings to N+1 windings. In this case, the necessary current may also change to keep the number of ampere turns constant. This variation has also an impact on several other electrical parameters like the coil's resistance, the coil's inductance, or the ramping voltage and the flattop voltage. Furthermore, the corresponding parameters of the power converters also change with the variations of the magnets' parameters. But there is not only an impact on the magnets' and power converters' electrical parameters. Also, the parameters of the NC magnets' cooling system may change due to fluctuations in the magnets' and the power converters' power losses resulting from the variations in the conductor's necessary cooling-channel diameter respectively the conductor's cross-section. Fluctuations in the energy consumption of the SC magnets' and the SF magnets' cooling system arise from the fluctuations in the magnets' cold mass, which result from the variation in the coil geometry and the yoke geometry. For the HCP magnets, uncertainties arise from the approximations of the magnets' inductance as well as the power converters capacitance. Thus, the energy consumption is not a continuous function but there there are significant fluctuations. Independent from the magnet type, these fluctuations resulting from the uncertainties in the model are approximately 20% on average.

To consider the energy consumption's fluctuations in the following recommendations, a trendline is fitted to the original data from the model. These trendlines represent the general behaviours of the different magnet types. Furthermore, bands are plotted around the estimated energy consumption. The width of these bands is chosen to be 20% representing the average fluctuations. If the fluctuations are larger than this, the width can also be manually modified to include preferably all data points inside the bands. The trendlines as well as the bands representing the model's fluctuations are also illustrated in figure 5.2 for the exemplary data set.

5.3 Investment Costs

In this section, the price estimates of the beamline's essential parts, namely the magnets, the power converters as well as the cooling systems, are introduced. Additional components such as steerers, beam diagnostics, or higher multipole correctors are not considered in this model. Also, spare parts and running costs for replacements are generally missing in these calculations. Furthermore, costs for R&D, which is necessary especially for SC, SF and HCP magnets, are not considered in the calculations. These costs can have significant impact on the total costs of a transfer line.

5.3.1 Magnets

The investment costs of magnets depend on several parameters. Among others, the investment costs depend on the material costs, purchase quantity, salaries, functional tests, tools, the complexity of the design, and the complexity of the individual production steps. Nonetheless, not all of these points can be considered in this work. To predict the prices as best as possible for every magnet type, series production is assumed. Hence, the following estimates are valid only for quantities of at least about 50 pieces. To scale the investment costs with the magnets' dimensions, i.e., the aperture size and the yoke length, the following calculation method was chosen. The model includes all essential parts of the magnets. However, not all details can be modelled, for example, special coil configurations, more compact yokes, or more radiation resistant designs cannot be considered, as these are special components deviating from the standard components assumed in this thesis. Extra costs for spare parts are not considered, as well. All prices are adjusted for inflation to give estimates for the year 2015. The resulting estimated investment costs are illustrated in appendix A.1.

The estimated costs for the NC magnets are approximated by calculating the cost estimates for a few exemplary magnets of different size, which base on cost estimates at GSI [34, 35]. The resulting costs are then plotted over the magnet mass, which can be approximated by the yoke mass. Then, a fit function is fitted to these data. This yields the estimated investment costs as a function of the NC magnets' yoke mass illustrated in figure A.1. The error of the NC magnets' costs estimates is 20% [34]. A similar method was chosen for the HCP magnets' investment costs. Here, the estimated investment costs as a function of the coil mass are fitted. These data base on the cost estimates offered by NTG [36]. In addition to the magnets, a capacitor bank of 5.0±2.5 kEUR and a switch of 20±10 kEUR are assumed. The resulting functions are shown in figure A.4. As for the SF magnets and the SC magnets only the estimated costs of the SIS100 magnets [37] respectively SIS300 magnets [18] were accessible, these costs are scaled with the magnets' cold mass, which is approximately the yoke mass. The material costs are assumed as 25%. Hence, an offset of 75% of the SIS100 estimates respectively the SIS300 estimates occur, which includes, i.a., construction, production, assembly and testing. The resulting estimated investment costs as a function of the magnets' cold mass are illustrated in figure A.2 and figure A.3. The investment cost of the Permanent Magnetic (PM) magnets are calculated by estimating the material costs. They consist of the price of the PM material of 300 EUR/kg

– an extrapolation of a value from literature [22] – and the price of the aluminium brackets (AL1100) of 7 EUR/kg [35]. The PM magnets' material costs are assumed to be approximately 40% of the total investment cost of this magnet type. Vacuum chambers are considered, as well. As the requirements and engineering designs differs a lot among the various accelerator types and magnet types, a price of 1500 EUR/m and a large error of ±50% are assumed [35].

The assumed material costs' errors are 20% and the assumed errors of the production costs are 50% for PM magnets. In the model, the material costs are assumed to be about 40% of the total investment costs, and the production costs are assumed to be about 60% of the total investment costs. Hence, a total error of 38% is assumed for the PM magnets. For the SC magnets, the SF magnets and the HCP magnets, for which more construction time and testing is especially necessary, the material costs are assumed to be only 30% of the total investment costs, and the production costs are assumed to be 70% of the total investment costs. With the errors of 20% for material costs and 50% for production costs, the resulting total error is 41%.

5.3.2 Power Converters

SM and SCR Power Converters for NC, SC, and SF Magnets

The SM and SCR power converters are used for the NC, SC, and SF magnets. For these power converters' investment costs, the price does not depend on the power converter type in the model but only on the supplied effective apparent power. The prices base on internal studies at GSI [38]. The resulting estimated investment costs as a function of the effective apparent power is illustrated in figure A.6. The assumed error depends on the apparent power, as well [28]. For an effective apparent power of up to 10 kVA, an error of 30% is assumed. For 10 kVA up to 200 kVA, the assumed error is 10%. For larger values of the effective apparent power, the error increases up to 30%.

Capacitor Charging High Voltage Power Supplies for HCP Magnets

For charging the capacitor banks in the HCP magnets, capacitor charging high voltage power supplies are used. To model the investment costs of those power converters, FuG provided a price list for 2015 of their spectrum of devices [29]. This price list covers the necessary field of application. The prices were plotted over the average power loss and a fit function is fitted to the data. The resulting correlation of the investment costs and the average power loss are shown in figure A.7.

5.3.3 Cooling

Water Cooling

The water cooling's investment costs depend on the water recooling capacity of the cooling system. The resulting investment costs illustrated in figure A.8 base on engineering estimates made at GSI for the new FAIR facility [30]. These data include the primary cooling system consisting of hybrid cooling towers for recooling the water, a secondary cooling system for cooling the magnets and power converters as well as measurement and control technology. The estimate for FAIR is scaled with the recooling capacity, which is assumed to be 10% more than the maximum required total power loss of the magnets and power converters [30]. The estimated investment costs' error is assumed as 30%.

Liquid-Helium Cooling

The cryogenic cooling system for the SC magnets and the SF magnets is identical for both magnet types. The power converters of these magnets require an additional water cooling. The cryogenic plant's investment costs consider the complete cooling system consisting of all essential components, such as compressors and helium tanks. The prices base on internal cost studies at GSI [14]. The resulting correlation of the liquid-helium cooling's estimated investment costs and the refrigerator capacity at 4.5 K is illustrated in figure A.9. Here, an error of 20% is assumed.

In addition, a cryogenic infrastructure is necessary to supply the magnets with liquid helium. These components yield the following additional investment costs: the investment costs for connections between the ends of the magnets (7.5 kEUR/connection), connection cryostats (10.0 kEUR/m), a 50 m long helium-transfer line from the cryo plant to the LHe feedbox (10.0 kEUR/m), a LHe feedbox and endbox (500 kEUR), current leads (200 kEUR/pair), and quench detection (7.5 kEUR/magnet). These prices base on engineering estimates for the SIS100 at FAIR [37]. For all these prices, an error of 50% is assumed.

5.4 Estimated Total Costs

The estimated total costs, which will be discussed in chapter 7, consist of the estimated operation costs due to electric energy consumption and water consumption, and the estimated investment costs of the magnets, the power converters, and the necessary cooling systems. The bands around the estimated total costs include the uncertainties from the fluctuations due to the model, which are approximately 20%, the specific errors assumed for the energy price and the water price, as well as the specific errors following from the investment costs of the components described in the previous section.

6 Comparison of Energy Consumption

In this chapter, the energy consumption of fictitious transfer lines in three different exemplary machines – an electron machine, a proton machine, and a heavy-ion machine – will be discussed. The transfer lines' beam parameters are comparable to the parameters of existing accelerator facilities, which will be introduced in the following section. The chosen beamline parameters shall reflect the values typically used in electron machines respectively proton machines or heavy-ion machines. However, the full spectrum of machines cannot be covered.

6.1 General Requirements of Different Accelerator Types

As the general physical properties of FODO beam transfer lines were discussed in chapter 3, the requirements for the beam transport system of different particle-accelerator types are introduced now. For this purpose, the particles' kinetic energy, the magnetic rigidity as well as the emittance respectively the normalised emittance are compared on the basis of a few examples of existing accelerator facilities. These properties are summarised in table 6.1 for electrons, in table 6.2 for protons, and in table 6.3 for heavy ions. Of course, no average accelerator facility representing the particle accelerators' majority exists. The requirements differ a lot among the different fields of application, such as industrial use or research. However, the following examples shall offer an overview on the common parameters of existing accelerator facilities for research use.

Due to the smaller mass of electrons compared to protons or heavy ions, electrons nearly reach the speed of light at a lower kinetic energy respectively a lower magnetic rigidity in comparison to protons or heavy ions. For the use in synchrotron light sources, an energy of a few GeV is common. The resulting magnetic rigidity varies from a few Tm to a few 10 Tm. The large γ factor of electron beams yields a small emittance in the range of μm mrad. As in synchrotron light sources a very small vertical emittance is desired, the value of the vertical emittance is often about 1% of the horizontal emittance in the storage rings. The repetition rates of such machines are in the range of several Hz. In the following calculations a typical electron accelerator beamline is associated with parameters similar to the PETRA III parameters at DESY. This exemplary beamline shall transport an exemplary beam with a kinetic energy of 6.0 GeV [39], a magnetic rigidity of 20.0 Tm [39], and a horizontal respectively vertical emittance of 2.0 μm mrad. The assumed emittance is larger than the emittance in PETRA III and shall partially account for dispersive effects.

The kinetic energy of protons common in existing accelerator facilities differs among the various fields of application. The protons' energy varies from a few 10 GeV at FAIR to TeV at CERN. In the following calculations, the exemplary proton beamline is associated with the J-PARC parameters, which contain a kinetic energy of 50.0 GeV [44] and a magnetic rigidity of 169.9 Tm [44]. As the emittance of 19.2 mm mrad [44] is rather large compared to other accelerator facilities, an emittance of 10.0 mm mrad is assumed for the exemplary proton beamline.

The exemplary heavy-ion beam's parameters are similar to the parameters of the FAIR reference beam, which uses U^{28+} ions [43]. The assumed heavy-ion beam has a kinetic energy

Electron Accelerators

	Particle accelerator	Particle energy	Magnetic rigidity	Horz./vert. emittance	Normalised emittance
PSI	SLS Booster	2.4 GeV	8.0 Tm	9.0 μm mrad 0.09 μm mrad	42.3 mm mrad 0.4 mm mrad
PSI	SLS	2.4 GeV	8.0 Tm	5.0 μm mrad 0.05 μm mrad	23.5 mm mrad 0.2 mm mrad
DESY	DESY II	6.0 GeV	20.0 Tm	350.0 μm mrad 35.0 μm mrad	4109.9 mm mrad 411.0 mm mrad
DESY	PETRA III	6.0 GeV	20.0 Tm	1.0 μm mrad 0.01 μm mrad	11.7 mm mrad 0.1 mm mrad

Table 6.1.: Overview on the beam parameters of PSI [4] and DESY [39, 40] as examples of electron accelerators. The values of the emittance are either taken from literature or calculated from the values in literature.

Proton Accelerators

	Particle accelerator	Particle energy	Magnetic rigidity	Horz./vert. emittance	Normalised emittance
CERN	PS Booster	1.4 GeV	7.2 Tm	1.1 mm mrad	2.5 mm mrad
CERN	PS	25.0 GeV	87.0 Tm	107.8 μm mrad	3.0 mm mrad
CERN	SPS	450.0 GeV	1500.0 Tm	7.2 μm mrad	3.5 mm mrad
CERN	LHC	7.0 TeV	23505.1 Tm	0.5 μm mrad	3.75 mm mrad
FAIR	SIS18	4.0 GeV	16.3 Tm	12.0 mm mrad 5.0 mm mrad	62.4 mm mrad 26.0 mm mrad
FAIR	SIS100	28.8 GeV	99.9 Tm	2.0 mm mrad 0.8 mm mrad	62.4 mm mrad 26.0 mm mrad
J-PARC	RCS	3.0 GeV	12.8 Tm	169.6 mm mrad	695.6 mm mrad
J-PARC	Main Ring	50.0 GeV	169.9 Tm	19.2 mm mrad	1047.6 mm mrad

Table 6.2.: Overview on the beam parameters of CERN [41], FAIR [42, 43], and J-PARC [44] as examples of proton accelerators. The values of the emittance are either taken from literature or calculated from the values in literature.

of 2.7 GeV/u respectively a magnetic rigidity of 100.0 Tm [43]. The emittance resulting from adiabatic damping of the FAIR beam is 6.3 mm mrad [43] at 100.0 Tm.

6.2 Dependency of Energy Consumption on Aperture Size, Repetition Rate, and Magnetic Rigidity

To compare the dependency of the energy consumption of NC, HCP, SC, SF and PM magnets on the aperture radius, the repetition rate, and the magnetic rigidity, the energy consumption is plotted as a function of these parameters. The bands around the graphs account for the uncertainties in the models, which were discussed in section 5.2 and are assumed to be at least 20%. More detailed plots of the original data from the model and the fitted functions can be found in appendix B.

As completely PM transport lines with a bend can only transport a beam with fixed magnetic rigidity, it is necessary to use a hybrid beamlines for beams with deviating energies: Those hybrid beamlines consist of, for example, PM quadrupoles and NC dipoles. This can be an interesting alternative for beamlines using beams with different magnetic rigidities. If a straight beam-transfer line is considered, a completely PM magnet system is also possible for varying

Heavy-Ion Accelerators

	Particle accelerator	Particle energy	Magnetic rigidity	Horz./vert. emittance	Normalised emittance
CERN	LEIR, Pb^{54+}	72.2 MeV/u	4.8 Tm	1.7 mm mrad	0.7 mm mrad
	PS, Pb^{54+}	5.9 GeV/u	86.7 Tm	137.6 μm mrad	1.0 mm mrad
	SPS, Pb^{82+}	176.4 GeV/u	1500.0 Tm	6.3 μm mrad	1.2 mm mrad
	LHC, Pb^{82+}	2.76 TeV/u	23347.9 Tm	0.5 μm mrad	1.5 mm mrad
FAIR	SIS18, U^{28+}	195.7 MeV/u	18.0 Tm	35.0 mm mrad 12.0 mm mrad	23.8 mm mrad 8.2 mm mrad
	SIS100, U^{28+}	1.5 GeV/u	63.7 Tm	9.9 mm mrad 3.4 mm mrad	23.8 mm mrad 8.2 mm mrad
BNL	Booster, Au^{32+}	107.8 MeV/u	9.5 Tm	76.2 mm mrad 35.8 mm mrad	37.7 mm mrad 17.7 mm mrad
	AGS, Au^{77+}	8.9 GeV/u	83.2 Tm	3.6 mm mrad	37.7 mm mrad
	RHIC, Au^{79+}	99.1 GeV/u	831.8 Tm	0.3 mm mrad	31.4 mm mrad

Table 6.3.: Overview on the beam parameters of CERN [41], FAIR [42, 43], and BNL [45] as examples of heavy-ion accelerators. The accerelated ions are listed beside each machine. The values of the emittance are either taken from literature or calculated from the values in literature.

	Electron transfer line	Proton transfer line	Heavy-ion transfer line
Horz./vert. emittance	2.0 μm mrad	10.0 mm mrad	6.3 mm mrad
Magnetic rigidity	20.0 Tm	169.9 Tm	100.0 Tm
Total length of transfer line	80 m	504 m	504 m
Total deflexion angle	90°	60°	60°
Number of FODO cells	10	21	21
Number of dipoles	20	42	42
Integral dipole field	1.6 Tm	4.2 Tm	2.5 Tm
Number of quadrupoles	20	42	42
Integral gradient	6.2 T	17.5 T	10.3 T
Drift length	4.0 m	12.0 m	12.0 m
Repetition rate	0.5 Hz	0.33 Hz	0.33 Hz
Horz./vert. aperture	varying	varying	varying

Table 6.4.: Parameters used for the comparison of energy consumption versus aperture radius. The chosen parameters of the exemplary beam-transfer lines are fictitious but shall reflect typical values for each kind of transfer-line type. All of the parameters are fixed except for the aperture radius.

magnetic rigidities (see chapter 3). In this chapter only PM-NC hybrid beamlines are discussed as the energy consumption of completely PM beam transport systems is zero anyway. For all of the calculations in this chapter, all parameters are fixed except for those ones of interest. These are the aperture radius, the repetition rate, and the magnetic rigidity.

6.2.1 Energy Consumption versus Aperture Radius

The energy consumption as a function of the aperture radius is shown in figure 6.1 for the exemplary beam-transfer lines. The corresponding beamline parameters are listed in table 6.4. As mentioned before, all parameters are fixed except for the aperture radius in this first comparison. As the field strengths are identical for all apertures, the beam envelope is also identical. This means that the ratio of acceptance and emittance A/ϵ differs among the different apertures. Hence, the transport of particles outside the RMS beam envelope (halo particles) will be better with larger apertures than with smaller apertures.

For the exemplary electron beamline in figure 6.1(a), HCP magnets cause the least energy consumption. The energy consumption of the NC magnets and the PM-NC magnets are so close to each other that no clear recommendation can be given. Many electron machines such as synchrotron-light sources use only one precisely defined energy. Then, it is also possible to use a completely PM magnet system, which results in zero energy consumption. The SC magnet system and the SF magnet system have a higher energy consumption than the NC magnet system or the PM-NC magnet system for small aperture radii up to about 15 mm but have a comparable energy consumption for apertures above this value. The energy consumption resulting from the model is lower for SC magnets than for SF magnets. However, the bands around the trendlines of the SC magnets and the SF magnets overlap; and therefore, no clear recommendation for one

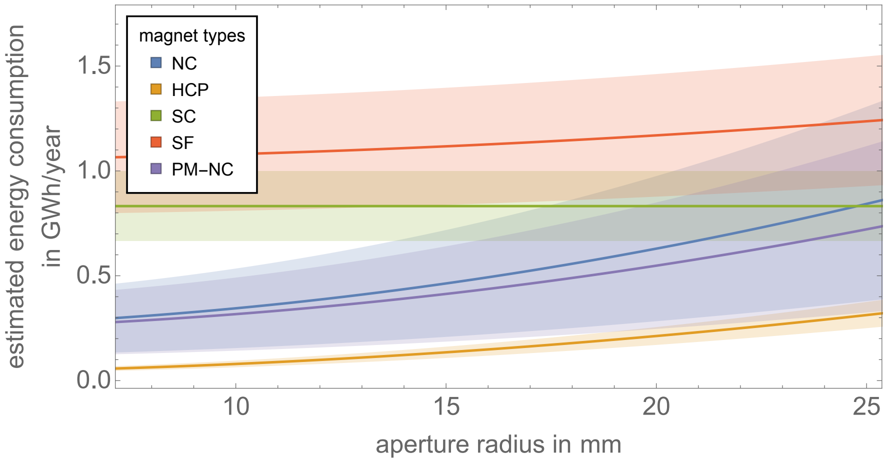

(a) Estimated energy consumption versus aperture radius of an exemplary beamline of an electron accelerator.

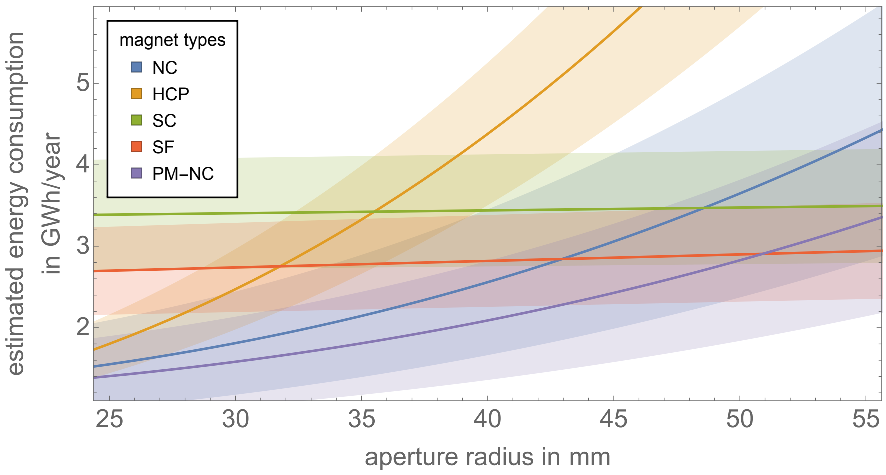

(b) Estimated energy consumption versus aperture radius of an exemplary beamline of a proton accelerator.

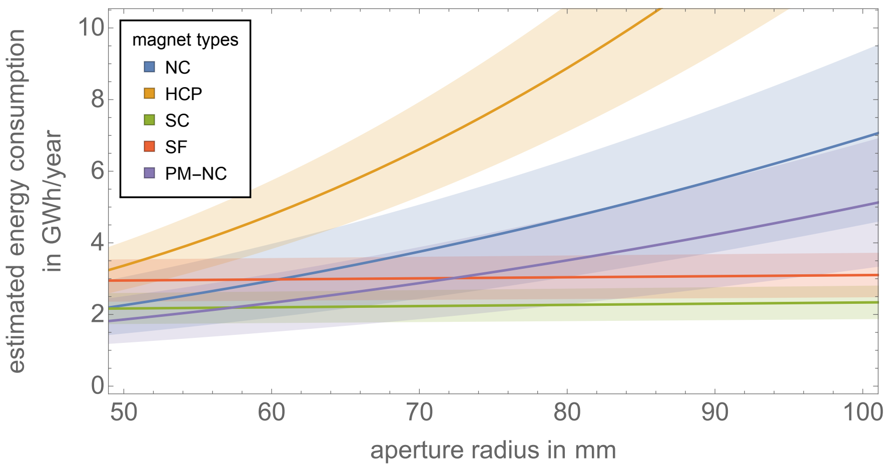

(c) Estimated energy consumption versus aperture radius of an exemplary beamline of a heavy-ion accelerator.

Figure 6.1.: Estimated energy consumption versus aperture radius for an exemplary beamline of an electron accelerator, a proton accelerator, and a heavy-ion accelerator. The parameters for each beamline are listed in table 6.4.

of these magnet types can be given. For apertures common for electron machines, HCP, NC or NC-PM respectively PM magnets are recommendable.

In figure 6.1(b), the energy consumption as a function of the aperture radius is shown for an exemplary proton line. In this example, the energy consumption of the HCP solution increases significantly with the aperture radius. The energy consumption of the NC and the PM-NC magnet system are similar for small apertures. As there are no power losses of the PM quadrupoles in the PM-NC solution. This concept is the most efficient one in this example. Especially for larger apertures, the energy consumption of the PM-NC solution becomes more and more efficient. However, for larger apertures manufacturing issues may exist for the PM magnets. Therefore, PM magnets are only applicable up to medium apertures. With increasing apertures the SC magnets and the SF magnets become more efficient because the energy consumption of both the NC magnets and the HCP magnets increase significantly with the aperture. The estimated energy consumption of the SC magnets and the SF magnets is comparable. The higher value of the SC magnets can be identified with higher power-converter losses. This difference accounts for the different modelling of the SC magnets and the SF magnets; the SF magnets' current is restricted to a maximum value. Thus, the number of windings is adapted to match with the requirements. Whereas the SC magnets' current is not restricted but their number of windings is restricted by the geometry. As both magnet types' dipole magnets reach their full load in the exemplary proton beamline, the properties following from the models result in a higher current; and hence, a higher energy consumption of the SC magnets.

The exemplary heavy-ions beamline's estimated energy consumption is illustrated in figure 6.1(c). With increasing aperture size, the SC solution and the SF solution become the most efficient solutions. This follows from the absence of resistive losses in the magnet. In contrast to the proton beamline, the SC magnets are more efficient due to the mentioned properties of the models. However, lower field strengths are necessary in this example. Hence, the SC magnets have a lower load and additionally the coils have many windings due to the large aperture; this large aperture yields lower currents compared to the SF magnets, which reach nearly their maximum current. The energy consumption of these magnets' cryogenic cooling system is nearly constant. The NC magnets' and the PM-NC magnets' estimated energy consumption increase significantly with the aperture. HCP magnets require an extremely high current for the generation of the necessary pole-tip fields for large apertures. This leads to a high energy consumption of HCP magnets in this example.

For small apertures (up to 30 mm aperture radius), generally NC, HCP, and PM-NC magnets (pure PM for single particle energy) are recommendable as these are the most energy efficient magnet systems. For larger apertures (up to 40 mm aperture radius), the NC magnets and the PM-NC magnets are more efficient. For apertures larger than this range, the SC solution and the SF solution will become more and more attractive.

6.2.2 Energy Consumption versus Repetition Rate

The second characteristic parameter investigated is the repetition rate. The estimated energy consumption of the three different example beamlines are shown in figure 6.2. The parameters are given in table 6.5. In this section, only the repetition rate is varied while the other parameters are constant.

The energy consumption as a function of the repetition is illustrated in figure 6.2(a) for the exemplary electron transfer line. For low repetition rates up to 1 Hz, the NC magnets and the

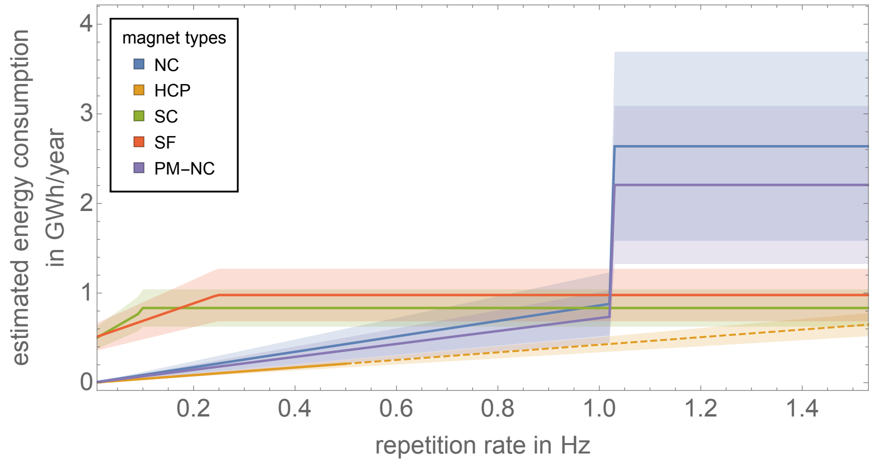

(a) Estimated energy consumption versus repetition rate of an exemplary beamline of an electron accelerator.

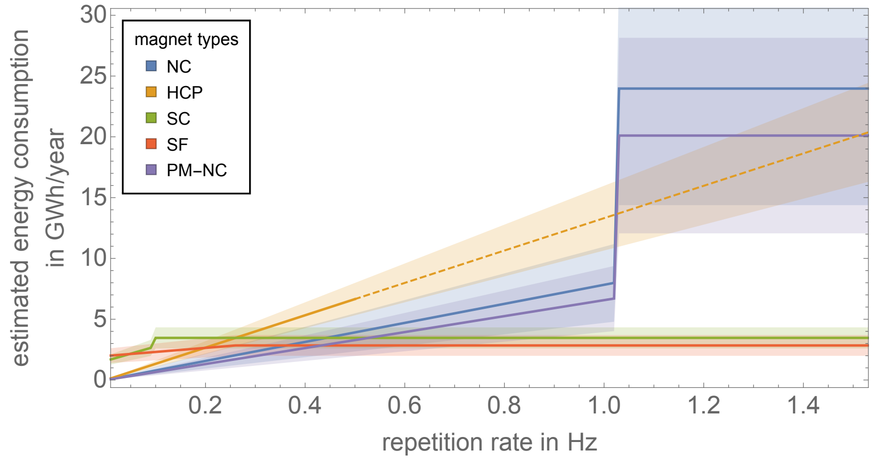

(b) Estimated energy consumption versus repetition rate of an exemplary beamline of a proton accelerator.

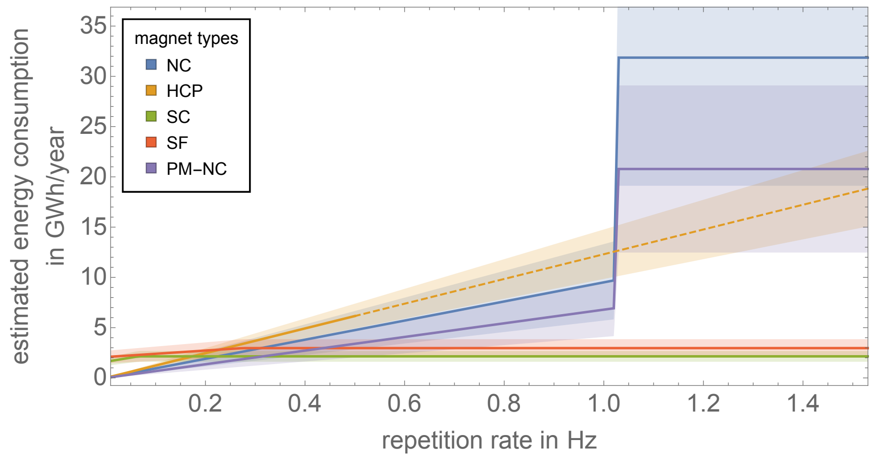

(c) Estimated energy consumption versus repetition rate of an exemplary beamline of a heavy-ion accelerator.

Figure 6.2.: Estimated energy consumption versus repetition rate for an exemplary beamline of an electron accelerator, a proton accelerator, and a heavy-ion accelerator. The parameters for each beamline are listed in table 6.5. Switching from AC operation to DC operation accounts for the jump in the energy consumption.

	Electron transfer line	Proton transfer line	Heavy-ion transfer line
Horz./vert. emittance	2.0 μm mrad	10.0 mm mrad	6.3 mm mrad
Magnetic rigidity	20.0 Tm	169.9 Tm	100.0 Tm
Total length of transfer line	80 m	504 m	504 m
Total deflexion angle	90°	60°	60°
Number of FODO cells	10	21	21
Number of dipoles	20	42	42
Integral dipole field	1.6 Tm	4.2 Tm	2.5 Tm
Number of quadrupoles	20	52	42
Integral gradient	6.2 T	17.5 T	10.3 T
Drift length	4.0 m	12.0 m	12.0 m
Repetition rate	varying	varying	varying
Horz./vert. aperture	40x40 mm^2	80x80 mm^2	110x110 mm^2

Table 6.5.: Parameters used for the comparison of energy consumption versus repetition rate. The chosen parameters of the exemplary beam-transfer lines are fictitious but shall reflect typical values for each kind of transfer-line type. All parameters are fixed except for the repetition rate.

PM-NC magnets show nearly the same energy consumption. The jump at 1 Hz is caused by the fact that the NC magnets shall reach their nominal field within less than 0.5 s in AC operation. This results in the energy consumption being considerably higher for repetition rates above 1 Hz, as the NC magnets run in DC operation in this range. The position of the jump can be shifted by varying the nominal value of the duration of ramping but this has an effect on the design of the power converters: For example, a shorter ramping duration demands a higher ramping voltage. An alternative for low repetition rates is a HCP magnet system. A repetition rate of up to 0.5 Hz is possible with the design of the HCP quadrupole prototype at GSI. Higher repetition rates are possible, in principle, either by allowing a higher operation temperature or by having an additional active cooling. Furthermore, the lifetime of the switch is limited. Thus, the switch has to be replaced more often for higher repetition rates. This causes additional maintenance costs, which have to be considered in the total costs. The energy consumption of the SC magnets and the SF magnets increases with increasing repetition rates; until they switch to DC operation, which is done if AC operation is not possible due to long ramping times or DC operation yields a lower energy consumption due to the absence of dynamic losses. The additional heat loads due to eddy currents in the magnets in AC operation requires additional cryogenic cooling. Hence, the SC magnets and the SF magnets are only efficient for low repetition rates in AC operation or for repetition rates higher than about 1 Hz when operated in DC mode. The position of switching from the AC mode to the DC mode can be shifted by changing the desired duration of ramping, as well.

For the exemplary proton machine, the energy consumption as a function of the repetition rate is shown in figure 6.2(b). The behaviour of the magnets are similar to the electron machine. Due to the larger aperture radius, the energy consumption of the NC solution and the PM-NC solution are higher; and therefore, these magnets are the most efficient ones for repetition rates up to 0.1-0.3 Hz. For higher repetition rates, the SC magnets or the SF magnets are more efficient. Due

	Electron transfer line	Proton transfer line	Heavy-ion transfer line
Horz./vert. emittance	2.0 μm mrad (at 20.0 Tm)	10.0 mm mrad (at 169.9 Tm)	6.3 mm mrad (at 100.0 Tm)
Magnetic rigidity	varying	varying	varying
Total length of transfer line	80 m	504 m	504 m
Total deflexion angle	90°	60°	60°
Number of FODO cells	10	21	21
Number of dipoles	20	42	42
Integral dipole field	0.2-2.0 Tm	1.6-7.6 Tm	0.5-5.0 Tm
Number of quadrupoles	20	42	42
Integral gradient	0.8-7.9 T	6.7-31.4 T	2.1-20.6 T
Drift length	4.0 m	12.0 m	12.0 m
Repetition rate	0.5 Hz	0.33 Hz	0.33 Hz
Horz./vert. aperture	40x40 mm^2	80x80 mm^2	110x110 mm^2

Table 6.6.: Parameters used for the comparison of energy consumption versus magnetic rigidity. The chosen parameters of the exemplary beam-transfer lines are fictitious but shall reflect typical values for each kind of transfer-line type. All parameters are fixed except for the magnetic rigidity and the integral dipole field respectively the integral gradient, which both depend on the magnetic rigidity. Furthermore, the horizontal and vertical emittance vary due to adiabatic damping.

to the high currents necessary to generate the field within the larger aperture, HCP magnets have a considerably higher energy consumption compared to the electron beamline. The behaviour of the energy consumption as a function of the repetition rate, which is illustrated in figure 6.2(c), is similar for the heavy-ion beamline. The absolute values are higher due to the larger apertures.

Summarising, two relevant ranges of the repetition rate exist: For low repetition rates up to 0.1 Hz, the NC magnets and the PM-NC magnets are energy efficient. Depending on the aperture size, HCP magnets are an option, as well. For higher repetition rates up to 1 Hz, the NC magnets and the PM-NC magnets are efficient (especially for the exemplary electron beamline) as long as they are operated in AC mode. The SC magnets and the SF magnets are more efficient for repetition rates higher than 1 Hz.

6.2.3 Energy Consumption versus Magnetic Rigidity

In this last section on comparing the energy consumption of different magnet types, the energy consumption as a function of the magnetic rigidity will be discussed. The beamlines' parameters are listed in table 6.6 and the plots are shown in figure 6.3. For each point in the plots, the energy consumption for especially the investigated value of the magnetic rigidity is calculated. This means that the data in this section are only valid for beamlines, which transport only beams with a fixed magnetic rigidity and not different beams with a variation of the magnetic rigidity. As the emittance depends on the magnetic rigidity due to adiabatic damping, the ratio of acceptance and emittance A/ϵ is not constant; and therefore, the transfer efficiency can differ like it does in the comparison in section 6.2.1. As the integral dipole field and the integral gradient increase with increasing magnetic rigidity, this section is also about the estimated energy consumption as a function of the integral dipole field respectively the integral gradient or furthermore the field strengths and magnet lengths.

The lowest estimated energy consumption of the exemplary electron beamline, which is illustrated in figure 6.3(a), is reached with HCP magnets. Due to the small aperture and the range of low magnetic rigidities in this example, the magnets do not reach their full load and the necessary field strengths can be generated highly energy efficient. This solution is followed by the NC magnets and the PM-NC magnets, which both have nearly identical energy consumption. These magnets reach their maximum value for the field strengths; and therefore, they are scaled in length to reach the required integral values. This yields a linear increase in energy consumption. The estimated energy consumptions of the SC magnets and the SF magnets are higher compared to the other solutions in this example. Here, SF magnets have a higher estimated energy consumption than SC magnets. This accounts for the fact that the SF magnets reach their limit on the magnetic field strength and grow in the magnet length while the SC magnets have a higher maximum field and increase the current further. Therefore, the load of the SC magnets is less than that of the SF magnets. The high energy consumption of both magnet types can be affiliated to the high power loss of the cryogenic cooling system.

Figure 6.3(b) shows the behaviour of the energy consumption for the exemplary proton machine. Here, the NC magnets and the PM-NC magnets are the most energy efficient solutions for the lower part of the investigated range of magnetic rigidity. For higher values of the magnetic rigidity, the SC magnets and the SF magnets become similar efficient or even more efficient. In fact, the SF magnets' model can yield a negative slope. This negative slope can be explained by the fact that the heat loads of the connection cryostats are higher than the heat loads of the magnets (c.f. table 4.1). Hence, for higher integral field strengths, the magnets become longer and the cryogenic cooling system's energy consumption decreases while the magnets reach their maximum field strength; and thus, the power converter losses are constant. The SC magnets can become more interesting for further increasing values of the magnetic rigidity, e.g., if the SF magnets would be too long to fit into the drift space. The SC magnets' energy consumption increases only that much until the maximum field strength is reached for both quadrupole and dipole magnets. Beyond this point, the energy consumption is almost constant like for SF magnets. HCP magnets have a higher energy consumption due to the high currents necessary for the high fields at large values of the magnetic rigidity.

The estimates for the heavy-ion example are similar to the estimates for the proton example. But in this example, also smaller values of the magnetic rigidity are investigated. In the lower end of this range, the HCP magnets are an alternative for the NC magnets and the PM-NC magnets because the HCP magnets' maximum field strength is not reached in this range; and thus, the load is low.

In general, it can be summarised that for small values of the magnetic rigidity the NC magnets, the PM/PM-NC magnets and the HCP magnets are efficient. For large values of the magnetic rigidity, high field strengths are necessary, which require high currents; and therefore, for this field of application the SC magnets and the SF magnets are efficient because of their absence of resistive losses.

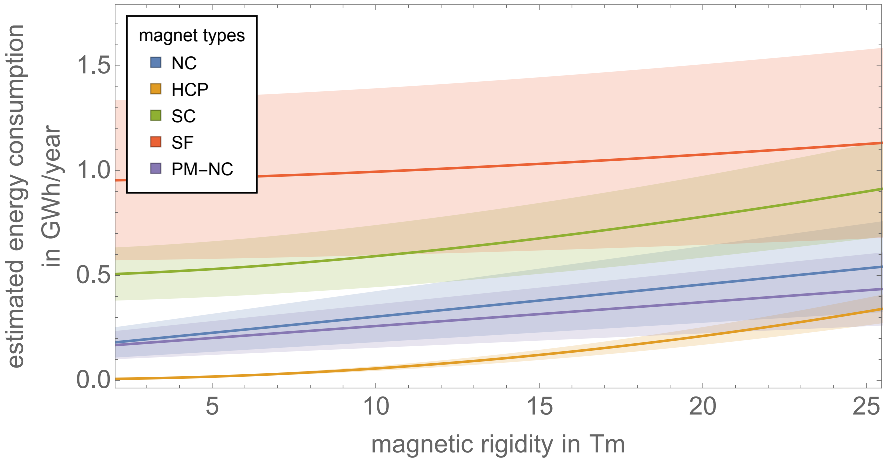

(a) Estimated energy consumption versus magnetic rigidity of an exemplary beamline of an electron accelerator.

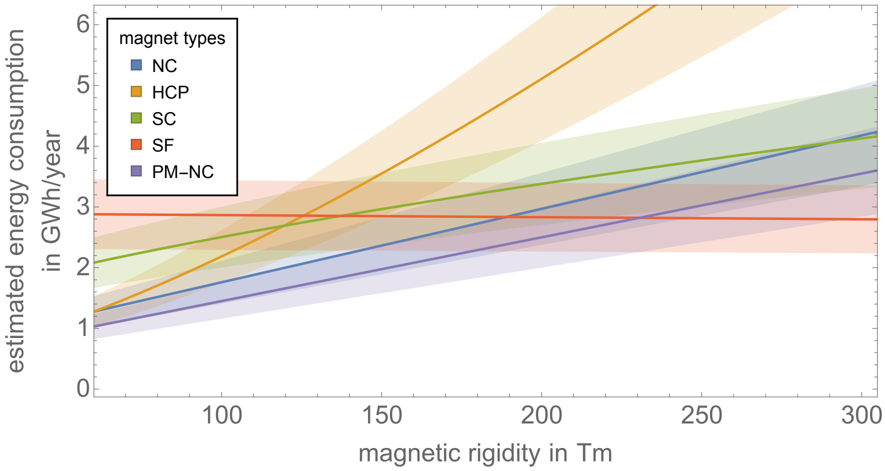

(b) Estimated energy consumption versus magnetic rigidity of an exemplary beamline of a proton accelerator.

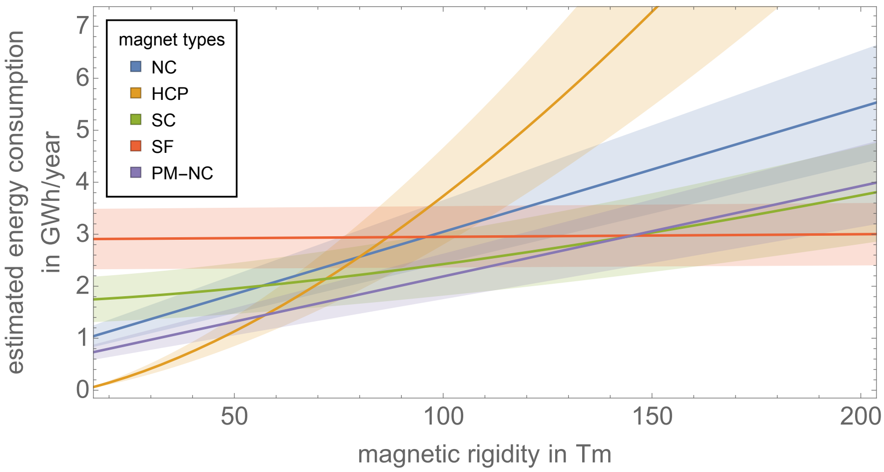

(c) Estimated energy consumption versus magnetic rigidity of an exemplary beamline of a heavy-ion accelerator.

Figure 6.3.: Estimated energy consumption versus magnetic rigidity for an exemplary beamline of an electron accelerator, a proton accelerator, and a heavy-ion accelerator. The parameters for each beamline are listed in table 6.6.

6.3 Conclusion on Energy Consumption Comparison

To summarise this chapter, the different magnet types' possible fields of application with respect to aperture size, repetition rate, and magnetic rigidity are listed here:

- **NC**: small and medium apertures (up to about 50 mm aperture radius), low and medium repetition rates (up to 0.1-1 Hz, higher repetition rates only if AC operation is possible), applicable for magnetic rigidities common for electron machines like synchrotron-light sources, proton machines and heavy-ion machines.
- **SF**: large apertures (greater than 50 mm aperture radius), DC operation efficient for high repetition rates (higher than about 1 Hz), AC operation can be efficient for low repetition rates, applicable for high-energy accelerators.
- **SC**: large apertures (greater than 50 mm aperture radius), DC operation efficient for high repetition rates (higher than about 1 Hz), AC operation can be efficient for low repetition rates, applicable for high-energy accelerators; especially for very high values of the magnetic rigidity, the SC magnet design is more compact than the SF magnet design.
- **HCP**: small apertures (up to about 30 mm aperture radius), low repetition rates (up to 0.1-0.5 Hz, higher repetition rates only possible with additional cooling), applicable for magnetic rigidities common for electron machines and medium energy proton machines or heavy-ion machines (up to about 50 Tm), high gradients are possible.
- **PM**: only applicable for single particle energy like in a synchrotron-light source or straight beamlines, aperture is limited due to manufacturing issues (up to 30-40 mm aperture radius), applicable for magnetic rigidities common for electron machines, proton machines and heavy-ion machines, sensitive to radiation.
- **PM-NC**: aperture of the PM magnets is limited due to manufacturing issues (up to 30-40 mm aperture radius), low and medium repetition rates (up to 0.1-1 Hz, higher repetition rates only if AC operation is possible), applicable for magnetic rigidities common for electron machines, proton machines, and heavy-ion machines.

7 Comparison of Total Costs

In this chapter, the total costs of the different magnet types are compared on the basis of case examples of exemplary transfer channels. These are modelled on the requirements of existing accelerator facilities and represent upgrade options or general possible savings. The total costs for the different magnet systems following from the investment costs and the operation costs will be calculated. The bands around the cost estimates indicate the errors of the investment costs and the uncertainties of the operation costs described in chapter 5. To cover a wide field of application, examples of a transfer lines in an electron accelerator, a proton accelerator, and heavy-ion accelerators with different aperture sizes are given. Only the periodic FODO part of the beamline is considered. Matching parts at the start and at the end of the beamline are not considered.

7.1 Electron-Accelerator Facilities

The first example is a fictional beam-transport line from PETRA III to the HERA tunnel at DESY [39]. An electron beam with a horizontal and vertical emittance of 2.0 μm mrad and a fixed magnetic rigidity of 20 Tm is assumed. The aperture of the beamline shall be 35x35 mm^2. The total deflexion angle is assumed to be about 75°. The total transfer length of 207 m and

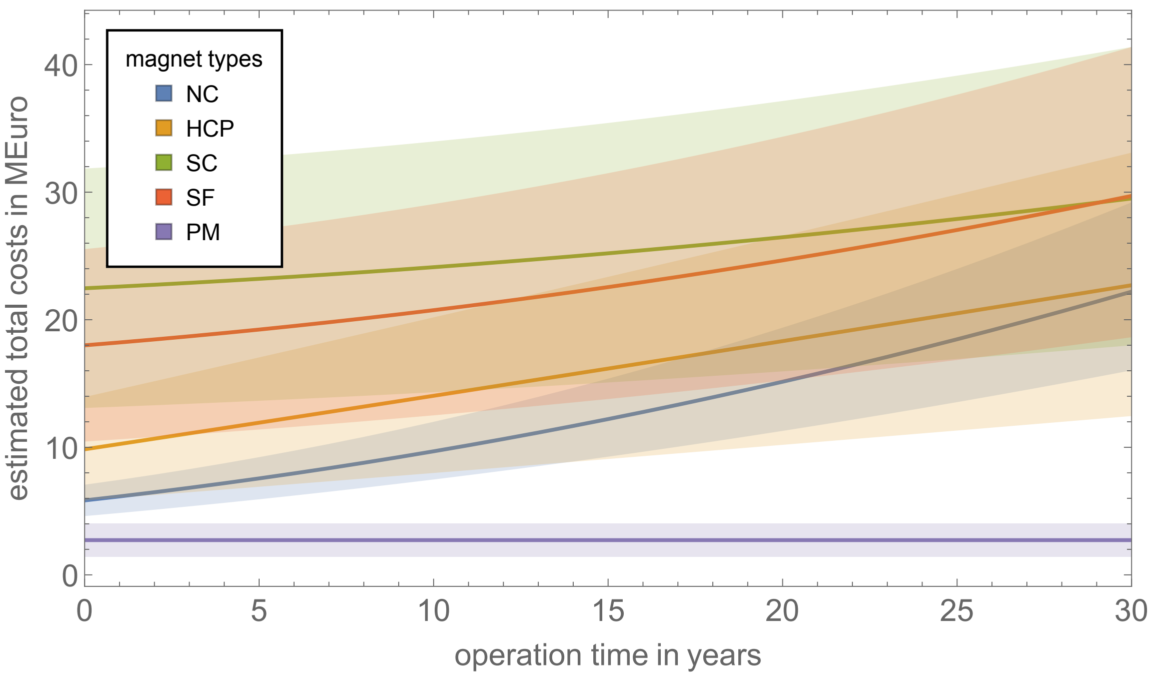

Figure 7.1.: Estimated total costs of NC, HCP, SC, SF and PM magnet systems for a fictional electron beamline from PETRA III to the HERA tunnel at DESY. The beamline parameters are described in section 7.1.

the drift length between the quadrupoles' centers of 4.5 m yield 23 identical FODO cells. The resulting integral gradient is 5.5 T, the integral dipole field is 0.6 Tm. For the repetition rate, a value of 1 Hz is assumed. The estimated total costs of this example are shown in figure 7.1.

As the magnetic rigidity is assumed to be fixed, a completely PM magnet systems can be used. Due to the small aperture and the low field strengths, this is significantly the cheapest configuration in total costs for this example. If variable field strengths are important, e.g., for a wider spectrum of particle energies, a NC solution or a hybrid PM-NC solution is an alternative. The NC magnets have the further advantage of a simple and well-known design. As the estimated total costs are low compared to the other current-based magnet types, the NC magnets are recommendable aside from the PM solution. In this example, the NC magnets are operated in AC mode. For higher repetition rates than the assumed 1 Hz in this model, the magnets switch to DC operation and the operation costs increase. Due to the generally higher investment costs of the SC and the SF magnets even for small apertures, these magnet types have significantly higher estimated investment costs than the other magnet types. Furthermore, it should be stated that much more R&D is necessary for the SF and SC solution, which is not included here but is increasing the real costs further. The SC and SF magnets are operated in DC operation in this example, and thus dynamic losses do not exist. This yields lower operation costs compared to the NC magnets. For very high repetition rates, the SC and SF magnets are the most economic solution for long-term operation.

The HCP solution has medium estimated investment cost in this example. The disadvantage of this configuration is the limited lifetime of the switches at the assumed repetition rate of 1 Hz. The resulting maintenance costs dominate the operation costs. Nevertheless, if this system is equipped with durable switches (eventually R&D is necessary), it can be an alternative, e.g., for high repetition rates, for which the NC magnets are operated in DC mode.

7.2 Proton-Accelerator Facilities

For the exemplary proton beamline, a fictional transfer line from the Main Ring at J-PARC [44] to a fictional future accelerator was chosen. This beamline shall transport a proton beam with a magnetic rigidity of 169.9 Tm. The corresponding horizontal and vertical emittance is 19.2 mm mrad. The beamline's total length is assumed to be 504 m and the total deflexion angle is 60°. The drift length between the quadrupoles' centers is 12.0 m. This yields 21 FODO cells. Following from the aperture size of 80x80 mm^2, the resulting integral dipole field strength is 4.2 Tm respectively the integral gradient is 17.5 T. As a cycle of the Main Ring lasts about 3 s [44], a repetition rate of 0.33 Hz is assumed.

The resulting estimates on the total costs as a function of the operation time are illustrated in figure 7.2. The lowest estimated total costs are obtained with the NC and the PM-NC magnets. The hybrid solution has higher investment costs due to the more expensive PM quadrupoles compared to the NC quadrupoles. In total, the estimates are comparable for an operation time of 30 years. The HCP solution has also investment costs comparable to the NC solution but has significantly higher operation costs. These high operation costs follow from the high current needed to generate the required dipole field strength. As the bands around the estimated total costs of all these magnet types overlap, no clear recommendation can be given; especially for shorter operation times up to about 10 years.

The SC and SF solutions have higher estimated total costs compared to the other magnet types. The difference in the SC and the SF magnets' investment costs result from the different

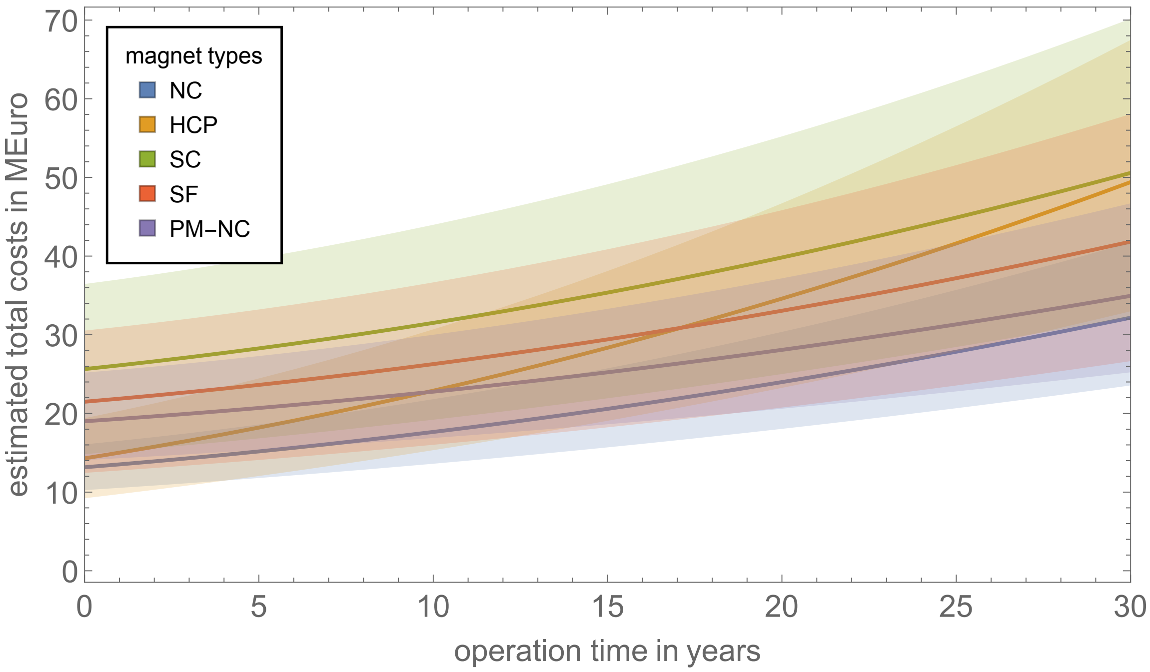

Figure 7.2.: Estimated total costs of NC, HCP, SC, SF and PM-NC magnet systems for a fictional proton beamline from the Main Ring at J-PARC to a fictional future accelerator. The beamline parameters are described in section 7.2.

load of these magnets in this example. The SF dipoles and quadrupoles reach respectively nearly reach their maximum field strength (cf. table 4.3) whereas the SC magnets have a low load due to the higher maximum field strengths. However, the SC magnets have a minimum magnet length of 1 m, which yields long magnets compared to the length following from the required integral field strengths and the magnets' maximum field strengths. As the investment costs scale with the length respectively the magnets' cold mass, the investment costs are higher for longer magnets. Furthermore, the operation costs are little higher for the SC solution due to the longer magnets. These effects could be compensated, if the minimum magnet length is decreased for the SC magnets. But then the edge fields resulting from the ends of the saddle coil have to be considered, which are neglected in this thesis.

7.3 Heavy-Ion-Accelerator Facilities

As the beamline parameters differ strongly among the fields of application for heavy-ion accelerators, in this section a few different types of heavy-ion beamlines will be discussed. These distinguish themselves in aperture size, emittance and magnetic rigidity.

7.3.1 Heavy-Ion-Accelerator Facilities (Small Aperture and Large Magnetic Rigidity)

The first exemplary heavy-ion beamline is a fictional upgrade of the BNL accelerator facility [46]. A beam-transfer line from RHIC to a fictional future accelerator or an experiment is assumed. For the beam parameters, an emittance range of 0.3 mm mrad up to 0.7 mm mrad and a range of the magnetic rigidity of 400.0 Tm up to 831.8 Tm are assumed. The total transfer length shall

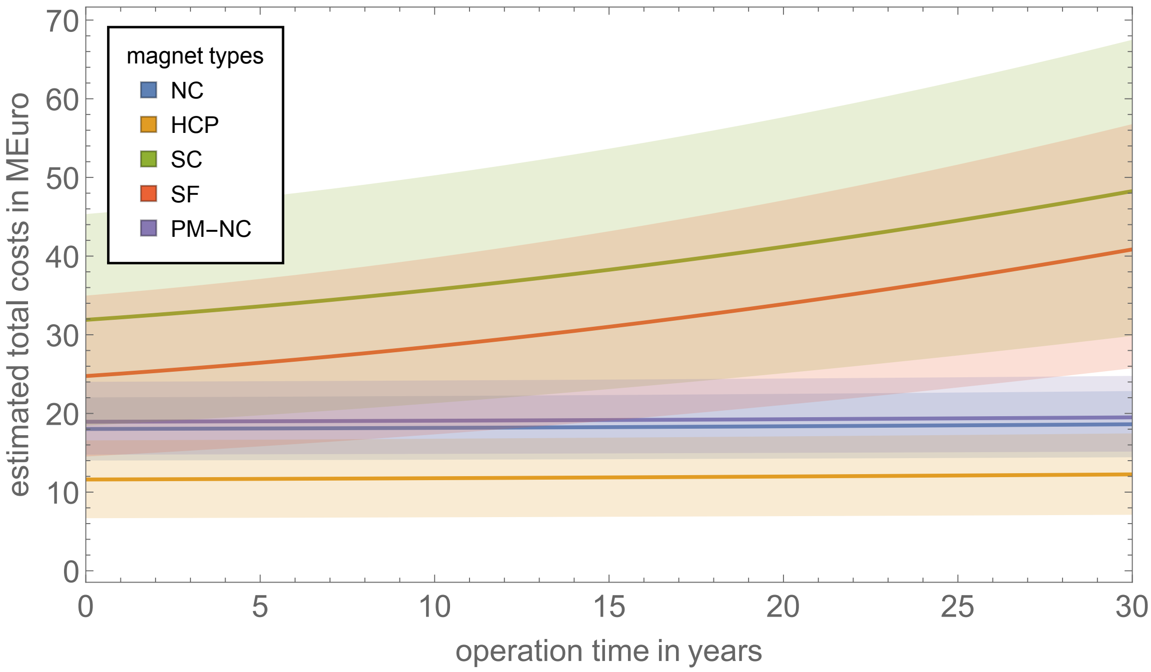

Figure 7.3.: Estimated total costs of NC, HCP, SC, SF and PM-NC magnet systems for a fictional heavy-ion beamline from RHIC at BNL to a fictional future accelerator. The beamline parameters are described in section 7.3.1.

be 750 m and the total deflexion angle shall be 45°. Due to the small emittance, an aperture of 40x40 mm^2 is assumed. This leads to a FODO design with an integral gradient of 33.0 T, an integral dipole field of 13.1 Tm, a drift length of 15.0 m, and a total number of 25 FODO cells. As a RHIC cycle lasts about 135 s [46], a repetition rate of 0.007 Hz results.

Figure 7.3 shows the estimated costs of this fictional beamline. As not only one species of ions is accelerated at BNL but a variety (they include protons, copper ions, or gold ions), and furthermore a large range of magnetic rigidity is assumed, a completely PM magnet system with fixed gradients and fixed dipole fields is not recommendable. Due to the low repetition rate and the small aperture size, HCP magnets as well as NC and PM-NC magnets are more economic than a SC or a SF solution for this example. For this kind of beamline, the HCP magnet system is the most economic solution. The total costs of the NC solution and the PM-NC solution are comparable. Larger values of the total deflexion angle result in higher integral field strengths. As the magnet length is limited due to the limited available space between the magnets, SC magnets – due to large values of the integral gradient respectively the integral dipole field are possible – will become more interesting with increasing deflexion angle, as well.

The significant difference in the SC magnets' and the SF magnets' investment costs is an effect of the used model. On the one hand, this difference follows from the differing loads as mentioned in the proton example. The quadrupole magnets of both the SC magnets and the SF magnets do not reach their full load whereas the dipole reach their maximum field strength allowed in the model. Thus, the SF quadrupole magnets are cheaper as they are shorter than the SC quadrupole magnets. On the other hand, the SC dipole magnets have a heavier cold mass compared to the SF magnets following from the higher field strengths and the resulting magnetic shielding used in the model. Hence, the investment costs of the SC dipole magnets

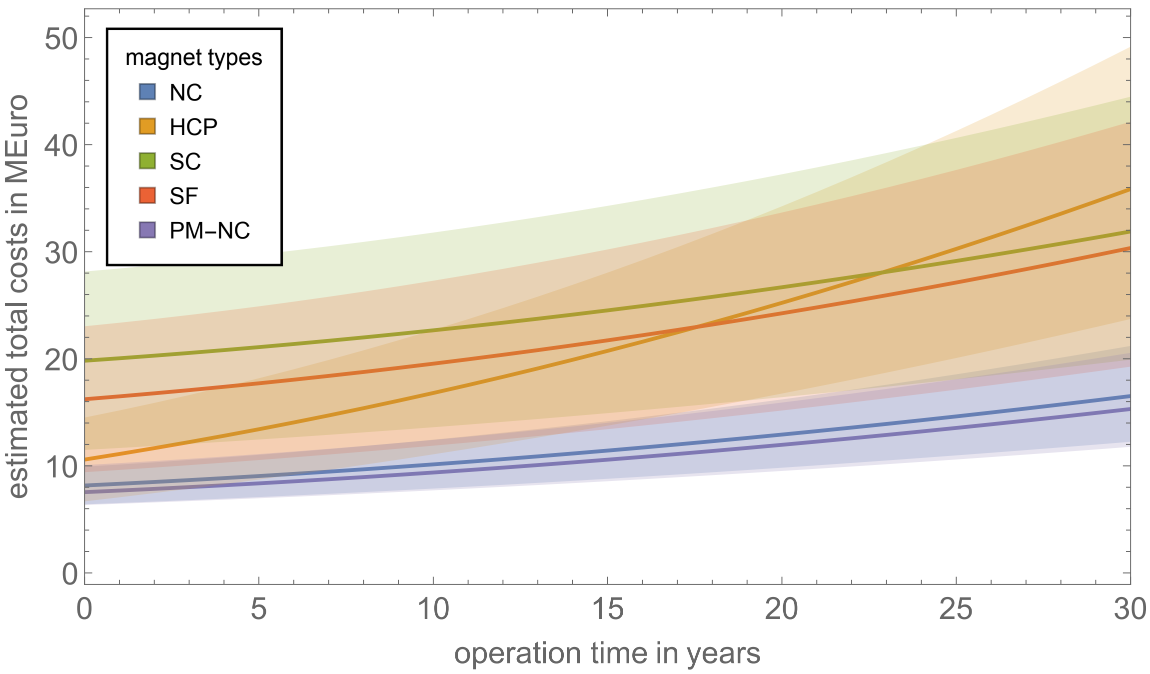

Figure 7.4.: Estimated total costs of NC, HCP, SC, SF and PM-NC magnet systems for a heavy-ion beamline from the SIS100 at FAIR to a target or an experiment. The beamline parameters are described in section 7.3.2.

are higher although their yoke is shorter than the one of the SF magnets. The investment costs of the cooling system are higher for the SC magnets due to the heavier cold mass, as well.

7.3.2 Heavy-Ion-Accelerator Facilities (Medium Aperture and Large Range of Magnetic Rigidity)

In this example, a beam-transfer line at FAIR is examined. This beamline could connect the SIS100 with an experiment target [43]. The beam parameters differ among the different accelerated ion species. To consider this in the calculations, a horizontal emittance range of 6.3-35.0 mm mrad, a vertical emittance range of 2.2-12.0 mm mrad, and a magnetic rigidity range of 18.0-100.0 Tm are assumed. The aperture is assumed to be elliptical and has a size of 100x60 mm^2. This requires an integral gradient of 2.5 T, an integral dipole field of 3.1 Tm, and a drift length of 9.0 m. The beamline in this example shall have a total length of 306 m and the total deflexion angle shall be 60°. Furthermore, the FAIR facility is designed for parallel operation of different experiments. As this cannot be considered in the model, a fixed repetition rate of 0.33 Hz is assumed to approximate an average operation. This follows from the SIS100's cycle lengths varying from about 0.2 s up to about 4.2 s [43].

The resulting estimates on the total costs as a function of the operation time are illustrated in figure 7.4. As a variety of different ions are accelerated at FAIR, a completely PM magnet system is not recommendable. The NC and the PM-NC magnets are recommendable for this type of beamline due to the lowest total costs and also the simple magnet design. The SF magnets and the SC magnets are less efficient. The difference in the investment costs is again resulting from the minimum magnet length of 1 m in the model of the SC magnets. Both the SC magnets and the SF magnets also need a complex cooling system, which is a further disadvantage compared to the NC solution. Due to the large aperture size requiring high currents, the HCP magnet system also has higher estimated total costs. Of course, the HCP magnets can only be used in the parts of the beamlines, which are not used for the transfer of slow extracted beams.

In reality, the transfer lines at FAIR do not have a uniform curvature. Thus, the dipole magnets are not all equal. This results in more than one dipole and one quadrupole design for each magnet type, and also more than one power-converter design for each type. These points cannot be covered by the model in this thesis. Furthermore, it is desired to control every quadrupole magnet individually as the optics is no real FODO lattice. Thus, every quadrupole needs its own power converter. But this is an issue especially for the superconducting magnets as in the model is only one magnet family is assumed for both the dipoles and the quadrupoles. An individual control of the magnets would lead to a significantly more complex design of the cryogenic infrastructure with respect to the large number of current leads and the large number of superconducting cables in the cryostat. This also result in additional heat loads in the cryogenic cooling system, which are not considered in the model. Thus, the total costs of this exemplary beamline should be higher than the estimates in this model; especially for the SC magnets and the SF magnets.

7.3.3 Heavy-Ion-Accelerator Facilities (Large Aperture and Small Magnetic Rigidity)

In a last example, a beam-transfer line similar to the Super-FRS at FAIR will be investigated. This beamline is positioned behind the production target, and therefore the emittance of 125.7 mm mrad is relatively large [47]. Moreover, all fragments shall be transported. This requires a large acceptance of the transport system. Thus, this beamline requires very large apertures of 380x200 m^2. The secondary particles have a magnetic rigidity of 20 Tm [47] in this example. The total deflexion angle of the 304 m long transfer channel is about 180°. Considering a drift length of 8.0 m, 19 FODO cells result. The integral dipole field strength is 1.7 Tm, the integral gradient is 3.1 T. The assumed repetition rate of 0.25 Hz results from the SIS100's cycle length of about 4 s for Super-FRS operation [43]. However, the Super-FRS is designed as a DC operated machine, which is supplied with a slow extracted beam from SIS100. A duration of the transfer of 2 s is assumed.

As the Super-FRS is a beamline for secondary particles behind a production target, it should be stated that the high-radiation environment requires a radiation hard magnet design, which differs from the introduced models. Therefore, the real total costs can deviate from the estimates due to a more complex design. To be compatible with the high-radiation environment, the Super-FRS at FAIR consists of a radiation hard NC part in the beginning of the beamline and a SF part. But such a hybrid beamline consisting of NC and SF magnets cannot be simulated with the model.

The resulting estimates on the total costs as a function of the operation time are illustrated in figure 7.5. The most energy efficient solutions are the SC one and the SF one. A clear recommendation cannot be given due to the nearly identical estimated total costs. The magnets' large aperture requires high currents to generate the magnetic field. Hence, superconducting magnets have an advantage over the other magnet types due to the absence of resistive losses in the magnets. Both the SC and the SF magnets are operated in DC mode in this example. NC magnets have comparable investment costs as the SC and the SF magnets have but have significantly higher energy consumption due to the slow extraction. As in this example a fixed

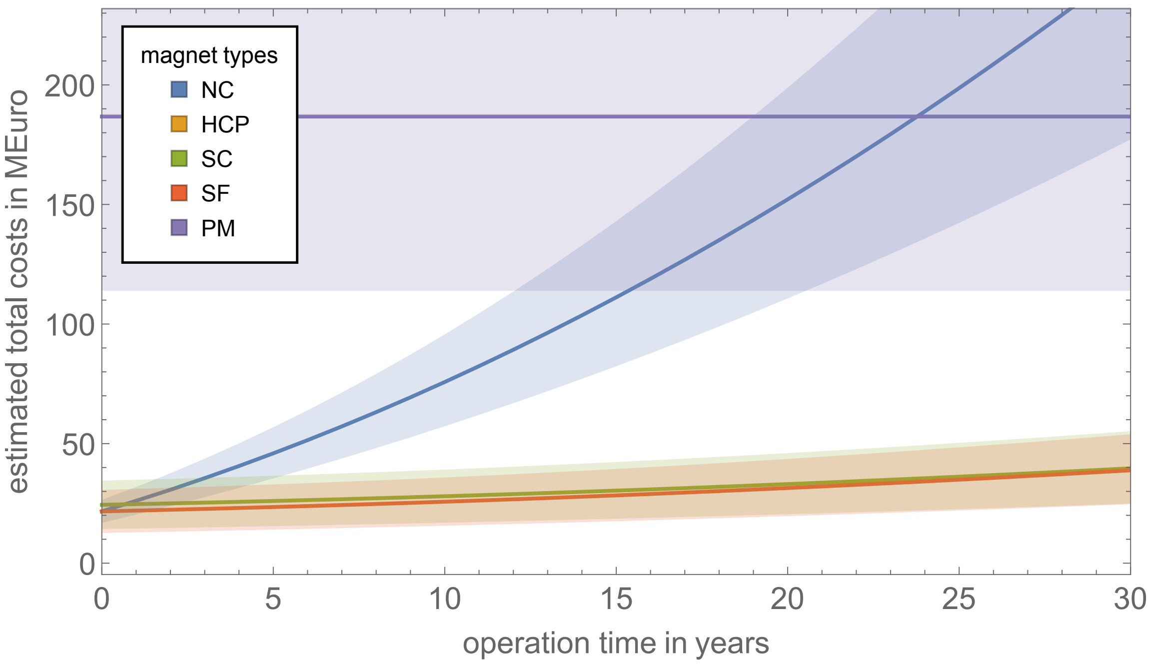

Figure 7.5.: Estimation of the total costs of NC, HCP, SC, SF and PM-NC magnet systems for a heavy-ion beamline similar to the Super-FRS at FAIR. The beamline parameters are described in section 7.3.3.

magnetic rigidity of 20 Tm is assumed, PM dipole magnets and quadrupole magnets can be used. The PM solution has significantly higher investment costs than the other magnet types due to the large amount of PM material necessary to generate the magnetic field. Probably, manufacturing issues occur for those large apertures needed and the magnets cannot be manufactured in this size anyway. Furthermore, the radiation hardness of PM magnets is rather poor. The HCP magnets are not compatible with the slow extraction, and thus cannot be used for this type of beamline.

8 Conclusion

8.1 Summary on Energy Consumption and Total Operation Costs of Different Magnets

The requirements of accelerator facilities strongly differ among the different fields of research and the accelerated particles. Thus, a generalised recommendation valid for every accelerator facility is barely possible. Too many parameters affect the operation and investment costs, which cannot be modelled in detail. Therefore, the model has to be more detailed to ensure more detailed investigations. Of course, a general recommendation, which is given in this deliverable report, cannot replace a detailed investigation of the magnet system for a specific accelerator facility. Therefore, further examinations have to follow for every individual case before a definitive recommendation can be given.

Nevertheless, it was found that more or less reasonable setups exist for the common fields of application in electron accelerators, proton accelerators, and heavy-ion accelerators. Of course, it is not possible to cover the full spectrum of accelerator facilities; especially facilities with special requirements, such as high radiation environments, high beam intensities, high repetition rates, or large acceptances, yielding large aperture sizes, are hardly possible to model sufficiently detailed. However, two ranges for the repetition rate were found, in which certain magnet types show significantly less total costs than others. These ranges are slow operation – i.e. with a repetition rate lower than 0.1 Hz – and fast operation – i.e. with a repetition rate above about 1 Hz. Between 0.1 Hz and 1 Hz, the magnets' operation mode is relevant: For example, the NC magnets are rather efficient when operated in AC mode, while the SC or the SF magnets are rather efficient in DC mode. A similar behaviour was found for the magnetic rigidity. Two ranges exist, in which a recommendation is partially possible – a small value of the magnetic rigidity of up to 10 Tm and a value of the magnetic rigidity larger than about 100 Tm. In the range between these values, often no significant difference in total costs is existent. Especially in the ranges for the repetition rate and the magnetic rigidity, in which no clear recommendation is possible, a more detailed investigation is necessary for every individual machine. For DC operation and small values of the magnetic rigidity, NC magnets or PM respectively PM-NC magnets – if manufacturable – are economic independently from the aperture size. For larger values, the SF magnets and the SC magnets are the most economic solution. It should be mentioned that SC magnets are often less efficient than SF magnets for small apertures or small values of the magnetic rigidity in the model. This can be explained with the SC magnets' low load. These magnets can also be suitable, if a shorter minimum magnet length than chosen in this model is used. The HCP magnets are especially applicable for very low repetition rates. The results of the study on the total costs of the different magnet types are summarised in table 8.1.

Furthermore, it was shown that the ion optical lattice primarily depends on the beam's emittance and the magnetic rigidity. For the design of the quadrupole magnets, it is important to know what the smallest value of the magnetic rigidity is. If the transport line is constructed for this value, the quadrupole magnets will transport beams even with larger magnetic rigidities. This was shown in chapter 3. Of course, this is valid for the quadrupole magnets only.

Dipole magnets with a fixed field strength would deflect particles with varying magnetic rigidities strongly different.

8.2 Outlook

The energy consumption as well as the investment costs depend on significantly more aspects than can be considered in this thesis. For the magnet models only a generalised standard type was introduced for every magnet technology. Other engineering designs exist, which can result in even lower energy consumption, more compact dimensions, or a better suitability in special environments such as high-radiation environments. Hence, an extension of the available magnet types in the model would be a considerable aspect.

Another point, which could be more detailed, is the operation. In the model, two kinds of operations are possible; namely an AC operation and a DC operation. For the AC operation, the duration of the flattop can be adjusted. To calculate the energy consumption, one single mode of operation is assumed during the whole time of operation. Facilities such as FAIR often do not run only one single experiment requiring one single operation scheme but provide a parallel operation of several experiments. Thus, a more flexible operation would be more adequate to model real accelerator facilities. Therefore, a more detailed time structure of the operation is needed for the model, which also considers varying flattop levels to provide a parallel operation of beams with different magnetic rigidities. At the moment, the model only supports one flattop level; and thus, the energy consumption is calculated for the beam's maximum magnetic rigidity. Hence, this is a worst case scenario due to the maximum load of all magnets. A more detailed time structure with various flattop levels would lead to a more realistic estimate; especially in the case of the dipole magnets, which may have a significantly lower energy consumption at lower field strengths.

The largest errors in the total costs arise from the errors assumed for the investment costs. A more detailed model including a dependency on the quantity of the manufactured devices would lead to more precise estimates. This dependency is not included in the current model. Furthermore, the investment costs also differ among the accelerator facility's location. Thus, the values are valid only for facilities in Europe respectively these values are valid especially for GSI. An adaption of costs for construction, assembly, or testing to other countries and currencies is missing in the model.

In the present model, only symmetric FODO structures are considered. Asymmetric structures – either asymmetric geometries or asymmetric field strengths – are not considered. Hence, further investigations could contain other concepts of beam-transfer channels than FODO transport channels, for example, a doublet focussing system or triplet focussing system, or beamlines, which are made of individually controllable magnets. Furthermore, only dipole magnets, quadrupole magnets, power converters, and cooling are considered. Further devices such as steerers, multipole correctors, or beam diagnostics are missing in the model, as well. Hence, the model cannot describe real beam-transport channels in detail and further investigations are necessary.

Transfer line type	Repetition rate	Magnetic rigidity $B\rho$: **Small** ($\leq$10 Tm)	Magnetic rigidity $B\rho$: **Medium** ($>$10 Tm, $\leq$100 Tm)	Magnetic rigidity $B\rho$: **Large** ($>$100 Tm)
Electron beamline (aperture radius 20±5 mm)	**DC operation**	NC or PM-NC; PM for fixed $B\rho$	SF or SC	SF or SC
	High ($\geq$1.0 Hz)	NC or PM-NC in AC operation; PM for fixed $B\rho$	NC or PM-NC; PM for fixed $B\rho$; SF or SC in DC operation	SF or SC in DC operation
	Medium ($\geq$0.1 Hz, $<$1 Hz)	NC or PM-NC; PM for fixed $B\rho$	NC or PM/PM-NC; SF or SC in DC operation; HCP in certain cases	SF or SC in DC operation
	Low ($<$0.1 Hz)	PM for fixed $B\rho$; PM-NC, NC, or HCP for variable $B\rho$	PM/PM-NC or NC depending on $B\rho$; HCP in certain cases	PM/PM-NC or NC depending on $B\rho$; HCP in certain cases
Proton beamline (aperture radius 40±5 mm)	**DC operation**	NC; alternatively PM-NC, if manufacturable	SF or SC	SF or SC
	High ($\geq$1.0 Hz)	NC or PM-NC in AC operation; HCP for lower repetition rates	HCP for lower repetition rates; SF or SC in DC operation	SF or SC in DC operation
	Medium ($\geq$0.1 Hz, $<$1 Hz)	NC; HCP in certain cases; PM-NC, if manufacturable	NC; HCP in certain cases; PM-NC, if manufacturable	SF or SC in DC operation
	Low ($<$0.1 Hz)	NC; HCP in certain cases; PM-NC, if manufacturable	NC; HCP in certain cases; PM-NC, if manufacturable	NC; HCP in certain cases; SF or SC for very high $B\rho$
Heavy-ion beamline (aperture radius 55±10 mm)	**DC operation**	NC; SF or SC; PM-NC, if manufacturable	SF or SC	SF or SC
	High ($\geq$1.0 Hz)	NC; PM-NC, if manufacturable; HCP for lower repetition rates; SF or SC in DC operation (especially for larger apertures)	HCP for lower repetition rates; SF or SC in DC operation (especially for larger apertures)	SF or SC in DC operation
	Medium ($\geq$0.1 Hz, $<$1 Hz)	NC; PM-NC, if manufacturable	NC, PM-NC, HCP, or SF/SC in DC operation depending on $B\rho$	SF or SC in DC operation; NC or PM-NC, if manufacturable
	Low ($<$0.1 Hz)	NC; PM-NC, if manufacturable	NC; HCP in certain cases; PM-NC, if manufacturable	NC; HCP in certain cases; SF or SC for larger apertures or very large $B\rho$

Table 8.1.: Overview on the general recommendations for beam-transport lines of electron accelerators, proton accelerators, and heavy-ion accelerators. These recommendations base on the calculations of the total costs for an assumed time of operation of 20 years. Maintenance costs are not considered, except for the HCP magnets' switches.

A Investment Costs

A.1 Magnets

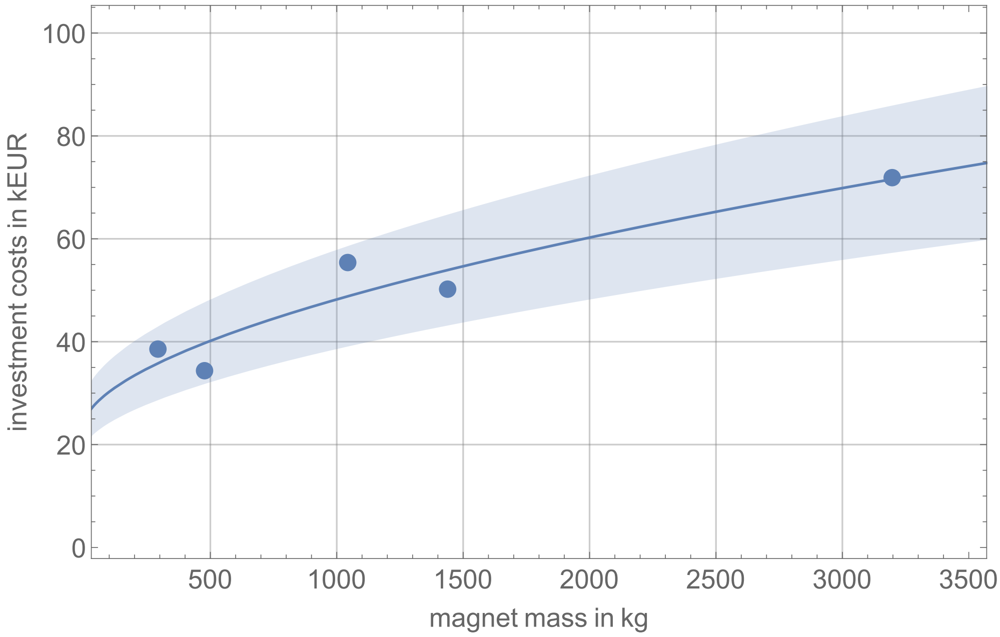

(a) Investment cost of NC quadrupoles as a function of the magnet mass.

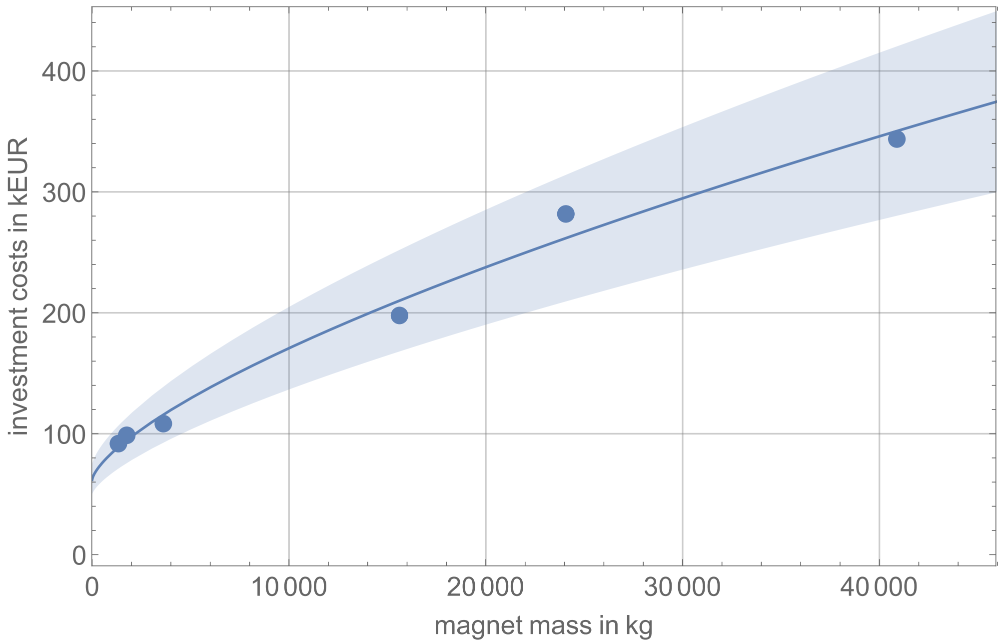

(b) Investment cost of NC dipoles as a function of the magnet mass.

Figure A.1.: Approximations for the cost estimates of NC magnets [34, 35].

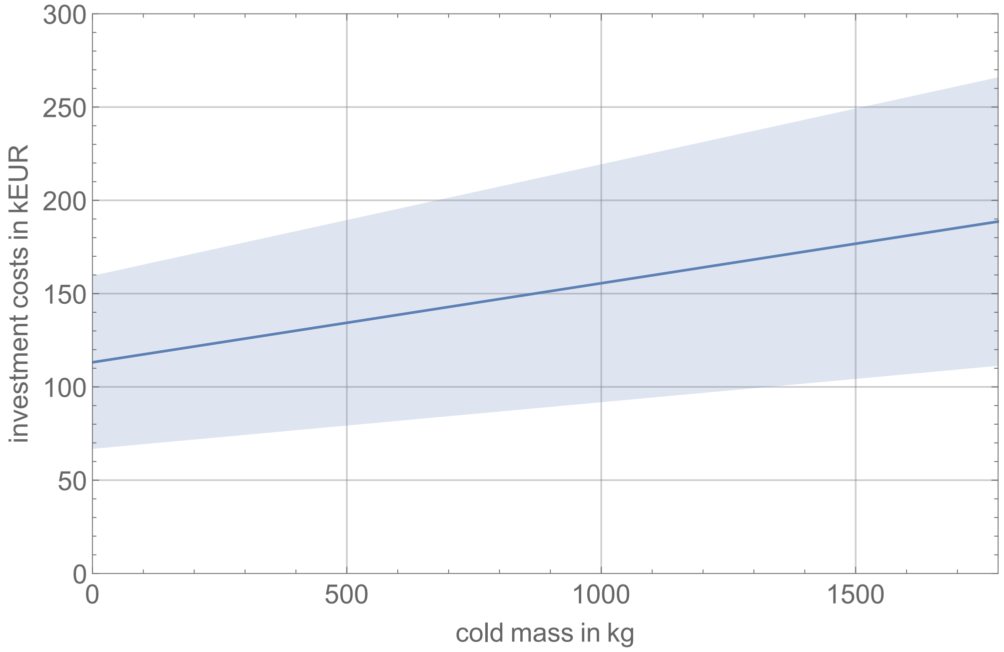

(a) Investment cost of SF quadrupoles as a function of the cold mass.

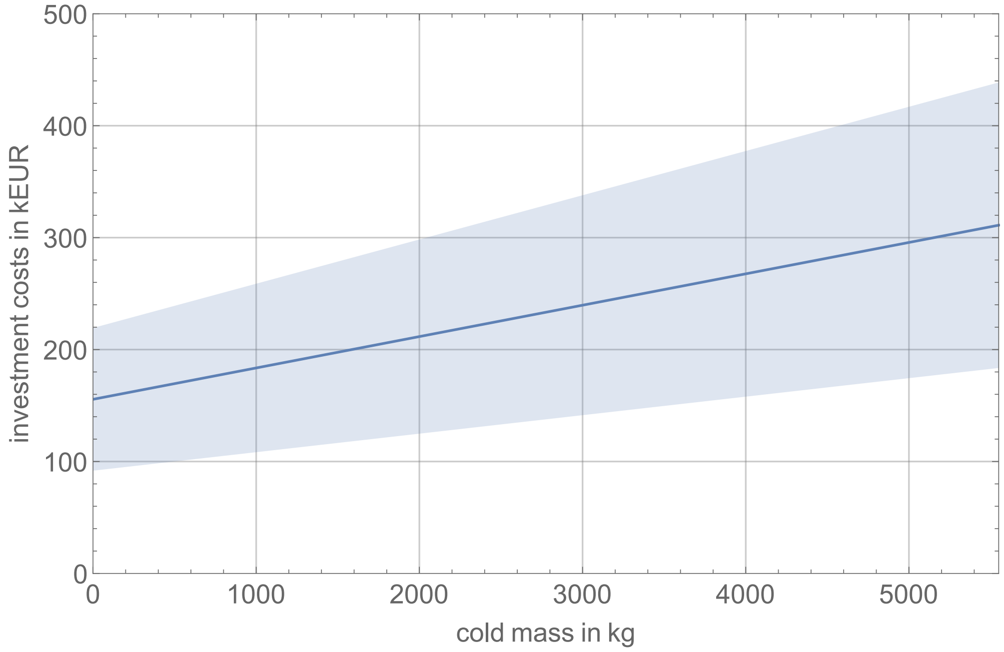

(b) Investment cost of SF dipoles as a function of the cold mass.

Figure A.2.: Approximations for the cost estimates of SF magnets [37].

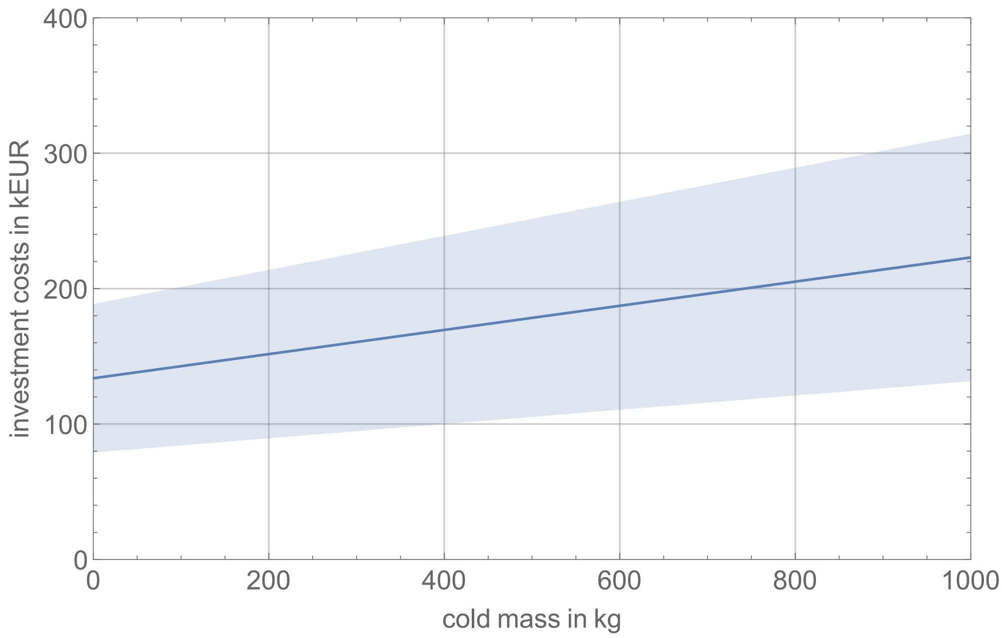

(a) Investment cost of SC quadrupoles as a function of the cold mass.

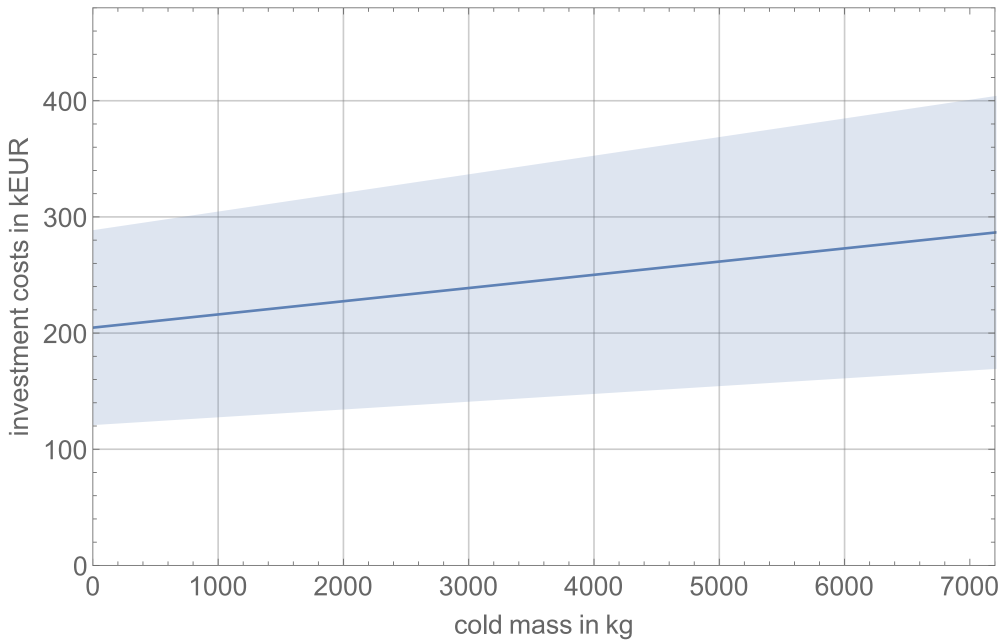

(b) Investment cost of SC dipoles as a function of the cold mass.

Figure A.3.: Approximations for the cost estimates of SC magnets [18].

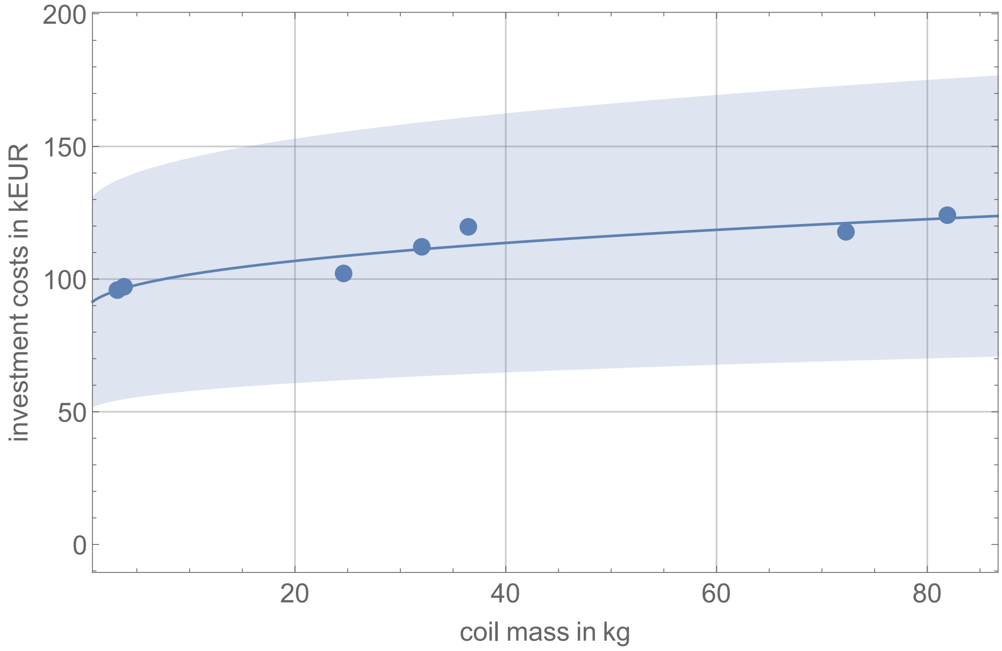

(a) Investment cost of HCP quadrupoles as a function of the coil mass.

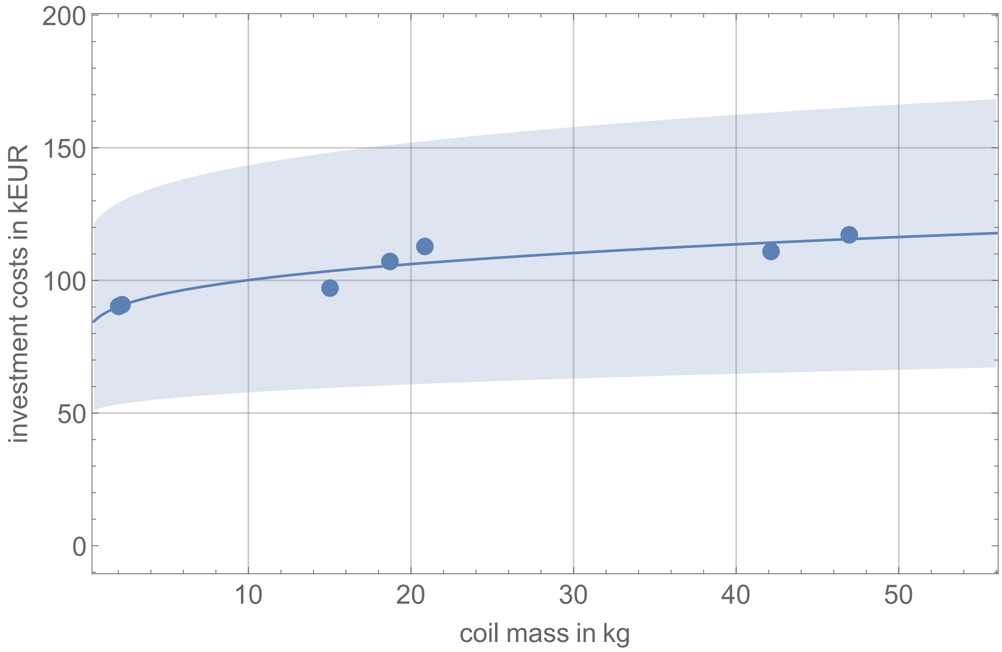

(b) Investment cost of HCP dipoles as a function of the coil mass.

Figure A.4.: Approximations for the cost estimates of HCP magnets including a capacitor bank and a switch [36].

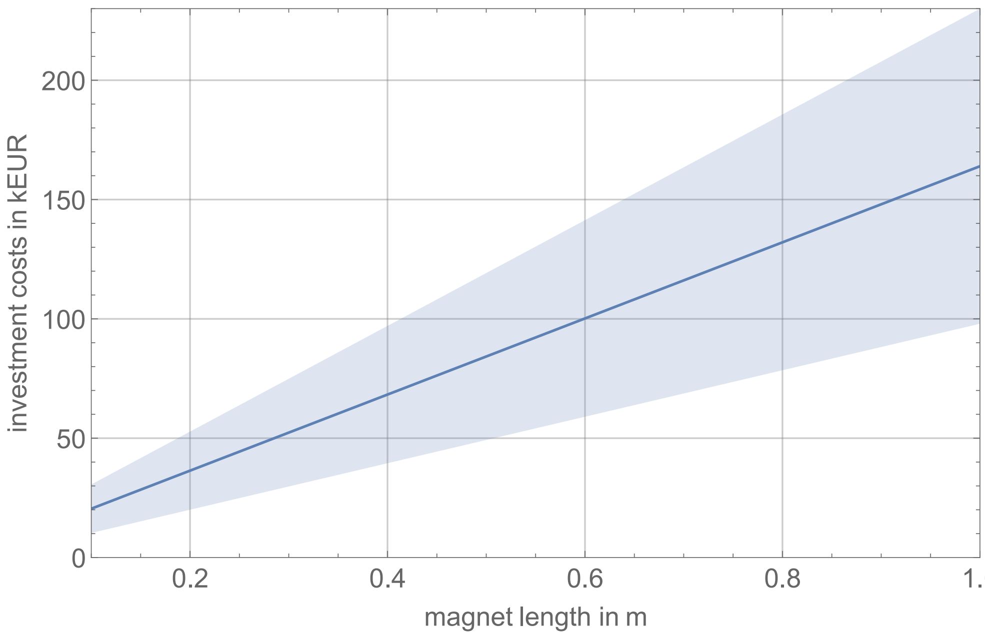

(a) Investment cost of PM quadrupoles as a function of the magnet length for an exemplary pole-tip radius of 25 mm and a pole-tip field of 1.5 T.

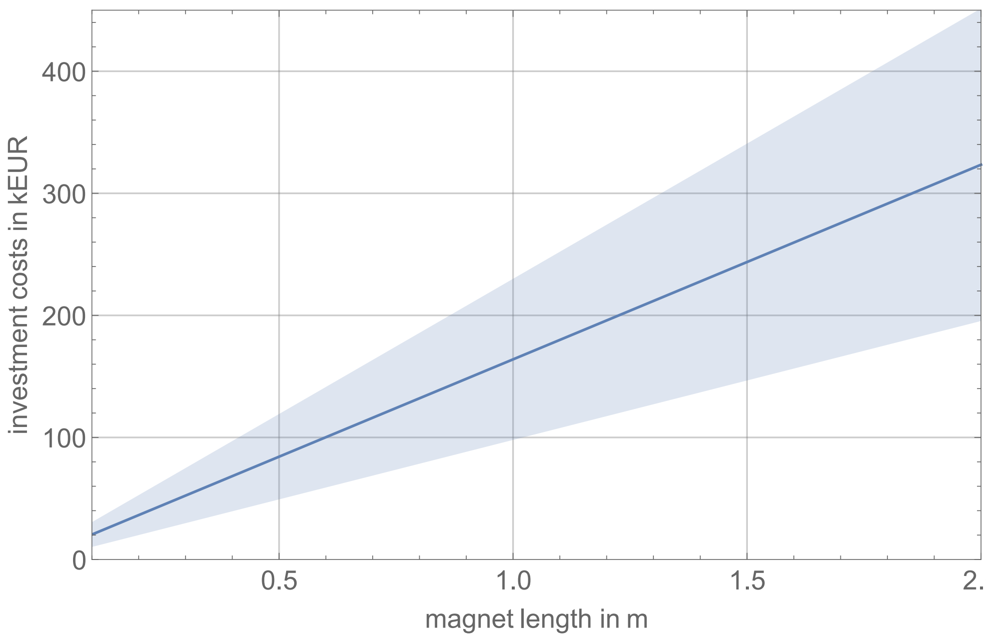

(b) Investment cost of PM dipole as a function of the magnet length for an exemplary pole-tip radius of 25 mm and a pole-tip field of 1.4 T.

Figure A.5.: Approximations for the cost estimates of PM magnets[22, 35].

A.2 Power Converters

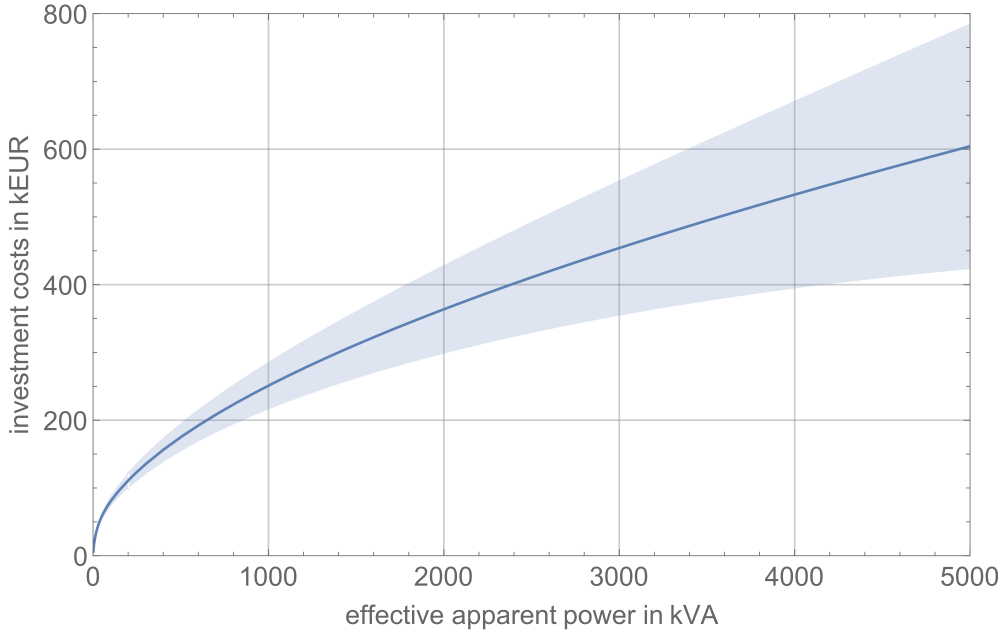

Figure A.6.: Investment costs of SM and SCR power converters as a function of the effective apparent power basing on the estimates calculated at GSI [38].

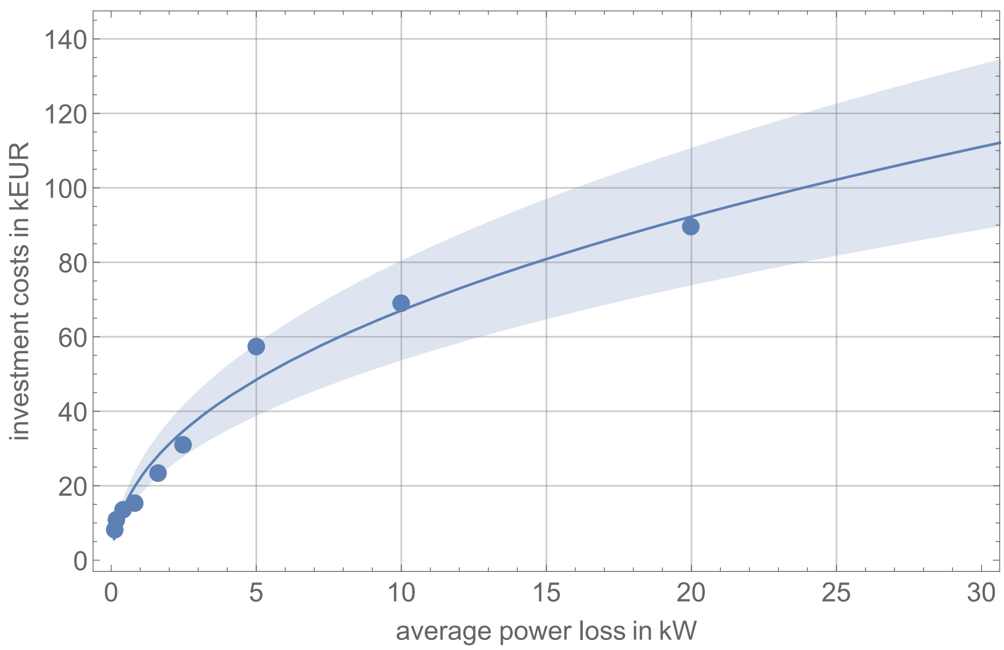

Figure A.7.: Investment costs of capacitor charging high voltage power supplies as a function of the average power loss basing on the price list of FuG from 2015 [29].

A.3 Water Cooling

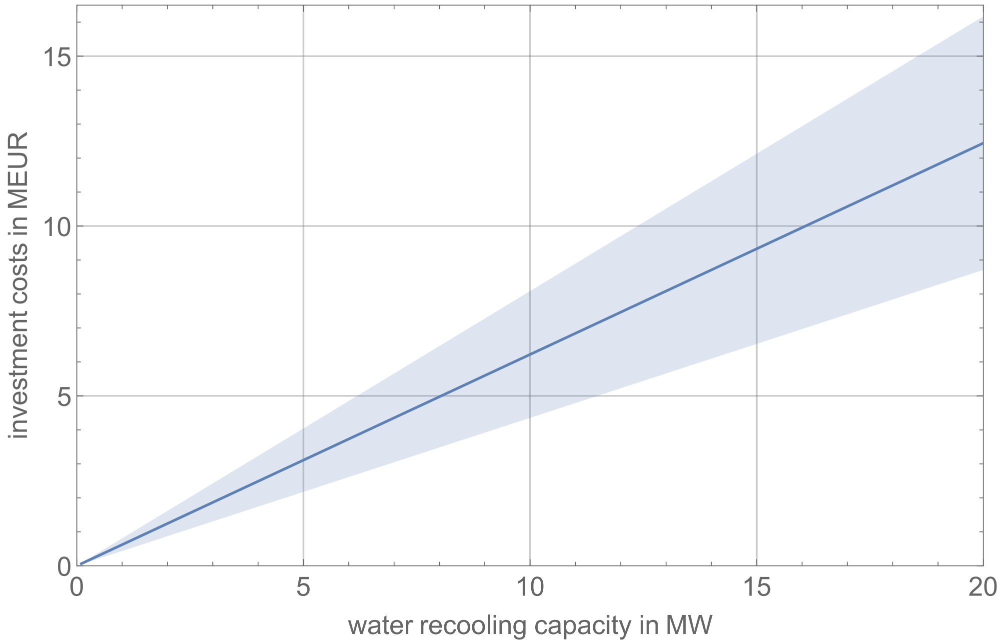

Figure A.8.: Investment costs of the water cooling system as a function of the water recooling capacity [30].

A.4 Liquid-Helium Cooling

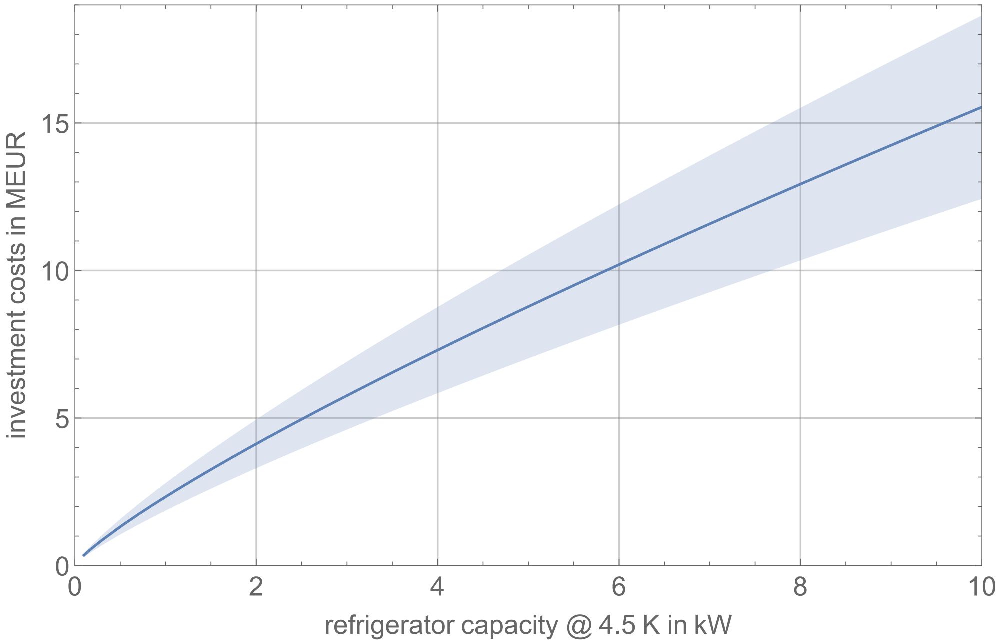

Figure A.9.: Investment costs of the liquid-helium-recooling plant as a function of the system's refrigerator capacity at 4.5 K [14].

B Raw Data for Comparison of Energy Consumption

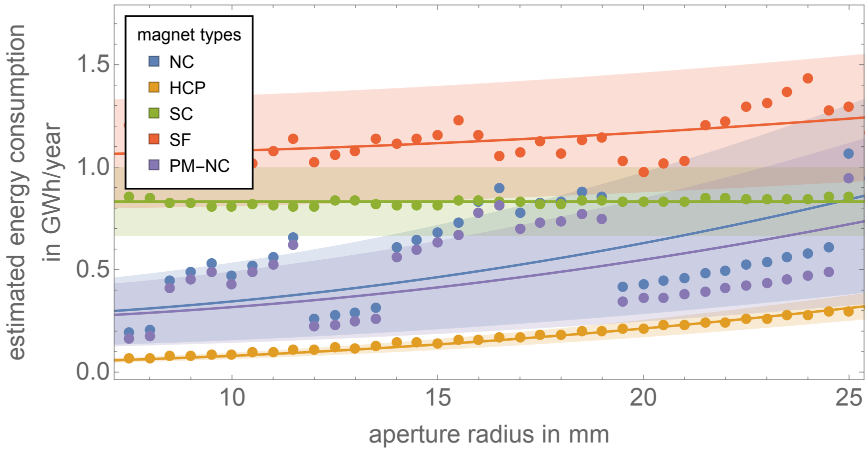

(a) Electron beamline.

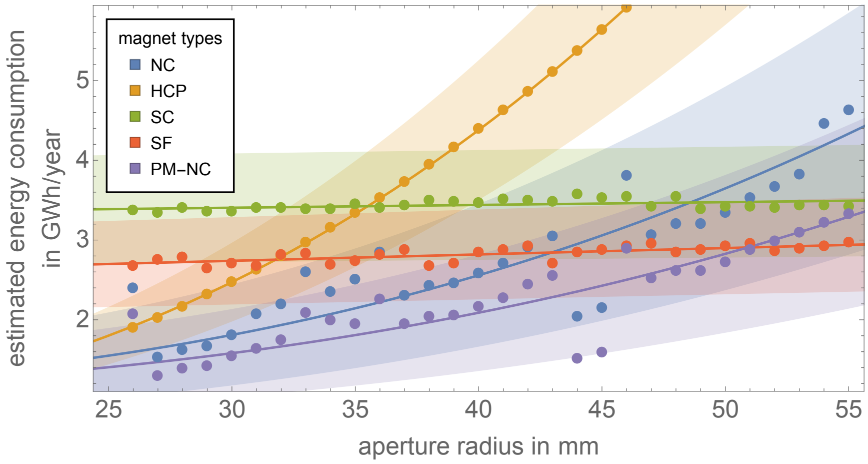

(b) Proton beamline.

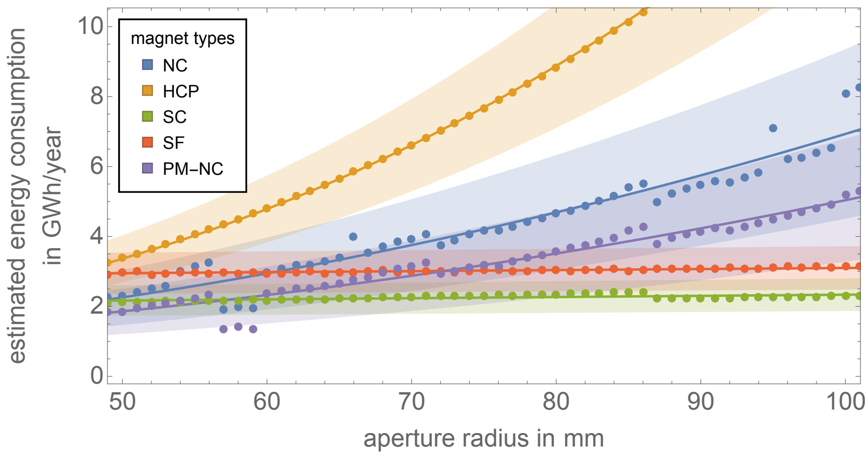

(c) Heavy-ion beamline.

Figure B.1.: Estimated energy consumption versus aperture radius for exemplary beamlines. The parameters for each beamline are listed in table 6.4.

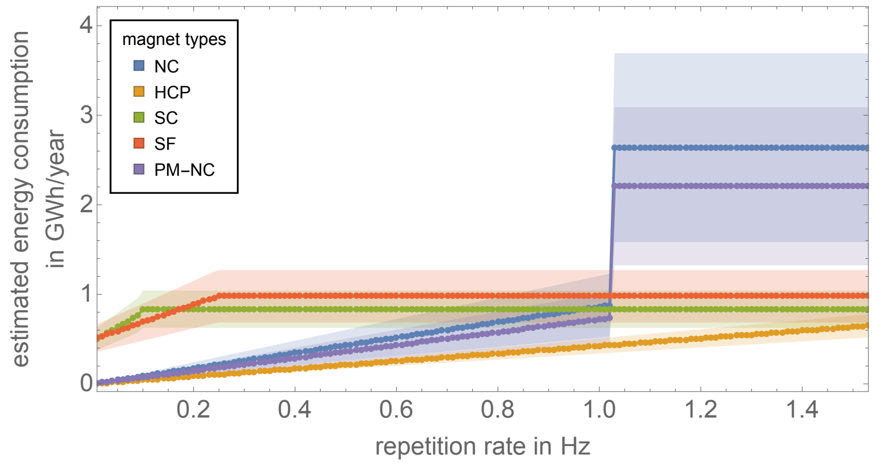

(a) Electron beamline.

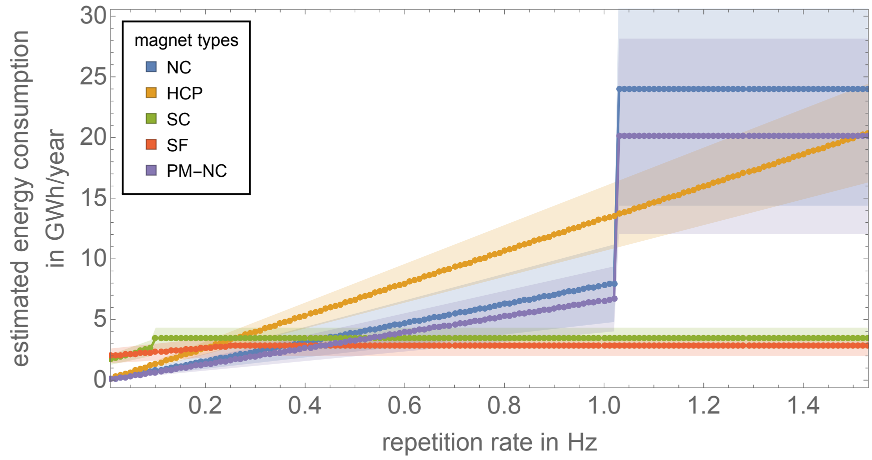

(b) Proton beamline.

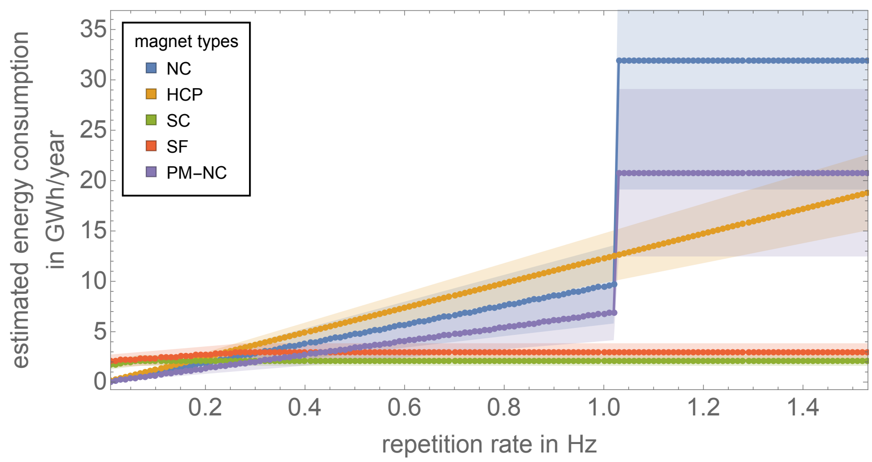

(c) Heavy-ion beamline.

Figure B.2.: Estimated energy consumption versus repetition rate for exemplary beamlines. The parameters for each beamline are listed in table 6.5.

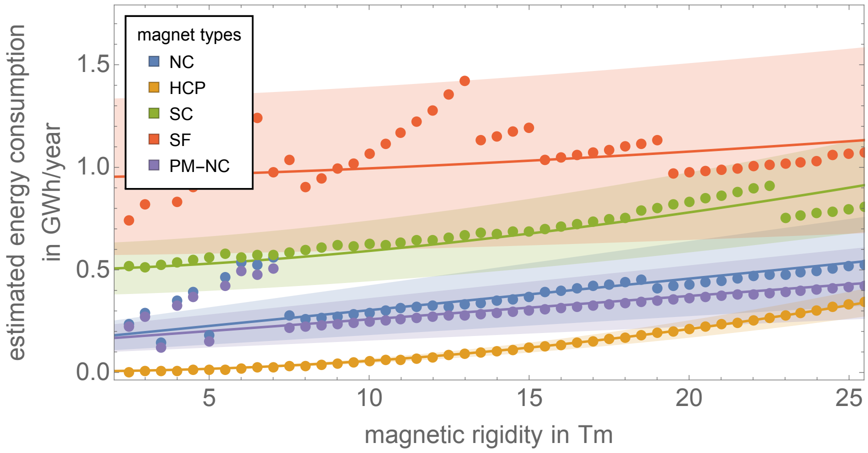

(a) Electron beamline.

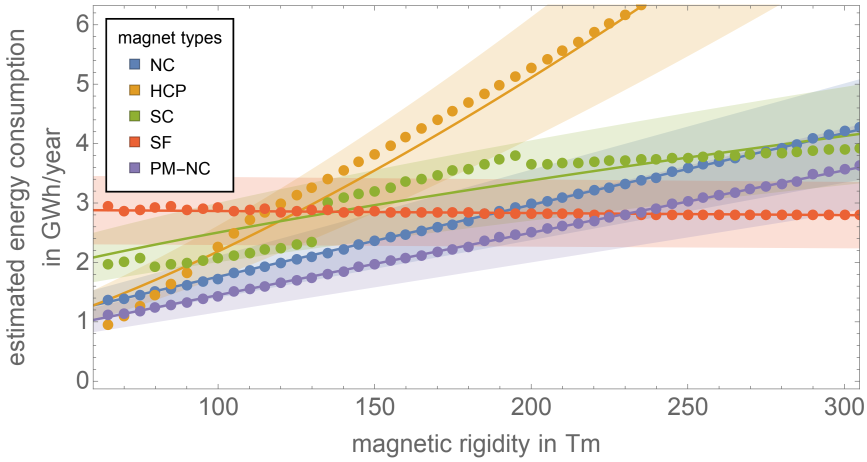

(b) Proton beamline.

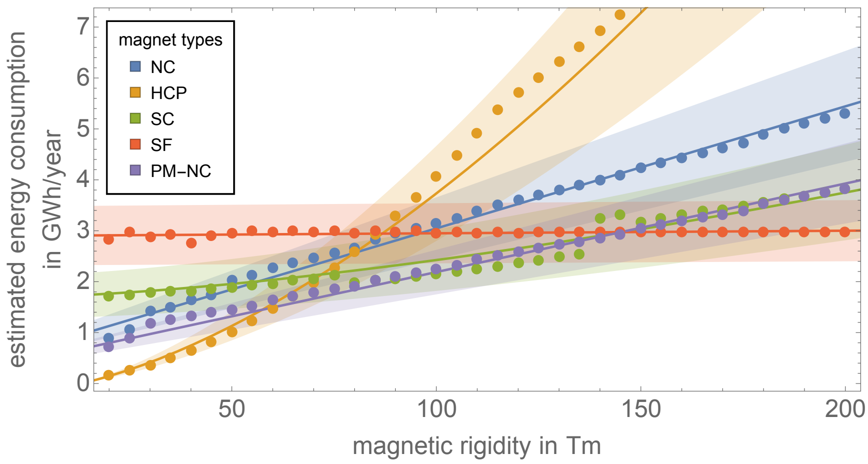

(c) Heavy-ion beamline.

Figure B.3.: Estimated energy consumption versus magnetic rigidity for exemplary beamlines. The parameters for each beamline are listed in table 6.6.

C Glossary

AC	Alternating Current
AGS	Alternating Gradient Synchrotron
BNL	Brookhaven National Laboratory
CERN	Conseil Européen pour la Recherche Nucléaire (European Organization for Nuclear Research)
DC	Direct Current
DESY	Deutsches Elektronen-Synchrotron
EuCARD^2	Enhanced European Coordination for Accelerator Research & Development
FAIR	Facility for Antiproton and Ion Research
GSI	GSI Helmholtzzentrum für Schwerionenforschung GmbH
HCP	High Current Pulsed
HERA	Hadron-Elektron-Ring-Anlage
J-PARC	Japan Proton Accelerator Research Complex
LEIR	Low Energy Ion Ring
LHC	Large Hadron Collider
LHe	Liquid Helium
NC	Normal Conducting
PETRA III	Positron-Elektron-Tandem-Ring-Anlage III
PM	Permanent Magnetic
PS	Proton Synchrotron
PS Booster	Proton Synchrotron Booster
PSI	Paul Scherrer Institute
RCS	Rapid Cycle Synchrotron
RHIC	Relativistic Heavy Ion Collider
SC	Superconducting
SCR	Silicon Controlled Rectifier (power converter)

SF	Superferric
SIS18	Schwerionensynchrotron (heavy-ion synchrotron, magnetic rigidity 18 Tm)
SIS100	Schwerionensynchrotron (heavy-ion synchrotron, magnetic rigidity 100 Tm)
SIS300	Schwerionensynchrotron (heavy-ion synchrotron, magnetic rigidity 300 Tm)
SLS	Swiss Light Source
SM	Switch Mode (power converter)
SPS	Super Proton Synchrotron
Super-FRS	Super Fragment Separator

Bibliography

[1] Gardlowski, P.: *Energy Efficiency of Beam Transfer Channels*. Deliverable D3.3, EuCARD2, Darmstadt, October 2015. EuCARD2-Del-D3-3-Final.doc.

[2] Hinterberger, Frank: *Physik der Teilchenbeschleuniger und Ionenoptik*. Springer-Verlag, Berlin Heidelberg, 2nd edition, 2008.

[3] Wille, Klaus: *Physik der Teilchenbeschleuniger und Synchrotronstrahlungsquellen*, chapter Lineare Strahloptik, pages 51–151. Teubner Studienbücher: Physik, Stuttgart, 2nd edition, 1996.

[4] Wrulich, A. *et al.*: *The SLS design handbook*. Technical report, PSI, Villingen, 1998.

[5] Assmann, R. *et al.*: *Emittance optimization with dispersion free steering at LEP*. Technical Report CERN-SL-2000-078-OP, CERN, Geneva, January 2001.

[6] Tipler, Paul A. and Gene Mosca: *Physik für Wissenschaftler und Ingenieure*. Spektrum Akademischer Verlag, Heidelberg, 6th edition, 2009.

[7] Lee, S. Y.: *Accelerator Physics*, chapter 2.II Linear Betatron Motion, pages 47–73. World Scientific Publishing, Singapore, 2nd edition, 2004.

[8] Tanabe, J.: *Iron Dominated Electromagnets - Design, Fabrication, Assembly and Measurements*. SLAC, Stanford, June 2006. SLAC-R-754.

[9] Rottländer, P. private communication, GSI Helmholtzzentrum für Schwerionenforschung GmbH, Darmstadt, July 2015.

[10] Zickler, T.: *Basic design and engineering of normal-conducting, iron-dominated electromagnets*. In Brandt, D. (editor): *CERN Accelerator School - Magnets*, number CERN-2010-004, pages 65–102, Geneva, November 2010. CERN. CERN-2010-004.

[11] Tommasini, D.: *Practical Definitions & Formulae for Normal Conducting Magnets*. Internal Note 2011-18, CERN, Geneva, September 2011.

[12] *Hollow conductors - square with round hole*. http://www.luvata.com/en/Products/Special-Products/Hollow-Conductors/Square-with-round-hole/, visited on 18.03.2015.

[13] Spiller, P. *et al.*: *FAIR Technical Design Report SIS100*. Technical Design Report, GSI Helmholtzzentrum für Schwerionenforschung GmbH, Darmstadt, December 2008.

[14] Kauschke, M. private communication, GSI Helmholtzzentrum für Schwerionenforschung GmbH, Darmstadt, April 2015.

[15] Wolff, S.: *Superconducting accelerator magnet design*. In Turner, S. (editor): *CERN Accelerator School - Fifth General Accelerator Physics Course*, volume II, pages 755–790. CERN, Geneva, January 1994. CERN 94-01.

[16] Todesco, E.: *Magnetic design of superconducting magnets*. In Bailey, R. (editor): *CERN Accelerator School - Superconductivity for Accelerators*, pages 269–292. CERN, Geneva, July 2014. CERN-2014-005.

[17] Perin, R.: *Field, forces and mechanics of superconducting magnets*. In Turner, S. (editor): *CERN Accelerator School - Superconductivity in Particle Accelerators*, pages 71–92. CERN, Geneva, May 1996. CERN 96-03.

[18] Spiller, P. *et al.*: *Technical Report SIS300*. Technical Report, GSI Helmholtzzentrum für Schwerionenforschung GmbH, Darmstadt, February 2005.

[19] Tenholt, C.: *Entwicklung eines hochstromgepulsten Luftspulen-Quadrupols*. PhD thesis, Johann Wolfgang Goethe-Universität, Frankfurt am Main, 2015.

[20] Wheeler, H. A.: *Inductance formulas for circular and square coils*. Proceedings of the IEEE, 70(12):1449–1450, Dec 1982.

[21] Petzenhauser, I. private communication, GSI Helmholtzzentrum für Schwerionenforschung GmbH, Darmstadt, March 2015.

[22] Meinander, T.: *Generation of magnetic fields for accelerators with permanent magnets*. In Turner, S. (editor): *CERN Accelerator School - Fifth General Accelerator Physics Course*, volume II, pages 983–997. CERN, Geneva, January 1994. CERN 94-01.

[23] Bahrdt, J.: *Permanent magnets including undulators and wigglers*. In Brandt, D. (editor): *CERN Accelerator School - Magnets*, number CERN-2010-004, pages 185–229, Geneva, November 2010. CERN. CERN-2010-004.

[24] Halbach, K.: *Design of permanent multipole magnets with oriented rare earth cobalt material*. Nuclear Instruments and Methods, 169(1):1 – 10, 1980.

[25] Modena, M.: *Electromagnetic and hybrid design experience for CLIC magnets R&D*. Workshop on "Compact and Low Consumption Magnet Design for Future Linear and Circular Colliders", CERN, Geneva, 26-28 November 2014.

[26] Shephard, B. *et al.*: *ZEPTO: Tunable Permanent Magnet Dipoles and Quadrupoles*. Workshop on "Compact and Low Consumption Magnet Design for Future Linear and Circular Colliders", STFC, Geneva, 26-28 November 2014.

[27] Welker, H.: *Estimated Power Losses of SM2 and SCR Power Converters*. private communication, GSI Helmholtzzentrum für Schwerionenforschung GmbH, Darmstadt, March 2015.

[28] Welker, H. private communication, GSI Helmholtzzentrum für Schwerionenforschung GmbH, Darmstadt, March 2015.

[29] Schmidt, T.: *Power Supplies Price List 15 EU*. private communication, FuG Elektronik GmbH, Rosenheim, September 2015.

[30] GSI Division PCCM: *Engineering Estimates on Watercooling System for FAIR*. private communication, GSI Helmholtzzentrum für Schwerionenforschung GmbH, Darmstadt, August 2015.

[31] Fuhr, V.: *Internal document: Verfahrenstechnische Anlagendimensionierung Kühlung*. private communication, GSI Helmholtzzentrum für Schwerionenforschung GmbH, Darmstadt, September 2015.

[32] Ramakers, H. private communication, GSI Helmholtzzentrum für Schwerionenforschung GmbH, Darmstadt, March 2015.

[33] Fuhr, V. private communication, GSI Helmholtzzentrum für Schwerionenforschung GmbH, Darmstadt, September 2015.

[34] Will, C. and C. Mühle: *Cost calculation procedure for normal conducting magnets*. In Große, K. (editor): *GSI Scientific Report 2012*, page 304. GSI, Darmstadt, May 2013.

[35] Will, C. private communication, GSI Helmholtzzentrum für Schwerionenforschung GmbH, Darmstadt, August 2015.

[36] Bechtold, A. private communication, NTG GmbH & Co. KG, Gelnhausen, July 2015.

[37] FAIR@GSI Primary Beams: *Engineering Estimates on SIS100*. private communication, GSI Helmholtzzentrum für Schwerionenforschung GmbH, Darmstadt, December 2015.

[38] Welker, H.: *Estimates for EOI Costbook 5 and Estimates for EOI 2009*. private communication, GSI Helmholtzzentrum für Schwerionenforschung GmbH, Darmstadt, March 2015.

[39] *Machine Parameters PETRA III (Design Values)*. `http://photon-science.desy.de/facilities/petra_iii/machine/parameters/index_eng.html`, visited on 21.11.2015.

[40] *DESY II*. `http://desy2.desy.de/`, visited on 21.11.2015.

[41] Benedikt, M., P. Collier, V. Mertens, J. Poole, and K. Schindl: *LHC Design Report Volume 3: The LHC Injector Chain*. Technical Design Report CERN-2004-003, CERN, Geneva, June 2004.

[42] Liebermann, H. and D. Ondreka: *FAIR and GSI Reference Cycles for SIS18*. Technical Report Version 1.0, GSI Helmholtzzentrum für Schwerionenforschung GmbH, Darmstadt, 13.11.2012.

[43] Liebermann, H. and D. Ondreka: *SIS100 Cycles*. Technical Report Version 2.3, GSI Helmholtzzentrum für Schwerionenforschung GmbH, Darmstadt, 03.09.2013.

[44] Yamazaki, Y. *et al.*: *Accelerator Technical Design Report for J-PARC*. Technical Design Report J-PARC-03-01, J-PARC, March 2003.

[45] Gardner, C. J.: *Parameters for the injection, acceleration, and extraction of gold and copper ions in Booster, AGS, and RHIC*. Technical Report BNL-98927-2012-IR, Brookhaven National Laboratory - Collider-Accelerator Department, Upton, November 2012.

[46] *RHIC Configuration Manual*, November 2006. `https://www.bnl.gov/cad/accelerator/docs/pdf/RHICConfManual.pdf`, visited on 12.12.2015.

[47] Geissel, H. *et al.*: *Technical Design Report on the Super-FRS*. Technical Design Report, GSI Helmholtzzentrum für Schwerionenforschung GmbH, Darmstadt, December 2008.

Danksagung

Ich möchte mich zunächst bei Prof. Dr. Dr. h.c./RUS Dieter H. H. Hoffmann für die Betreuung dieser Thesis bedanken. Vor allem bin ich ihm dankbar für die Motivation zu einer Miniforschung an der GSI im dritten Semester meines Studiums sowie die Vermittlung an die GSI-Kollegen. Dies ermöglichte mir sowohl eine interessante Bachelorthesis als auch eine sehr vielseitige Masterthesis.

Den GSI-Kollegen der Abteilung Primary Beams möchte ich für die freundliche Aufnahme und die Hilfsbereitschaft danken. Vor allem Dr. Peter Spiller und Dr. David Ondreka gilt mein besonderer Dank. Sie haben mich während meiner Arbeit mit sehr viel Engagement betreut und mir mehrere Reisen zu aufschlussreichen Workshops und Konferenzen ermöglicht. Bei meinen Reisen stand mir zudem Dr. Jens Stadlmann sowohl bei den Vorbereitungen als auch vor Ort stets unterstützend zur Seite. Den Kollegen des EuCARD^2-Projekts danke ich für die Unterstützung und die Bereitstellung von Daten.

Besonders möchte ich mich auch bei meinen Eltern, Sylvia und Wolfgang Gardlowski, sowie meinen Großeltern, Brigitte und Roland Stöhr, bedanken. Durch ihre Unterstützung wurde mir mein Studium ermöglicht. Auch in anstrengenden Phasen des Studiums haben sie mich stets motiviert und ermutigt. Weiterhin gilt mein Dank meiner Verlobten Theresa Schickedanz. Sie musste zugunsten dieser Arbeit viele Stunden auf mich verzichten. Dennoch stand sie immer voll hinter mir und meiner Arbeit und bestärkte und unterstützte mich in ihr.